The Morphological and Molecular Basis of Hypoxic Chemotransduction and Transmission in Neuroepithelial Cells of Zebrafish (*Danio rerio*)

Wen Pan

Thesis submitted to the
University of Ottawa
in partial fulfillment of the requirements for the
Doctorate in Philosophy degree in Biology

Department of Biology
Faculty of Science
University of Ottawa

ACKNOWLEDGEMENTS

First, I would like to thank my supervisor Dr. Michael Jonz for accepting me into the lab and providing all the guidance along my studies. During my PhD, I had a lot of difficulties in my studies and life problems that almost led me to quit. I am thankful that Mike didn't give up on me, worked through it with me and gave me the opportunity to succeed. I would also like to thank all my thesis advisory committee members, Dr. Marie-Andrée Akimenko, Dr. Tuan Bui, Dr. Vance Trudeau and Dr. Xuhua Xia. Thank you for all the advice and guidance you provided. I surely learned a lot from you. Thanks to Dr. Jonathan Wilson and Dr. Diane Lagace for accepting to be my thesis examiners.

I would like to thank all my labmates. Michael Country, who has been a great friend and provided support and help during those difficult times. Ben Campbell, who was so positive and inspirational, and made my first few months in the lab so pleasant. Thanks to Maddy and Nicole for being such cheerful labmates during this difficult lockdown time. Thanks to all the undergraduate students that worked with me and my collaborators who have made my projects possible.

Finally, I would also like to express my gratitude to my family. Thanks to my husband Rafael Soares Godoy for being so supportive and patient. Thanks to my lovely son Royce Pan Godoy who tolerated my terrible mood swings during those difficult times. I want to thank my mom for all the emotional support and the long talks to help me find my life goals.

ABSTRACT

O_2 is essential to many animals. Vertebrate species rely on specialized chemoreceptive cells to "sense" O_2 changes in order to make appropriate physiological adjustments to maintain homeostasis. Aquatic vertebrates are especially prone to fluctuations in environmental O_2 availability and have adapted respiratory and cardiovascular responses to cope with hypoxia, a condition characterized by a low level of O_2. In teleost fish, such as zebrafish (*Danio rerio*), neuroepithelial cells (NECs) present in the gill epithelium are the putative O_2 chemoreceptors that mediate hypoxic signals to facilitate such responses. NECs contain the neurotransmitter serotonin (5-HT) and exhibit extensive neural innervation. They are sensitive to hypoxia, as isolated NECs undergo membrane depolarization and vesicular recycling when exposed to acute hypoxia. Other neurotransmitters, such as dopamine (DA), acetylcholine (ACh) and adenosine triphosphate (ATP), have also been suggested to regulate the ventilatory responses to hypoxia. However, the presence of these neurotransmitters or targeted receptors in gills are not well explored. In my PhD studies, I identified cellular and molecular components involved in chemotransduction and transmission for hypoxic signals in NECs of zebrafish through various experimental approaches. First, using the existing transgenic zebrafish line, *ETvmat2:GFP*, I established a method to reliably identify gill NECs. I showed that these cells could be distinguished based on their high expressions of the reporter gene GFP *in vitro, in situ* and in cytometric analyses. GFP-labeled NECs also displayed increases in cell size and population in response to chronic hypoxia. Second, using immunohistochemistry and confocal microscopy, I localized cholinergic cells and dopaminergic cells, sources of DA and ACh secretion respectively, in the gills. These cells present distinct populations from serotonergic NECs. In addition, I found purinergic P2X3 receptors, targets of ATP, to be present in gill NECs and other

neurons. These findings offered different avenues in which hypoxic signals could be regulated. Lastly, using the single cell RNA sequencing approach, I determined the transcriptomic profile of NECs. NECs showed high expressions of G protein regulators, similar to those found in the mammalian O_2 chemoreceptors, and they expressed high levels of genes likely to be involved in O_2 signal transduction and transmission. Within the gill cell atlas generated using the single cell sequencing data, I localized a number of 5-HT, ACh and DA receptors in various gill cell populations, providing evidence for the 5-HT fast synaptic excitatory neurotransmission, paracrine and endocrine regulation of the signal. The studies overall provide compelling evidence to support a role for NECs as the primary O_2 chemoreceptor in zebrafish, and further our understanding of signal modulation in the hypoxic response.

RÉSUMÉ

L'O_2 est essentiel pour de nombreux animaux. Les espèces de vertébrés s'appuient sur des cellules chimioréceptives spécialisées pour «détecter» les changements d'O_2 afin d'effectuer les ajustements physiologiques appropriés pour maintenir l'homéostasie. Les vertébrés aquatiques sont particulièrement sujets aux fluctuations de la disponibilité d'O_2 dans l'environnement et ont des réponses respiratoires et cardiovasculaires adaptées pour faire face à l'hypoxie, une condition caractérisée par un faible niveau d'O_2. Chez les poissons téléostéens, comme le poisson-zèbre (*Danio rerio*), les cellules neuroépithéliales (CNE) présentes dans l'épithélium branchial sont les chémorécepteurs O_2 putatifs qui médient les signaux hypoxiques pour faciliter ces réponses. Les CNE contiennent le neurotransmetteur sérotonine (5-HT) et présentent une innervation neurale étendue. Ils sont sensibles à l'hypoxie, car les CNE isolés subissent une dépolarisation membranaire et un recyclage vésiculaire lorsqu'ils sont exposés à une hypoxie aiguë. D'autres neurotransmetteurs, tels que la dopamine (DA), l'acétylcholine (ACh) et l'adénosine triphosphate (ATP), ont également été suggérés pour réguler les réponses ventilatoires à l'hypoxie. Cependant, la présence de ces neurotransmetteurs ou récepteurs ciblés dans les branchies n'est pas bien explorée. Dans mes études de doctorat, j'ai identifié les composants cellulaires et moléculaires impliqués dans la chimiotransduction et la transmission des signaux hypoxiques dans les CNE du poisson-zèbre à travers diverses approches expérimentales. En premier lieu, en utilisant une lignée de poisson-zèbre transgénique existante, *ETvmat2:GFP*, j'ai établi une méthode pour identifier de manière fiable les CNE branchiales. J'ai montré que ces cellules pouvaient être distinguées sur la base de leurs expressions élevées du gène rapporteur GFP *in vitro*, *in situ* et dans des analyses cytométriques. Les CNE marqués par la GFP ont également montré des augmentations de la taille des cellules et de la population en réponse à l'hypoxie chronique.

Deuxièmement, en utilisant l'immunohistochimie et la microscopie confocale, j'ai localisé des cellules cholinergiques et des cellules dopaminergiques, sources de sécrétion de DA et d'ACh respectivement, dans les branchies. Ces cellules présentent des populations distinctes de CNE sérotoninergiques. De plus, j'ai trouvé des récepteurs purinergiques P2X3, cibles de l'ATP, présents dans les CNE branchiales et d'autres neurones. Ces résultats ont offert différentes voies dans lesquelles les signaux hypoxiques pourraient être régulés. Enfin, en utilisant l'approche de séquençage d'ARN à cellule unique, j'ai déterminé le profil transcriptomique des CNE. Les CNE ont montré des expressions élevées des régulateurs de la protéine G, similaires à celles trouvées dans les chimiorécepteurs O_2 de mammifères, et ils ont exprimé des niveaux élevés de gènes susceptibles d'être impliqués dans la transduction et la transmission du signal O_2. Dans l'atlas de cellules branchiales généré à l'aide des données de séquençage de cellules uniques, j'ai localisé un certain nombre de récepteurs 5-HT, ACh et DA dans diverses populations de cellules branchiales, fournissant des preuves de la neurotransmission excitatrice synaptique rapide 5-HT, de la paracrine et de la régulation endocrinienne du signal. Globalement, les études fournissent des preuves convaincantes pour soutenir le rôle des CNE en tant que chimiorécepteur principal de l'O_2 chez le poisson-zèbre, et approfondir notre compréhension de la modulation du signal dans la réponse hypoxique.

TABLE OF CONTENTS

LIST OF FIGURES

LIST OF TABLES

LIST OF ABBREVIATIONS

$[Ca^{2+}]_i$	Intracellular calcium ion concentration
5-HT	5-Hydroxytryptamine
ACh	Acetylcholine
AMP	Adenosine monophosphate
ATP	Adenosine triphosphate
ATPγS	Adenosine 5′-O-(3-thio)triphosphate
Ca^{2+}	Calcium ion
$CaCl_2 2H_2O$	Calcium chloride dihydrate
CB	Carotid body
ChAT	Choline acetyltransferase
ChN	Chain neuron
Cl^-	Chloride ion
CO_2	Carbon dioxide
CV	Coefficient of variation
d.p.f	Days post fertilization
DA	Dopamine
DAPI	4’,6-diamidino-2-phenylindole
DAT	Dopamine active transporter
DE	Differential gene expression
EDTA	Ethylenedinitriotetraacetic acid
eFA	Efferent filamental artery
ENPC	Epidermal neural progenitor cell

ETC	Electron transport chain
FBS	Fetal bovine serum
FITC	Fluorescein isothiocyanate
FSC	Forward scatter
G2M	Growth phase 2 or metaphase
GABA	Gamma-aminobutyric acid
GDNF	Glial cell line-derived neurotrophic factor
GFP	Green fluorescent protein
h	Hour
H^+	Proton
H_2S	Hydrogen sulfide
HIF	Hypoxia inducible factor
HR	H^+-ATPase-rich
HSPC	Hematopoietic stem and progenitor cell
K^+	Potassium ion
K_B	Background K^+ channel
KCl	Potassium chloride
KH_2PO_4	Potassium phosphate monobasic
$MgSO_47H_2O$	Magnesium sulfate heptahydrate
MLS	Mitochondrial localizing signal
mM	Millimolar
Na^+	Sodium ion
Na_2HPO_4	Sodium phosphate dibasic

Na_2S	Sodium sulfide
NaCl	Sodium chloride
NADH	Nicotinamide adenine dinucleotide
NADPH	Nicotinamide adenine dinucleotide phosphate
NaR	Na^+/K^+-ATPase-rich
NEB	Neuroepithelial bodies
NEC	Neuroepithelial cell
O_2	Oxygen
PBS	Phosphate buffered solution
PBS-TX	Permeabilizing solution containing 2% Triton X-100 in PBS
PCA	Principal component analysis
PNEC	Pulmonary neuroendocrine cell
PO_2	Partial pressure of oxygen
PPADS	Pyridoxalphosphate-6-azophenyl-2',4'-disulfonic acid
ROS	Reactive oxygen species
RT-PCR	Reverse transcription polymerase chain reaction
s	Second
SNN	Shared nearest neighbour
SSC	Side scatter
stGFP	Strong GFP-expressing
SV2	Synaptic vesicle glycoprotein
TH	Tyrosine hydroxylase
UMAP	Uniform manifold approximation projection

VAChT	Vesicular acetylcholine transporter
VAH	Ventilatory acclimatization to hypoxia
vmat2	Vesicular monoamine transporter 2
μm	Micrometer
μM	Micromolar

CHAPTER 1

General introduction

1.1 Introduction

Molecular oxygen (O_2) is essential to all aerobic organisms. It serves as the terminal electron acceptor of the electron transport chain in aerobic respiration and is responsible for most ATP production that fuels cellular processes. When O_2 is deficient, ATP production decreases and cells are forced to switch to anaerobic respiration, which may result in loss of functions or even cell death. Having excessive O_2 however also poses oxidative stress to the cell and causes damage through increased reactive oxygen species (ROS) (Finkel and Holbrook 2000). Thus, sensing, regulating O_2 uptake and maintaining O_2 homeostasis are critical for organisms living in environments with dynamic O_2 availability.

1.2 O_2 chemoreceptors in mammals

In the mammalian system, various organs have been found as sites for oxygen sensing. Specialized O_2 chemoreceptors include type I (glomus) cells of the carotid body (González et al. 1992; Montoro et al. 1996), neuroepithelial bodies of pulmonary airways (Cutz and Jackson 1999) and the adrenal chromaffin cells during early development (Thompson et al. 1997; Nurse et al. 2009). Among these, type I cells of the carotid body have been studied extensively and well characterized as a model for oxygen sensing and chemosensory transduction in vertebrates (Peers and Buckler 1995; Lopez-Barneo et al. 2001; Nurse and Piskuric 2013).

The carotid body (CB) is a small, paired, well irrigated organ located at the bifurcation of the common carotid artery (Gonzalez et al. 1994). It is made up of mainly clusters of chemoreceptive type I cells and supporting sustentacular type II cells (López-Barneo et al. 2008). The CB is composed of a profuse network of capillaries and afferent sensory nerve fibres joining the glossopharyngeal nerves, that are in close contact with type I (glomus cells) and type II cells.

Owing to its location, the carotid body is a major arterial chemoreceptor organ that functions to rapidly detect chemical composition changes in the blood (Gonzalez et al. 1994). The CB is the site of polymodal receptors and has been shown to respond to a variety of stimuli including acute hypoxia, hypercapnia, acidosis and hypoglycemia (Peers and Buckler 1995; Lopez-Barneo et al. 2001; García-Fernández et al. 2007; Zhang et al. 2007). The stimulation of the CB initiates a series of systemic reflexes including increased ventilation, tachycardia, vasoconstriction and adrenaline release from the adrenal medulla (Kumar 2009; Thompson et al. 2016).

The CB is a special neural and paraneural organ that increases in size and vasculature upon exposure to chronic hypoxia (McGregor et al. 1984; Wang and Bisgard 2002). Such adaptive responses have been observed in humans acclimated to high altitude or in patients with cardiopulmonary disease who suffer from hypoxemia (Edwards et al. 1971; Arias-Stella and Valcarcel 1976; Heath et al. 1982). The CB also exhibits considerable plasticity and has been shown to be a functionally active germinal niche (Pardal et al. 2007; Sobrino et al. 2018, 2020). Although the underlying process of organ growth is unknown, it has been suggested that at least some type II cells are dormant stem cells that proliferate and differentiate into new type I cells in response to physiological hypoxia (Pardal et al. 2007; Navarro-Guerrero et al. 2016; Annese et al. 2017). In rats, sustained hypoxic exposure caused type I cell proliferation that mainly occurred within the first 3 days of exposure and long-lasting changes in morphology (Wang et al. 2008).

The major sensory units of the CB are the type I cells, the most abundant cell type in the CB. They express a wide variety of voltage- and ligand-gated ion channels, transient receptor potential and background K^+ channels (Duchen et al. 1988; López-Barneo et al. 1988; Prabhakar and Overholt 2000). They contain secretory dense-core vesicles packed with neurotransmitters

such as ATP, dopamine and acetylcholine (Nurse 2005). Type I cells are electrically excitable, and the activation of type I cells leads to stimulation of adjacent chemoafferent fibres that relay sensory information to the central nervous system (Gonzalez et al. 1994).

1.2.1 Model of CB O_2 sensing

Type I cells of the CB, the major sensory units, are polymodal arterial chemoreceptors, sensitive to a number of stimuli including hypercapnia, extracellular acidosis, hypoglycemia and most notably hypoxia (Dasso et al. 2000; Lopez-Barneo et al. 2001; Pardal and López-Barneo 2002). While a bulk of evidence suggests that type I cells are the initial site of transduction (Verna et al. 1975; Ponte and Sadler 1989; Montoro et al. 1996; Zhong et al. 1997), the molecular mechanism underlying O_2 sensing remains unclear. There have been two main hypotheses proposed to explain the transduction process which eventually triggers the release of neurotransmitters. One hypothesis, regarded as the "metabolic hypothesis", assumes an O_2 sensor being a heme protein and/or a redox-sensitive enzyme, and an associated biochemical event triggers the transduction cascade (Mulligan and Lahiri 1982; Acker et al. 1989; Biscoe et al. 1989; Buerk et al. 1994). The other hypothesis, regarded as the "membrane model", suggests a mechanism by which certain membrane K^+ channels are responsible for sensing O_2 and inhibition of such channels by hypoxia leads to membrane depolarization and subsequent transduction events (López-Barneo et al. 1988, 1997; Prabhakar 2000).

A number of enzymes or proteins have been suggested to be O_2 sensors as suggested in the first hypothesis. Those include reduced nicotinamide adenine dinucleotide phosphate (NADPH) oxidase, mitochondrial uncouplers, prolyl/asparagyl hydroxylases and haemoxygenase-2 (López-Barneo et al. 2008). NADPH oxidases have been found in neutrophils

and CB, and they generate superoxide which can in turn oxidize ion channels and other molecules (Cross et al. 1990). Mutations of several NADPH oxidase subunits altered the function of these enzymes; however, they did not affect CB hypoxic responsiveness (Archer et al. 1999; Fu et al. 2000; He et al. 2002). Evidence seems to suggest that NADPH oxidases are not directly involved in CB O_2 sensing but contribute indirectly through modulation of O_2-sensitive K^+ channels (Fu et al. 2000). Mitochondrial dysfunction has also been investigated as a mechanism of O_2 sensing. Application of electron transport chain (ETC) or mitochondrial uncoupler inhibitors have been shown to increase the afferent activity of the carotid sinus nerve, similar to what has been observed in the hypoxic response (Mills and Jöbsis 1972). Mitochondrial uncouplers were shown to increase intracellular Ca^{2+} and decrease K^+ permeability in type I cells (Duchen and Biscoe 1992; Buckler and Vaughan-Jones 1998). It is as though mitochondrial function alters membrane ion conductance in the presence of hypoxia. In addition, the decrease in intracellular ATP in hypoxia could result in direct closure of ATP-dependent background K^+ channels and AMP kinase activation (Varas et al. 2007). The increase in the AMP/ATP ratio, as a result of mitochondrial dysfunction, can also modulate membrane ion channels (Wyatt et al. 2008). Despite the above evidence, saturating concentrations of mitochondrial inhibitors at proximal and distal complexes failed to inhibit neurotransmitter release from type I cells in hypoxia (Ortega-Saenz et al. 2003). However, a selective inhibition of mitochondrial complex I by rotenone occluded responsiveness to hypoxia, suggesting sensitivity to hypoxia is linked to a rotenone-sensitive molecule present in complex I (Ortega-Saenz et al. 2003). Similar to NADPH oxidases, research involving prolyl/asparagyl hydroxylases and haemoxygenase-2 also failed to prove a direct O_2 sensor as inhibition of these enzymes did not alter type I cell responsiveness to hypoxia (López-Barneo et al. 2008).

In regard to the "membrane model", several O_2 sensitive K^+ channels have been found in type I cells and their open probability decreases upon hypoxic stimulation (Ganfornina and López-Barneo 1992a, b). Since the discovery of O_2-sensitive ion channels including K^+, Na^+, Ca^{2+} and Cl^- channels in type I cells, much attention has been focused on O_2-sensing by membrane channels (Shirahata and Sham 1999), although the identity of a specific O_2 sensor remains controversial. The existence of several classes of O_2-sensitive K^+ channels in type I cells, including some voltage-gated channels (Ganfornina and López-Barneo 1992a; Chou and Shirahata 1996), maxi-K^+ channels (Wyatt and Peers 1995; Williams et al. 2004) and background K^+ channels (Delpiano and Hescheler 1989; Buckler 1997; Kim et al. 2009), has made it unlikely that a single O_2 sensor directly or indirectly regulates the function of a specific K^+ channel to transduce the signal (López-Barneo 1994; Prabhakar and Overholt 2000). Different K^+ channels found in type I cells operate in different ranges of membrane potential and it has been suggested that they all contribute to O_2 detection, in a promiscuous signalling manner (Prabhakar and Overholt 2000). When type I cells are at rest, background K^+ channels constitute most of the K^+ conductance (Kim 2013). Upon exposure to low O_2, K^+ channels were inhibited, reducing K^+ conductance, leading to cell membrane depolarization and increased firing of action potentials (Lopez-Barneo et al. 2001). Opening of membrane Ca^{2+} channels causes the increase of cytosolic Ca^{2+} by extracellular Ca^{2+} influx and leads to catecholamine release from hypoxic type I cells. Aside from background K^+ channels, other channels like maxi-K^+ and voltage-dependent K^+ channels also contribute to the action potential and the potentiation of cell depolarization during hypoxic stimulation as pharmacological inhibition of these K^+ channels successfully induced a secretory response to hypoxia (López-López and Pérez-García 2007; Gomez-Niño et al. 2009; Donnelly et al. 2011). In addition, genetic ablation of genes encoding

ion channel subunits which contribute to the O_2-sensitive background K^+ conductance failed to prevent a powerful secretory response to hypoxia, supporting the notion that other K^+ channels are also involved (Ortega-Sáenz et al. 2010). The cellular responses to acute hypoxia, in terms of cytosolic Ca^{2+} increase and catecholamine release, appeared to be dose-dependent and matched almost perfectly to the hyperbolic correlation between arterial O_2 tension and the afferent discharges of the CB sinus nerve (López-Barneo et al. 2008).

Although experimental evidence exists to support both the "metabolic hypothesis" and "membrane model", both theories are interrelated and not mutually exclusive. While neither is fully supportive on its own, the O_2 sensing mechanism of type I cells of the CB may be a combination of both theories.

1.2.2 Neurotransmitters and neurochemicals involved in chemosensory transmission

The sensory units of the carotid body, type I cells, have been proposed to be the primary loci for transduction of chemical stimuli. Following a hypoxic stimulation, type I cells depolarize through a fast and reversible inhibition of one or multiple K^+ currents which in turn increases the intracellular [Ca^{2+}] and eventually leads to the release of one or more transmitters and modulators (Prabhakar 2000). Among several of the molecules present in type I cells, dopamine (DA), acetylcholine (ACh) and 5'-adenosine-triphosphate (ATP) have been proposed to be the excitatory transmitters in the carotid body. Other molecules that modulate the chemosensory process either through direct effects on type I cells and/or carotid body vessels include nitric oxide and endothelin-1 (Summers et al. 1999; Chen et al. 2000; Campanucci et al. 2006).

Type I cells contain several biogenic amines, most predominantly dopamine, as they express tyrosine hydroxylase (TH), the rate-limiting enzyme in the production of catecholamine

(Gonzalez et al. 1994). DA was once suggested to be an excitatory neurotransmitter, as the pioneering study by Fidone and colleagues found that the increase in DA release had been correlated with hypoxic stimulation in a Ca^{2+} dependent manner in rabbit carotid body and type I cells (Fidone et al. 1982a, b). Similar observations were made in carotid body tissue from cats and rats in later studies (Rigual et al. 1986; Vicario et al. 2000). Moreover, using radiolabelled catecholamines, Fidone *et al.* found the amount of catecholamines, which were mainly DA, released from rabbit carotid body was proportional to the level of hypoxic stimulation (1982b). The chemosensory activity recorded from the rabbit carotid sinus nerve, appeared to correlate to the radiolabelled catecholamine release in response to hypoxia. However, the excitatory transmitter role of DA has more recently fallen out of favour as it was later demonstrated that DA depletion with reserpine had little or no effect on the hypoxia-induced increase in central sinus nerve discharge (Donnelly 1996).

Another candidate of an excitatory neurotransmitter found in type I cells is ACh (Eyzaguirre and Zapata 1984). The biosynthetic machinery and degradation of ACh have been found in type I cells of a number of species, although attempts in rats have not been successful (Nurse and Zhang 1999; Fitzgerald 2000; Gauda et al. 2004). However, the vesicular acetylcholine transporter (VAChT), a typical cholinergic marker, has been localized to the type I cells in the rat carotid body *in situ* (Zhang and Nurse 2004). Other measures such as electrochemical analysis and immunocytochemistry with antibodies specific to ACh have also been used to localize ACh expression in carotid body type I cells (Kim et al. 2004). The excitatory role of ACh appeared controversial as blockers of both nicotinic and muscarinic ACh receptors could not completely abolish the carotid body response to natural stimulation (Douglas 1954; Fitzgerald 2000). It has been suggested that a co-release of ACh and ATP may be the main

mechanism that mediates the hypoxic chemotransmission (Zhang et al. 2000). In the intact CB-sinus nerve preparation from rats and cats, a combination of nicotinic and purinergic blockers was required to block chemosensory discharge from the sinus nerve (Zhang et al. 2000; Varas et al. 2003). ACh and ATP have also been shown to excite petrosal neurons through ionotropic P2X and nicotinic receptors respectively, when applied to soma in electrophysiological experiments (Zhang et al. 2000; Varas et al. 2003). Furthermore, electrophysiological, single cell RT-PCR and immunofluorescence studies have suggested that the purinergic receptors consist of heteromeric P2X2 and P2X3 subunits, where P2X2 subunits may be critical in the hypoxic response (Prasad et al. 2001), and transgenic mice lacking P2X2 subunits showed an attenuated ventilatory response to hypoxia and a reduction in neural discharge (Rong et al. 2003). Taken together, the co-release of ACh and ATP is a plausible mechanism in the chemotransmission of hypoxic signals in type I cells.

In addition to excitatory neurotransmitters, a number of neuroactive agents have also been found in the CB to modulate chemosensory signalling. Dopamine, for instance, has been found to have a dual excitatory and inhibitory role in goat CB, where the excitatory action was through the postsynaptic, serotonergic 5-HT_3 receptors on afferent nerve terminals, while it acts on dopaminergic D_2 receptors on type I cells to inhibit L-type Ca^{2+} channels to create negative feedback regulation (Herman et al. 2003). In addition, hypoxia has been shown to stimulate histamine release in rat CB type I cells *in situ* while a number of histamine receptors were found to be expressed in CB (Koerner et al. 2004). The evidence suggested that histamine may have modulating effects on chemosensory function. Moreover, 5-HT (serotonin) and gamma-aminobutyric acid (GABA) have been suggested as positive and negative neuromodulators, respectively, in type I cells of rodents (Oomori et al. 1994; Fearon et al. 2003; Zhang et al.

2003). Zhang and Nurse showed exogenous application of 5-HT could induce membrane depolarization or rhythmic-like spiking in type I cell clusters, whereas the 5-HT receptor blocker, ketanserin, inhibited the spontaneous discharge commonly present in these cells (2000). However, a later study showed that hypoxia did not elicit 5-HT release in intact rat CB (Jacono et al. 2005), making the modulating role of 5-HT unclear and to be elucidated in future studies. GABA, on the other hand, acts to supress the magnitude of the receptor potential through G-protein coupled $GABA_B$ autoreceptors in type I cells (Fearon et al. 2003). During hypoxia, the activation of these autoreceptors inhibits protein kinase A activity, leading to the augmentation of a background K^+ current. Thus, the suppression of the receptor potential by GABA will produce a negative feedback mechanism.

1.3 Oxygen chemoreceptors in fish

Aquatic vertebrates face particular challenges in acquiring O_2 as O_2 availability in an aqueous environment is relatively low compared to that of the terrestrial environment due to low O_2 solubility. Similar to mammals, aquatic vertebrate species are sensitive to hypoxia (Burleson and Milsom 2003; Perry et al. 2009). When fish experience hypoxia, they hyperventilate, increase ventilatory amplitude, decrease heart rate and increase gill vascular resistance (Randall 1982). These reflex responses are initiated by O_2 chemoreceptors whose locations have been proposed in various sites including the brain (Smatresk et al. 1986), the vasculature (Randall 1982) and the gills (Sundin et al. 2000; Reid and Perry 2003; Burleson and Milsom 2003). Respiratory gills are the primary sites for O_2 chemoreception and neuroepithelial cells (NECs) located in the gills are putative O_2 chemoreceptors (Jonz et al. 2004; Milsom and Burleson 2007).

During early life in zebrafish, gills start to develop at 3 days post-fertilization (d.p.f) (Kimmel et al. 1995) and become innervated and functional at 7 d.p.f (Jonz and Nurse 2005). However, before the formation of functional gills, larval zebrafish displayed hypoxia sensitivity (Padilla and Roth 2001) and this was attributed to the O_2 chemoreception by NECs on the skin (Coccimiglio and Jonz 2012). Skin NECs are distributed throughout the surface of the larva and are morphologically similar to NECs in the gills (Coccimiglio and Jonz 2012). Their population increases as zebrafish transition from anoxia-tolerant embryos to hypoxic-sensitive larvae (Mendelsohn et al. 2008) and decreases in coordination with gill development (Coccimiglio and Jonz 2012). During chronic exposure to hypoxia, the progressive disappearance of skin NECs during development is delayed.

NECs in the primary epithelium of fish gills were first described in 1982 in a few species of teleosts and elasmobranchs (Dunel-Erb et al. 1982). Using formaldehyde-induced fluorescence, both isolated and clustered populations of NECs were found in close proximity to neurons with characteristic dense-core vesicles containing monoamines (Dunel-Erb et al. 1982). These cells appear to be conserved across a number of species including zebrafish, rainbow trout, channel catfish, nile tilapia and the amphibious fish, mangrove rivulus (Jonz and Nurse 2003; Burleson et al. 2006; Monteiro et al. 2009; Zhang et al. 2011; Regan et al. 2011). In addition, serotoninergic NECs of similar morphology and innervation are found in the gills of *Xenopus* larvae at several developmental stages (Saltys et al. 2006).

Past studies have implicated the involvement of several neurotransmitters including 5-HT, ACh, catecholamines, ATP, nitric oxide and hydrogen sulfide, in the hypoxic chemotransmission in various fish species (Porteus et al. 2012). Exogenous application of the 5-HT_2 receptor antagonist, ketanserin, inhibited the hyperventilatory response to hypoxia

(Shakarchi et al. 2013), suggesting that hypoxia-stimulated release of 5-HT might be a mediator of the hypoxic response. Nicotine, an agonist for cholinergic receptors, increased ventilation frequency in larval zebrafish (Rahbar et al. 2016), implicating cholinergic control in O_2 sensing. Moreover, cholinergic cells containing ACh were found in the gill filaments as a distinct population from serotonergic NECs (Zachar et al. 2017b). Furthermore, purinergic P2X3 receptors were suggested to be involved in inducing the hyperventilatory response to hypoxia (Rahbar et al. 2016).

For a while, NECs were believed to be neural crest-derived and homologous to mammalian carotid body chemoreceptors. It was not until recently that homology was shown between gill NECs and pulmonary neuroendocrine cells (PNECs) in mammalian lungs (Hockman et al. 2017). Using lineage-tracing and neural crest-deficient mutant zebrafish, Hockman and colleagues found that NECs of gills are endoderm-derived, like PNECs, while a small population of catecholaminergic cells in the gills were neural crest-derived. Although evidence suggests that NECs of gills and carotid body type I cells are of different embryonic origins, they still share mechanisms at the cellular level. Thus, knowledge from the carotid body chemoreceptors can still be used to make comparisons with gill NECs.

1.3.1 Distribution and innervation of NECs

NECs are located within the efferent filament epithelium, facing the incident flow of water, and are adjacent to the efferent filamental artery (Jonz and Nurse 2003; Perry et al. 2009), which returns oxygenated blood to the systemic circulation. The positions of NECs in the primary epithelium have made them ideal to detect changes in both external and arterial partial pressure of O_2 (PO_2). NECs contain 5-HT and have been identified using antibodies targeting 5-

HT and a transmembrane synaptic vesicle marker (SV2) (Jonz and Nurse 2003; Saltys et al. 2006; Zaccone et al. 2019). Although early studies have focused mostly on NECs present in the efferent filament epithelium, immunohistochemical study revealed NECs identified based on 5-HT immunoreactivity were also seen in other parts of the gill epithelium in zebrafish (Jonz and Nurse 2003). Based on morphology and location, NECs can be divided into two major populations. The larger (~6.9 μm in diameter), irregular-shaped 5-HT-immunoreactive NECs found along the longitudinal axis of the filament and the smaller (~5.1 μm in diameter), spherical 5-HT immunoreactive NECs found in the respiratory lamellae (Jonz et al. 2004). The larger NECs found in the filament are present in the efferent side in all hemibranchs of gill arches, with a particular concentration at the distal end of filaments. The more abundant, smaller NECs found in the lamellae are primarily concentrated in the proximal region in all gill arches and are commonly directly exposed to the external environment. Only NECs in the filaments have been shown to be hypoxia sensitive through physiological studies (Jonz et al. 2004) and more investigation will be required to determine the role of NECs in lamellae. All 5-HT-positive NECs were also immunoreactive to SV2 (Jonz and Nurse 2003), indicating the presence of synaptic or secretory vesicles and their secretory role as in previous studies (Dunel-Erb et al. 1982; Bailly et al. 1992).

NECs of both the filaments and lamellae receive abundant neural innervation (Jonz and Nurse 2003). NECs in the filaments were found to be associated with zn-12-immunoreactive neuronal processes emanating from the superficial proximal neurons (Jonz and Nurse 2003). These neurons are intrinsic to the gill filaments and are situated near the base of the efferent filamental artery and may present afferent terminals or exert local vascular control (Jonz and Nurse 2003). In addition, innervation patterns of NECs in trout seemed to indicate that NECs

form synapses with catecholaminergic nerve fibres of afferent or efferent terminals (Dunel-Erb et al. 1982; Bailly et al. 1992). Moreover, denervation experiments with gill explant culture in zebrafish showed NECs of the filaments were innervated by both intrinsic neurons and extrinsic nerve fibres, while NECs of the lamellae were only innervated by extrinsic nerve fibres (Jonz and Nurse 2003). The evidence seems to suggest a difference in impact between NECs of the filaments and lamellae; however, specific roles of these cells need to be examined further.

1.3.2 Mechanism of O_2 chemotransduction in NECs

NECs are polymodal chemoreceptors. Aside from hypoxia, they are also sensitive to ammonia (Zhang et al. 2011) and acidic hypercapnia (Qin et al. 2010; Abdallah et al. 2015a). The complete response mechanism of NECs to external stimuli has yet to be determined although physiological evidence has proven their O_2 sensitivity. Early studies on a putative chemosensory mechanism showed that the glossopharyngeal and vagus nerves in gills from yellowfin tuna and rainbow trout exhibited increased neuronal discharge under hypoxia (Milsom and Brill 1986; Burleson and Milsom 1993). In addition, neurotransmitters found in CB type I cells such as ACh, DA and 5-HT were also shown to elicit an increase in afferent activity in perfusion of excised gills, similar to the response to hypoxic stimulation (Burleson and Milsom 1995a). This early evidence indicated the sites of O_2 sensing were in the gills.

Physiological investigation of isolated NECs provided more insights on the cells responsible for O_2 sensing. Similar to what was observed in type I cells of mammals (Lopez-Barneo et al. 2001; Buckler 2007), isolated NECs of the filaments from zebrafish exhibit an outwardly rectifying O_2-sensitive current that gets inhibited by hypoxia in a dose-dependent manner (Jonz et al. 2004). The following electrical characterization and pharmacological

inhibition of this current indicated that it was a K^+ current conducted by background K^+ channels. Current-clamp recordings showed that upon exposure to hypoxia, NECs undergo a reversible membrane depolarization (Jonz et al. 2004). The O_2 sensitivity of NECs has also been shown in channel catfish although the specific membrane channel was not defined (Burleson et al. 2006). In addition, background K^+ channel inhibition and membrane depolarization were also observed in NECs in response to increasing levels of CO_2 (Qin et al. 2010). In zebrafish, however, calcium imaging experiments on isolated NECs indicated that intracellular Ca^{2+} concentration increased in response to acidic hypercapnia and isocapnic acidosis, suggesting a response to the increase in the H^+ concentration associated with hypercapnia, rather than directly to CO_2 (Abdallah et al. 2015a). In goldfish, voltage-gated Ca^{2+} channels have been located in gill NECs (Zachar et al. 2017a). Furthermore, injection of the styryl dye, FM1-43, to gill NECs and subsequent hypoxic exposure had shown increased vesicular activity, suggesting secretory activity in response to acute hypoxia (Jonz et al. 2015). Although the precise mechanism of O_2 sensing in gill NECs is still unclear, a proposed O_2 sensing model can be drawn from the above evidence and our knowledge of the mechanism in mammalian systems.

As organized by Zachar and Jonz (2012), the proposed model of O_2 sensing starts with a drop in intracellular PO_2. This change in PO_2 is detected by a molecular O_2 sensor within NECs which causes inhibition of an outward K^+ current through background K^+ channels. While the outward K^+ current is responsible for generating polarized resting membrane potential under normoxic conditions, inhibition of it leads to membrane depolarization. Changes in the membrane potential activates the voltage-gated Ca^{2+} channels in the membrane to allow influx of Ca^{2+} into the cytosol and it may be accompanied by a Ca^{2+} release from intracellular storage.

Then the cytosolic Ca^{2+} increases and facilitates fusion of secretory vesicles with the plasma membrane and neurotransmitter release into the synaptic cleft.

More recently, hydrogen sulfide (H_2S) has been proposed as a molecular oxygen sensor in NECs. Intrabuccal injection of H_2S elicited dose-dependent cardioventilatory responses in trout, similar to responses observed with hypoxia (Olson et al. 2008). Synthesizing enzymes for H_2S have also been located in branchial tissue in trout (Olson et al. 2008), and inhibition of these enzymes in zebrafish blunted or abolished the hyperventilatory response to hypoxia (Porteus et al. 2014a). In addition, exposure of H_2S and hypoxia induced similar levels of depolarization and sodium sulfide (Na_2S), an H_2S donor, elicited an increase in intracellular Ca^{2+} in isolated zebrafish NECs (Olson et al. 2008; Porteus et al. 2014a). The above evidence suggests that the production of H_2S plays a part in mediating the hypoxic signal; however, more investigation will be needed to confirm its role as a molecular oxygen sensor.

1.4 Respiratory consequences of chronic hypoxia

Hypoxia is a condition in which an organism lacks adequate amount of oxygen to meet the demand for metabolism. Many animal species experience hypoxia as a result of changes in their environment. In particular, aquatic species are susceptible to environmental hypoxia as the O_2 availability in water varies. Consequently, fish species develop organismal, cellular and genetic response to hypoxia (Gracey et al. 2001).

Ventilatory acclimatization to hypoxia (VAH) is a well described adaptive response to chronic hypoxia in mammals. It is a time-dependent increase in ventilation which occurs within hours to months of chronic hypoxic exposure, that aims to increase O_2 delivery (Powell et al. 1998). The time course is species dependent and many ventilatory changes found in mammals

arise from the increase in tidal volume. This phenomenon is also found in fish (Burleson et al. 2002; Vulesevic et al. 2006). In addition, fish exhibit a behavioural response when the PO_2 drops below the critical point (Abdallah et al. 2015b). This behaviour, termed aquatic surface respiration, is characterized by an increase in swimming at the water surface, in an attempt to increase O_2 uptake. These behavioural changes are examples of adaptation that fish have acquired to combat the stress of chronic hypoxia.

1.4.1 Fish show changes in ventilation pattern following chronic hypoxia

In fish, VAH can be manifested as a change in ventilation pattern following chronic hypoxia. It was shown that severe chronic hypoxia of 30 mmHg for 4 weeks caused carp (*Cyprinus carpio*) to change its periodic ventilation in normoxia to continuous ventilation in hypoxia (Lomholt and Johansen 1979). However, the ventilation volume did not change with hypoxic acclimation. In flounder (*Platichthys flesus*), ventilatory frequency and amplitude both increased in hypoxic-acclimated fish (Kerstens et al. 1979). In air-breathing catfish (*Clarias mossambicus*), hypoxic acclimation of 18 mmHg for 27 days also resulted in increased ventilation (Johnston et al. 1983). After a week of acclimation in hypoxia of 75 mmHg, channel catfish (*Ictalurus punctatus*) showed an increase in breathing amplitude but no change in gill ventilation frequency (Burleson et al. 2002).

Similarly, a change in ventilation pattern was observed in zebrafish. In the study by Vulesevic et al. (2005), 20% of adult zebrafish exhibit an episodic breathing pattern composed of breathing and non-breathing periods. After exposure to 30-40 mmHg of chronic hypoxia for 28 days, the resting breathing frequency was significantly reduced such that no episodic breathing

was observed. Although the change in ventilation pattern varies between fish species, the response to chronic hypoxia overall shows an increase in ventilation.

1.4.2 Changes in chemoreceptor O_2 sensitivity contribute to VAH

It is widely accepted that the O_2 sensitivity of chemoreceptors is a main contributor of VAH in mammals (as reviewed by Powell *et al.* 1998). In goats, 6 hours of hypoxia caused an increase in carotid body chemoreceptor afferent activity (Bisgard and Neubauer, 1995), whereas the exposure time required in cats was 48 hours (Vizek et al. 1987). The time course required for this change is consistent with the time course required for VAH in each of these two species (Powell et al. 1998), suggesting correlation. Additionally, it was shown that the cellular mechanism behind increased O_2 sensitivity during chronic hypoxia involved changes in K^+ and Ca^{2+} channels in carotid body chemoreceptors (Hempleman 1995, 1996).

In fish, the change in O_2 sensitivity was also observed following chronic hypoxia. Burleson *et al.* showed in 2002 that hypoxic acclimated channel catfish displayed increased ventilatory sensitivity to hypoxia as the breathing amplitude increased during subsequent acute hypoxia. In zebrafish, chronic hypoxia causes hypertrophy and increased neural innervation of NECs, and an increase in the population of putative NEC progenitor cells (Jonz et al. 2004). This change in morphology and cell population may underlie a change in function, such as O_2 sensitivity.

As discussed, chronic hypoxia affects respiration in fish and changes were seen in behaviour and O_2 chemoreceptors. However, the specific changes that occur at the cellular level are not clear. Thus, another goal of the current study was to investigate the effects of chronic

hypoxia on cell composition and the genetic expression profiles of O_2 chemoreceptors to determine how adaption to hypoxia occurs.

1.5 Hypotheses

Gill NECs in teleost fish display O_2 sensitivity, as evidenced by signal transduction at the plasma membrane in response to hypoxia, as well through neurotransmitter storage and synaptic vesicle activity. While it has been widely accepted that NECs in the gills are putative O_2 chemoreceptors in fish, the specific mechanism of O_2 sensing needs to be elucidated. The current research aimed to further examine O_2 sensing, and the hypoxic chemotransduction and transmission processes in NECs of zebrafish. In addition, I aimed to explore other cell types that could potentially regulate or modulate the O_2 signal to better understand the signalling process. The first two research chapters of the thesis localized and identified potential chemoreceptors while the last research chapter identified a number of gill cell populations, and provides characterization based on transcriptomes to understand O_2 sensing by NECs and their interactions with other cells.

1.5.1 Visualization of GFP-positive NECs in the gill of ETvmat2:GFP transgenic zebrafish

Owing to the challenge in reliably identifying serotonergic NECs *in situ* and *in vitro,* I acquired an existing transgenic zebrafish line with the reporter gene green fluorescent protein (GFP) expressed under the control of vesicular monoamine transporter 2 (vmat2) regulatory elements. While vmat2 is responsible for facilitating monoamine transport into synaptic vesicles and has been shown to be expressed in dopaminergic cells in the zebrafish brain, I hypothesized that the GFP expression from *ETvmat2:GFP,* which recapitulates the expression of vmat2, labels

serotonergic NECs and other serotonergic neurons in the gill. I predicted that GFP-positive cells along the gill filaments and in the epithelium of respiratory lamellae would colocalize with cells immunoreactive to 5-HT. In addition, I predicted that GFP labelled serotonergic NECs in the filaments would respond to chronic hypoxia through morphological changes. To test my hypothesis, I used immunohistochemistry and confocal microscopy to determine the expression of GFP and verify cell identity. In addition, I used flow cytometric analysis to isolate filamental NECs and determined their response to chronic hypoxia.

1.5.2 Distribution of purinergic, cholinergic and dopaminergic cells in the gills

In this chapter, I discuss the presence of purinergic, cholinergic and dopaminergic cells in the gills. Purinergic, cholinergic and dopaminergic control of hyperventilatory responses to hypoxia have been demonstrated in zebrafish, I thus hypothesized that cells exerting these controls were present in gill tissue. I predicted that immunolabelling using antibodies targeting P2X3 receptors and VAChT and would localize purinergic and cholinergic cells, respectively, while the transgenic zebrafish Tg(*dat:tom20 MLS-mCherry*) with a mCherry reporter gene labelling a dopamine transporter would localize dopaminergic cells. To test my hypothesis in this chapter, I used immunohistochemistry and confocal microscopy to localize and characterize these cells.

1.5.3 Single cell transcriptomic analysis of NECs and gill cells in response to chronic hypoxia

The role and function of O_2-sensitive gill NECs have remained somewhat mysterious. In this chapter, I will discuss genes that may play critical roles in O_2 sensing, chemosensory transduction and transmission in gill NECs and genes involved in response to chronic hypoxia.

Based on the proposed model of O_2 sensing in NECs and our understanding of the mechanism in the homologous mammalian CB, I hypothesized that various genes involved in the chemotransduction pathway including membrane channel proteins, Ca^{2+} binding proteins and neurosecretory facilitating proteins would be present in the NEC population. Through single cell transcriptomic analysis, I determined the relative expression of those genes to test my hypothesis and I predicted that their levels of expression were significant in NECs. In addition, I predicted that these genes would be highly regulated after 2 weeks of chronic hypoxia in NECs.

CHAPTER 2

Identification of oxygen-sensitive neuroepithelial cells through an endogenous reporter gene in larval and adult transgenic zebrafish

Published as: Pan W, Scott AL, Nurse CA, Jonz MG (2021) Identification of oxygen-sensitive neuroepithelial cells through an endogenous reporter gene in larval and adult transgenic zebrafish. Cell Tissue Res 384:35-47.

I performed all experiments and analyses presented in this chapter, wrote the manuscript, and prepared all figures for publication.

2.1 Introduction

Oxygen (O_2) sensing is an essential mechanism for the survival of vertebrates and their adaptation to low environmental O_2, or hypoxia. Oxygen-sensory systems have been found in mammals, including the carotid body (Gonzalez et al. 1994; López-Barneo et al. 2009) and neuroepithelial bodies (NEBs) of the pulmonary epithelium (Youngson et al. 1993; Cutz and Jackson 1999). In teleost fish, peripheral O_2-sensitive chemoreceptors, called neuroepithelial cells (NECs), have been localized to the gills in several species, including the zebrafish, *Danio rerio* (Dunel-Erb et al. 1982; Zaccone et al. 1992; Jonz and Nurse 2003; Saltys et al. 2006; Coolidge et al. 2008), and are homologues of mammalian O_2 chemoreceptors (Milsom and Burleson 2007; Hockman et al. 2017). During early developmental stages, before the formation of functional gills, oxygen-sensitive NECs are present in the skin of zebrafish (Coccimiglio and Jonz 2012). The zebrafish, in particular, makes an ideal model organism for studies on fish O_2 sensing due to the ease in husbandry and a vast number of available genetic tools.

Zebrafish gills contain four pairs of branchial arches with numerous filaments that are organized into two rows or hemibranchs (Karlsson 1983). The first pair of arches receives innervation from cranial nerves IX (glossopharyngeal) and X (vagus), while the last three pairs are innervated only by the vagus nerve (Sundin and Nilsson 2002). Each gill filament gives rise to a large number of respiratory lamellae that run perpendicular to the filaments and maximize surface area for gas exchange. NECs reside within the gill epithelium (Dunel-Erb et. al 1982; Jonz and Nurse 2003). The larger filamental NECs are found on the efferent epithelium of the gill, between the incident flow of water and the efferent filamental artery. They are primarily concentrated near the distal region of the filaments. The smaller lamellar NECs, present within

the epithelium of the respiratory lamellae, are more abundant near the proximal regions of the gill filaments.

All NECs in fish exhibit the monoamine neurotransmitter, serotonin (5-hydroxytryptamine, 5-HT) (Dunel-Erb et al. 1982; Zaccone et al. 1992; Jonz and Nurse 2003; Saltys et al. 2006; Coolidge et al. 2008), which has been identified as an important transmitter or modulator in O_2 sensing in mammals (Fu et al. 2002; Nurse 2014). In addition, NECs express the synaptic vesicle protein, SV2 (Jonz and Nurse 2003); and acute stimulation of NECs by hypoxia or cyanide (a potent chemoreceptor stimulant) induced dense-cored vesicle degranulation at the ultrastructural level (Dunel-Erb et al. 1982), and vesicular recycling as measured by the styryl dye, FM1-43 (Jonz et al. 2015; Zachar et al. 2017a). Neurosecretion in NECs is thought to occur in a Ca^{2+}-dependent manner as a result of hypoxia-induced inhibition of background K^+ channels and membrane depolarization (Jonz et al. 2004; Zachar and Jonz 2012). NECs are also responsive to changes in CO_2 and H^+ (Qin et al. 2010; Abdallah et al. 2015a). NECs are innervated by neuronal processes that arise from proximal neurons located at the base of the filament, and by extrabranchial nerves, which are also SV2-positive (Jonz and Nurse 2003). In chronic hypoxia, NECs have been shown to increase in size and shape, suggesting an O_2-dependent change in morphology (Jonz et al. 2004; Porteus et al. 2014b) .

NECs are conventionally identified using the vital dye, Neutral Red, in live cell imaging experiments (Youngson et al. 1993; Jonz et al. 2004). Although Neutral Red labels NECs *in vitro*, it may diffuse out of the cell quickly, reducing its efficacy for experiments of long duration. In addition, labelling by Neutral Red is not confined to NECs, and the dye has been shown to label only 87% of gill NECs in goldfish (*Carassius auratus*; Zachar et al. 2017). In addition, identification of NECs using Neutral Red *in situ* is problematic due to poor selective

uptake in whole tissue. This study aimed to provide a new method to identify NECs *in vitro* and *in situ* using a transgenic zebrafish line. *ETvmat2:GFP* contains a reporter gene for green fluorescent protein (*GFP*) under the expression of the vesicular monoamine transporter (*vmat2*). The vesicular monoamine transporter (Vmat2) is an integral membrane protein that mediates storage of monoamines, such as 5-HT, into synaptic vesicles. Owing to the retention of 5-HT by NECs, we predicted that expression of *vmat2* would be indicative of NECs. We found that, based on GFP expression levels, morphology and distribution, gill filamental and lamellar NECs, associated neurons, and skin NECs in larval fish could be identified. In addition, we established a protocol to use the endogenous expression of GFP in *ETvmat2:GFP* to separate the filamental NEC population for high throughput flow cytometric analyses. Lastly, we showed that filamental NECs changed in size, gene expression and number following two weeks of *in vivo* exposure to chronic hypoxia.

2.2 Materials and methods

2.2.1 Animals

Transgenic *ETvmat2:GFP* zebrafish (*Danio rerio*), previously described by Wen et al. (2008), were obtained from the Becker Laboratory at the University of Edinburgh. Zebrafish were raised and maintained at 28°C on a 14-10 h light-dark cycle (Westerfield 2007) at the Laboratory for the Physiology and Genetics of Aquatic Organisms at the University of Ottawa. Larval fish were obtained by breeding from 12-month adult zebrafish and maintained in 150 mm Petri dishes at 28°C until 2 days post fertilization (d.p.f.). All procedures for animal use were carried out in accordance with institutional guidelines according to protocol BL-1760, along with guidelines provided by the Canadian Council on Animal Care (CCAC). Adult zebrafish were

euthanized by a blow to the head and decapitated. Larvae were euthanized by hypothermic shock by immersion in an ice bath for 20 min.

2.2.2 Immunohistochemistry and confocal microscopy

Techniques for tissue extraction, immunolabelling and confocal imaging were carried out as described by Jonz and Nurse (2003) and Coccimiglio and Jonz (2012). Whole gill baskets were removed and quickly immersed in ice-cold phosphate buffered solution (PBS) containing (mM): NaCl 137, Na_2HPO_4 15.2, KCl 2.7, and KH_2PO_4 1.5; pH 7.8 (Bradford et al. 1994). After a rinse in PBS, gill baskets were immersed in 4% paraformaldehyde in PBS to allow fixation overnight at 4°C. Tissues were removed from the fixative and rinsed in PBS three times at 3 min before permeabilization for 24 h at 4°C. Permeabilizing solution (PBS-TX) contained 2% Triton X-100 in PBS (pH 7.8). After 3 rinses in PBS, gill baskets were separated into individual gill arches and subsequently treated with primary and secondary antisera. Whole larvae were fixed and permeabilized in the same way but without dissection.

For certain specimens, the endogenous green fluorescent protein (GFP) signal of *ETvmat2:GFP* was enhanced after fixation using mouse anti-GFP (cat. no. A-11120, Invitrogen, Burlington, ON, Canada) at a dilution of 1:500 and localized with goat anti-mouse secondary antiserum conjugated with Alexa 488 at 1:100 (cat. no. A-11029, Invitrogen, Burlington, ON, Canada). Neuroepithelial cells, intrinsic nerve fibres and neurons were identified using antisera against serotonin (5-HT) and the synaptic vesicle protein SV2. Labelling of these structures in the zebrafish gills and skin by 5-HT and SV2 antibodies has been previously characterized (Jonz and Nurse 2003; Coccimiglio and Jonz, 2012). Polyclonal rabbit anti-5-HT (cat. no. S5545, Sigma-Aldrich, Oakville, ON, Canada) was used at 1:250 and localized with goat anti-rabbit secondary antiserum conjugated with Alexa 405 (1:50, cat. no. A31556, Life Technologies Inc.,

Burlington, ON, Canada). In some cases, labelling by Alexa 405 (blue) was changed to magenta to improve contrast. Monoclonal mouse antibodies against SV2 (Developmental Studies Hybridoma Bank, University of Iowa, IA, USA) were used at 1:100 and targeted by goat anti-mouse secondary antiserum conjugated with Alexa 594 at 1:100 (cat. no. A11005, Invitrogen, Burlington, ON, Canada). All antisera were diluted using PBS-TX. Gill arches and whole larvae were incubated in primary antisera for 24 h at 4°C. Tissues were rinsed with PBS three times at 3 min and immersed in secondary antisera for 1 h at room temperature in darkness. Gill arches and larvae were then rinsed with PBS before they were mounted onto a glass microscopic slide with Prolong Diamond antifade mountant (Thermo Fisher Scientific, Burlington, ON, Canada) and covered with a 1.2 mm glass coverslip.

Whole-mount preparations were examined using an upright microscope platform (FN1, Nikon) with motorized XYZ control and a confocal scanning system (A1RsiMP, Nikon) equipped with continuous laser lines at 405 nm, 488 nm and 561 nm. Images were viewed and captured with confocal imaging software, NIS Elements (Nikon). Each image is presented as a composite projection of multiple optical sections, each separated by 0.5–1.0 μm and combined to produce a total tissue thickness of 20–60 μm. Images in Figure 2.5a and a' are of single optical sections. Processing of images was made through the open source software Fiji (Schindelin et al. 2012) and Illustrator CS 6 (Adobe).

2.2.3 Chronic hypoxia

To facilitate exposure to chronic hypoxia, adult *ETvmat2:GFP* zebrafish were housed in static 2 l aquaria. Fish were kept at 28°C, subjected to a natural 14-10 h light-dark cycle, and were fed twice and given 2 water changes per day. The partial pressure of O_2 (PO_2) of water was

controlled by mixing compressed air and 100% N_2 through a Pegas 4000 MF gas mixer (Columbus Instruments, Columbus, OH, USA). The mixture was delivered by air stones suspended in the water. A group of 3 fish were acclimated to severe hypoxia by gradual decrease of water PO_2 from 158 mmHg to 35 mmHg in intervals of ~30 mmHg over the period of 1 week. Fish were maintained at a PO_2 of 35 mmHg for an additional week for a total 14-day exposure. This PO_2 level is above the critical O_2 tension (Barrionuevo and Burggren 1999) and was chosen to minimize fish mortality while maximizing morphological changes in NECs associated with chronic hypoxia. In the control group, 3 fish were given continuously aerated water throughout the treatment period.

2.2.4 Flow cytometry

Tissue dissection and cell dissociation were all performed under sterile conditions in a laminar flow hood and followed those of Jonz et al. (2004). Whole gill baskets were removed with scissors and forceps and rinsed in a wash solution containing 2% penicillin/streptomycin (cat. no. 15140122, Life Technologies Inc., Burlington, ON, Canada) in PBS three times at 3 min on ice. For all gill arches, the distal region of gill filaments, areas rich in NECs, were selectively removed and placed into 0.25% trypsin/EDTA (cat. no. 25200072, Life Technologies Inc., Burlington, Canada). Filament tissues were treated with trypsin for 1 h at room temperature, minced with fine forceps and triturated in a 15 ml centrifuge tube with a 1 ml Pasteur pipette. 10% fetal bovine serum (FBS, cat. no. 10438018, Life Technologies Inc., Burlington, ON, Canada) was added to stop the trypsin reaction and cells were passed through a 40 µm Falcon cell strainer (Fisher Scientific, Pittsburgh, PA, USA) to eliminate cell clumps. The cell suspension was centrifuged at 1,300 rpm for 3 min and the cell pellet was rinsed with PBS

through gentle trituration. The cell pellet was centrifuged again, resuspended in PBS and kept on ice until analysis. Cell viability of between 86–93% (depending on dissociation) was measured by plating cells in 35 mm glass-bottomed Petri dishes (see Jonz et al. 2004) and using an automated cell counter (EVE^{TM}, NanoEntek, Seoul, Korea) with 0.4% trypan solution (cat. no. 15250061, ThermoFisher Scientific, Waltham, MA USA) to stain dead cells.

Single-cell analysis was conducted using a Gallios Flow Cytometer (Beckman Coulter, IN, USA) equipped with 3 solid state lasers with excitations at 405 nm, 488 nm, and 638 nm. Fluorescence was collected by the forward scatter (FSC, Fourier design with 488 nm filter) and side scatter (SSC, independently-focused photodiode with electronic attenuation and 488 nm filter) channels. The native GFP signal of the *ETvmat2:GFP* gill cell suspension was detected through fluorescence channel FL1 with a 525 BP40 filter. A negative control of endogenous GFP fluorescence was prepared in the same way using unstained gill cells dissociated from wild type zebrafish. The amplification voltages were set based on negative and positive controls (FSC – 639 V, SSC – 174 V, 488 nm – 375 V). For each biological sample (i.e. all gill cells dissociated from one adult zebrafish), 100,000 events were collected with a rate of ~330 events per second. A forward scatter threshold of 30 was applied to minimize noise. Fluorescence measurement data was visualized in the Gallios acquisition software, Kaluza (Beckman Coulter, Indianapolis, IN, USA), during acquisition.

2.2.5 Data analysis

Analysis of flow cytometry data was made in FlowJo™ 10.6.1 (Becton Dickinson & Company, NJ, USA). A representative gating strategy, as outlined in Fig. 7, was applied to separate single, strong GFP-positive cell populations from debris, aggregates and GFP-negative

cells. Data of biological samples from the same treatment group was combined through the FlowJo™ concatenation function before further analysis. Parametric analysis was conducted using the built-in statistics function and the non-parametric analysis was done using the compare population package in FlowJo™.

2.3 Results

2.3.1 Neuroepithelial cells of the skin in ETvmat2:GFP larvae were GFP-positive

For better visualization following tissue fixation, the endogenous GFP signal of *ETvmat2:GFP* was enhanced by an anti-GFP antibody coupled with a secondary antibody with the Alexa 488 fluorophore. In all *ETvmat2:GFP* larvae examined, a population of GFP-positive cells was present across the entire skin surface, as shown in a confocal image collage of a 2 d.p.f. larva (Figure 2.1a). Immunolabelling with antibodies against 5-HT confirmed that all 5-HT-positive skin NECs were GFP-positive (arrows, Figure 2.1b, c); however, a smaller proportion (10.7 ± 2.5%) of cells were GFP-positive but were 5-HT negative (arrowheads, Figure 2.1b). GFP-positive skin NECs appeared irregular in shape and were situated in an epidermal layer superficial to pigment cells of the skin. Many NECs extended small processes (arrows, Figure 2.1b). They were most abundant in the head region (Figure 2.1b), on the yolk sac and the trunk (Figure 2.1c). Cells were dispersed in these regions and did not form clusters. GFP-positive skin NECs were present on the tail but were less abundant (Figure 2.1d).

2.3.2 Neuroepithelial cells of the gills in adult ETvmat2:GFP zebrafish were GFP-positive

The GFP expression of adult *ETvmat2:GFP* zebrafish labelled a large number of cells in the gills, as shown in Figure 2.2a. These cells displayed two distinct levels of expression, termed

strong GFP-expressing (stGFP) and weak GFP-expressing, indicated by a high GFP intensity and a lower GFP intensity, respectively. The difference in GFP expression in cells was prominent and could be demonstrated through a pseudocolour image showing different GFP intensities in Figure 2.2b’’’’. stGFP-positive cells, denoted by bright yellow in the pseudocolour image, were found on the efferent side of each gill filament with a higher concentration at the distal region. These cells were immunoreactive to 5-HT and SV2 (arrows, Figure 2.2b’, b’’) and identified as filamental NECs. stGFP-positive NECs at the distal region of the filament were organized closely to each other and typically formed one or more rows (Figure 2.2c). stGFP-positive NECs further away from the distal end were more distant from each other. They were elongated with prominent processes. Although rare, 2.0 ± 1.1% of stGFP-positive cells on the filaments were found to be SV2-positive and 5-HT-negative (double arrow, Figure 2.2b–b’’, c–c’’’). Adjacent to stGFP-positive NECs in the longitudinal axis of the filaments are weak GFP-expressing cells (double arrowheads, Figure 2.2b–b’’). They were 5-HT-negative and morphologically similar to stGFP-positive NECs. In addition, a small number of weak GFP-expressing cells were also SV2-positive.

Other weak GFP-expressing cells were distributed over the respiratory lamellae of the gills (Figure 2.3a). These cells were smaller than stGFP-positive NECs and were abundant on lamellae near the proximal filament regions. There were two distinct populations. One population of round-shaped cells was identified as lamellar NECs based on their immunoreactivity with 5-HT (arrows, Figure 2.3a, b). These cells were numerous, showed low GFP expression, and a granular labelling pattern that often revealed a dark nuclear region. The other population of weak GFP-expressing cells were irregularly-shaped (arrowheads, Figure 2.3b). They were negative for 5-HT and were located near the distal tips of lamellae.

2.3.3 Endogenous GFP labelled neurons in gill filaments of adult ETvmat2:GFP zebrafish

Along the longitudinal axis of the filament, the endogenous GFP labelled a population of bipolar neurons (arrows, Figure 2.4), called "chain neurons" (Jonz and Nurse, 2003). These cells displayed lower GFP intensity compared to stGFP-positive NECs and the GFP expression was primarily concentrated within the cell bodies. Chain neurons showed immunoreactivity to SV2, which revealed a series of puncta associated with GFP-positive nerve fibres (Figure 2.4b', b''). These neurons resided deeper within the filaments, compared to NECs (Figure 2.5a).

The endogenous GFP was also present in the proximal region of the filament and labelled the superficial and deep proximal neurons, two clusters of neurons of the proximal filaments that contribute fibres to the larger nerve bundles of the superficial or deeper regions of the filaments (see Jonz and Nurse, 2003). Similar to the chain neurons, the GFP intensity of these neurons was also weak compared to that of stGFP-positive NECs. The multipolar GFP-positive superficial proximal neurons resided within the superficial layer of the efferent filament near the gill arch junction. They appeared long with nerve fibres extending to the gill arch (arrows, Figure 2.5b). Beneath these neurons were GFP-positive deep proximal neurons (arrowhead, Figure 2.5b'), whose nerve fibres innervated chain neurons that ran along the filament. The spatial orientation of both superficial and deep proximal neurons is better illustrated in a spatial colour-coded composite of multiple optical sections with features at different sections coded in a different colour (Figure 2.5b'').

2.3.4 Flow cytometry and the effects of chronic hypoxia on stGFP-positive neuroepithelial cells

Filamental NECs exhibited a distinct endogenous GFP expression following dissociation from the gills of adult *ETvmat2:GFP* zebrafish (Figure 2.6). This characteristic was applied to sort filamental NECs from other gill cells, and the effects of chronic hypoxia on single NECs were examined using flow cytometric analysis. Cells from individual biological samples were processed separately. First, stGFP-positive NECs in gill filaments were identified using the GFP fluorescence parameter. After applying the gating strategy to filter out debris and aggregates shown in Figure 2.7, stGFP-positive cells formed a distinct cluster based on endogenous GFP fluorescence in both normoxia and hypoxia groups (Figure 2.7d, e). These cells were extracted for further analysis on frequency of cells, GFP fluorescence intensity and relative size. The frequency of stGFP-positive cells was measured as a proportion of stGFP-positive cells in the overall filtered cell population. In normoxia, the mean frequency of stGFP-positive cells was 0.78% with a standard deviation of 0.14% (Table 2.1). In hypoxia, the mean frequency of stGFP-positive cells increased to 1.17% with a standard deviation of 0.24%.

As seen in histogram plots for GFP fluorescence in Figure 2.8a, the stGFP-positive cell populations in hypoxia showed higher GFP fluorescence intensity when compared to normoxia. Both mean and mode GFP fluorescence of the hypoxia group, measured by the fluorescence channel, were significantly higher than those of the normoxia group (Table 2.1). The coefficient of variation (CV) among biological samples did not differ between groups, showing no significant change in variation after chronic hypoxia. In addition, the histogram plot of concatenated data from biological triplicates revealed that stGFP-positive cells of the hypoxia group showed a broader range of GFP fluorescence and a clear right shift on the GFP intensity

scale, when compared to normoxia (Figure 2.8b). The population comparison test verified that GFP fluorescence intensity in hypoxia was significantly different from normoxia (Chi-squared T(X) score of 97.22). The relative cell size of stGFP-positive cells was measured by the parameter of forward scatter area, where a greater reading indicated a greater cell size. In Figure 2.8c, biological samples from hypoxia showed larger stGFP-positive cells compared to the normoxia group. The difference in cell size was clearer in numerical measures, as the hypoxia group had a greater mean and mode in forward scatter area than normoxia (Table 2.1). The CV of forward scatter area was greater in normoxia, indicating a greater variation among individual samples than hypoxia. Similar to GFP fluorescence, the concatenated data showed a wider range of cell size and a right shift of the distribution along the relative cell size scale in hypoxia than normoxia (Figure 2.8d). The population comparison test showed the difference in relative cell size between hypoxia and normoxia was significant (Chi-squared T(X) score of 25.40).

2.4 Discussion

The present study showed that the transgenic zebrafish line *ETvmat2:GFP* labelled oxygen-sensitive NECs in the skin of developing larvae and in the gills of adult fish through GFP expression. In addition to oxygen chemoreceptors, neurons within the gill filaments were also labelled by GFP in this line. The labelled cells displayed unique characteristics and dynamic GFP expression, which allowed clear distinction between different cell populations. In addition, we demonstrate that GFP-positive NECs could be isolated *in vitro* and that they undergo morphological changes following exposure to chronic hypoxia.

2.4.1 Skin NECs are GFP-positive

At 2 d.p.f., *ETvmat2:GFP* larval fish showed GFP-positive cells across the skin surface. The majority of the cells labelled by GFP on the skin were shown to be serotonergic NECs and the distribution of these cells was consistent with previous reports (Coccimiglio and Jonz 2012; Dean et al. 2017). However, a few GFP-positive cells on the skin were found to be 5-HT-negative. The GFP in *ETvmat2:GFP* recapitulates the expression of *vmat2*, as this reporter gene was inserted into the enhancer region of the *vmat2* gene (Wen et al. 2008). *vmat2* expression is expected to include, but is not limit to, cells that express 5-HT. This line has been previously used for labelling dopaminergic neurons in the brain (Wen et al. 2008). Thus, GFP-positive cells that are 5-HT negative may represent another monoaminergic cell population. Nevertheless, the current study showed that 5-HT-positive cells on the skin were GFP-positive, making the endogenous GFP an indicator of skin NECs at this stage.

Zebrafish rely on cutaneous respiration during embryonic and early larval stages (Rombough 2007). In addition, evidence suggests that the skin is a site of oxygen sensing in zebrafish, before the development of functional gills (Jonz and Nurse, 2005; Coccimiglio and Jonz 2012; Shakarchi et al. 2013). As in the gills, skin NECs were identified by 5-HT and SV2 immunolabelling; moreover, acclimation to hypoxia or hyperoxia were shown to alter the natural decline of skin NEC number with age, and denervation of skin NECs eliminated the hyperventilatory response to hypoxia (Coccimiglio and Jonz 2012). More recently, it was demonstrated that nitric oxide may act as an excitatory neurotransmitter to mediate O_2 sensing by skin NECs (Porteus et al. 2015), and these cells may also sense changes in CO_2 to initiate cardiac reflexes (Miller et al. 2014). However, there is a lack of direct physiological evidence at the cellular level for the function of skin NECs as respiratory chemoreceptors, possibly due to the

difficulty in identifying these cells in live specimens. The present work offers a convenient tool for identifying skin NECs without invasive measures to allow future physiological experimentation.

2.4.2 Gill NECs are GFP-positive

The GFP expression in the *ETvmat2:GFP* line clearly labelled filamental and lamellar NECs in the gills of adult zebrafish. Labelling of stGFP-positive cells overlapped with that of 5-HT-positive NECs and SV2-positive cells in the filaments. NECs of the gill filaments are polymodal (Jonz 2018) and respond directly to hypoxia, hypercapnia and extracellular acidosis in isolated cell preparations (Jonz et al. 2004; Qin et al. 2010; Abdallah et al. 2015). Although previous studies have relied on *in vitro* isolation of NECs using the dye, Neutral Red, the present study showed that *ETvmat2:GFP* labels filamental NECs with a distinct level of GFP expression, which enabled definitive identification of chemoreceptive NECs in isolated cell or whole-tissue preparations. This method of identification is more reliable as it eliminates identification errors associated with exogenous application of non-specific indicators. In addition, the high GFP expression in filamental NECs might indicate a higher level of *vmat2* expression in these cells, compared to other GFP-positive cells with weaker expression. This is suggestive of higher monoamine storage, possibly leading to enhanced secretory activity, which aligns well with the role of an oxygen chemoreceptor.

A small fraction of stGFP-positive cells were 5-HT-negative but SV2-positive, and this is consistent with similar 5-HT-negative NECs that were previously described (Jonz and Nurse, 2003). *ETvmat2:GFP* also labelled another group of cells in the filaments that expressed lower levels of GFP and were immunonegative for both 5-HT and SV2. Since these cell types

expressed *vmat2*, they are likely to be monoaminergic but may not be serotonergic. Another possibility is that they are precursor cells that are in the process of differentiation but have not yet synthesized or obtained 5-HT. This is consistent with a previous report that identified a population of putative precursor cells in the zebrafish gills that were 5-HT-negative (Jonz and Nurse 2003).

GFP and *vmat2* expression was lower in NECs of the lamellae. Although lamellar NECs have not yet been tested for chemosensitivity, they possess patterns of innervation that are similar to NECs of the filaments (Jonz and Nurse, 2003). However, the lower *vmat2* activity of lamellar NECs might suggest a minor secretory or neuroendocrine role.

2.4.3 Other GFP-positive neurons in the gills

In addition to chemoreceptors, chain neurons together with superficial and deep proximal neurons were also labelled by GFP in *ETvmat2:GFP.* These neurons exhibited lower levels of GFP expression, compared to filamental NECs, and were identified based on their morphology and immunolabelling of SV2. Chain neurons are bipolar neurons that run deep in the filament tissue and extend from the base of the filament to the distal tip. They were previously shown to exhibit varicosities that may form connections with other structures within the filament (Jonz and Nurse 2003). Their close association with the efferent filamental artery and central venous sinus also suggested a mechanism of vascular control (Jonz and Nurse 2003). Furthermore, GFP also labelled superficial and deep proximal neurons at the base of gill filaments. This is consistent with previous findings that both superficial and deep proximal neurons were intrinsic and serotonergic (Jonz and Nurse 2003). In the present study, GFP labelling allowed simultaneous visualization of filamental NECs and intrabranchial neurons, and their relative positions. This

may provide an opportunity for future studies to investigate the interplay between NECs and neurons within the gill filaments.

2.4.4 Effects of chronic hypoxia on the stGFP-positive cell population

The transgenic zebrafish *ETvmat2:GFP* labels multiple cell populations with distinct characteristics in the gills. Among all GFP-positive cells, filamental NECs displayed a significantly higher level of GFP expression that distinguished them from other cells. In this study, we showed that when the proper gating strategies were applied to flow cytometry, stGFP-positive cells from the gill, which represent the filamental NEC population, formed a distinct cluster and could be separated for cytometric analysis. After two weeks of hypoxic treatment, the filamental NEC population from individual samples was shown to increase in frequency of detection, size and GFP intensity. Sixty days of chronic hypoxia was previously shown to induce hypertrophy and process extension in serotonergic gill NECs in zebrafish; in addition, this treatment caused proliferation of non-serotonergic NECs, with only a marginal increase in the number of serotonergic NECs (Jonz et al. 2004). While our current findings agree with this previous report, the present investigation was conducted on a larger cell population. The current results further show that as little as two weeks of hypoxic exposure was sufficient to induce changes in morphology; further, the number of stGFP-positive cells, which are predominantly serotonergic, increased with chronic hypoxia. The increase in frequency and size of NECs indicates an expansion of this cell population within the gill filaments in response to prolonged exposure to hypoxia, and correlates with modifications in the hyperventilatory response to hypoxia (e.g. breathing amplitude and frequency) in fish that occur within the range of approximately 1-4 weeks of chronic hypoxia (Kerstens et al. 1979; Johnston et al. 1983;

Burleson et al. 2002). The increase in GFP intensity following hypoxia may be indicative of an increase in Vmat2 protein production in NECs, suggesting an increased level of vesicular transport and storage of monoamines, such as 5-HT.

2.5 Conclusion

Here we report the first use of a transgenic animal with endogenous GFP expression to identify oxygen chemoreceptors during development, and in adults, in an aquatic vertebrate. While multiple cell populations are labelled in the gills of *ETvmat2:GFP*, the distinct expression profiles of each cell type allowed for straightforward identification. This non-invasive labelling approach will allow for reproducibility and scalability with important implications in live cell imaging and high-throughput experimentation, such as pharmacological screening or flow cytometric analysis. For example, we have demonstrated that, in NECs dissociated from the gills of *ETvmat2:GFP* zebrafish, changes in morphology, cell number, and vesicular transporter expression could be observed following chronic hypoxia.

Table 2.1 Quantification of stGFP-positive gill cell size and GFP parameters in *ETvmat2:GFP* transgenic fish in normoxia and chronic hypoxia.

Parameters‡	Normoxia	Hypoxia
Frequency of stGFP cells	0.79 ± 0.14%	1.17 ± 0.24%
Mean GFP	358,822 ± 36,219	491,000 ± 37,207*
Mode GFP	365,929 ± 70,251	525,000 ± 103,346*
CV GFP	28.9	26.8
Mean FSC-A	65,694 ± 4,565	72,619 ± 6,307
Mode FSC-A	60,075 ± 6,968	68,540 ± 6,038
CV FSC-A	27.1	23.5

‡*Standard deviations obtained from biological triplicates.*

*****Values significantly different ($p<0.05$) from control.*

Figure 2.1 Neuroepithelial cells (NECs) of the skin in *ETvmat2:GFP* larvae were GFP-positive. **a** Distribution of GFP-positive cells in the skin of a 2 d.p.f. *ETvmat2:GFP* zebrafish. Lateral view of a whole larva showing that GFP in green co-localizes with 5-HT-immunolabelling in blue. Regions within dashed boxes are enlarged in subsequent panels. Scale bar = 100 μm. **b** Distribution of GFP- and 5-HT-positive cells in the skin of the head region. Arrows show GFP- and 5-HT-positive cells exhibiting cell processes. Arrowheads indicate cells positive for GFP and negative for 5-HT. **c** Distribution of GFP- and 5-HT-positive cells on the surface of the yolk sac. Arrows indicate cells positive for both GFP and 5-HT. **d** Distribution of GFP- and 5-HT-positive cells in the skin of the tail. Scale bars in b'' = 100 μm and applies to all panels in b–d.

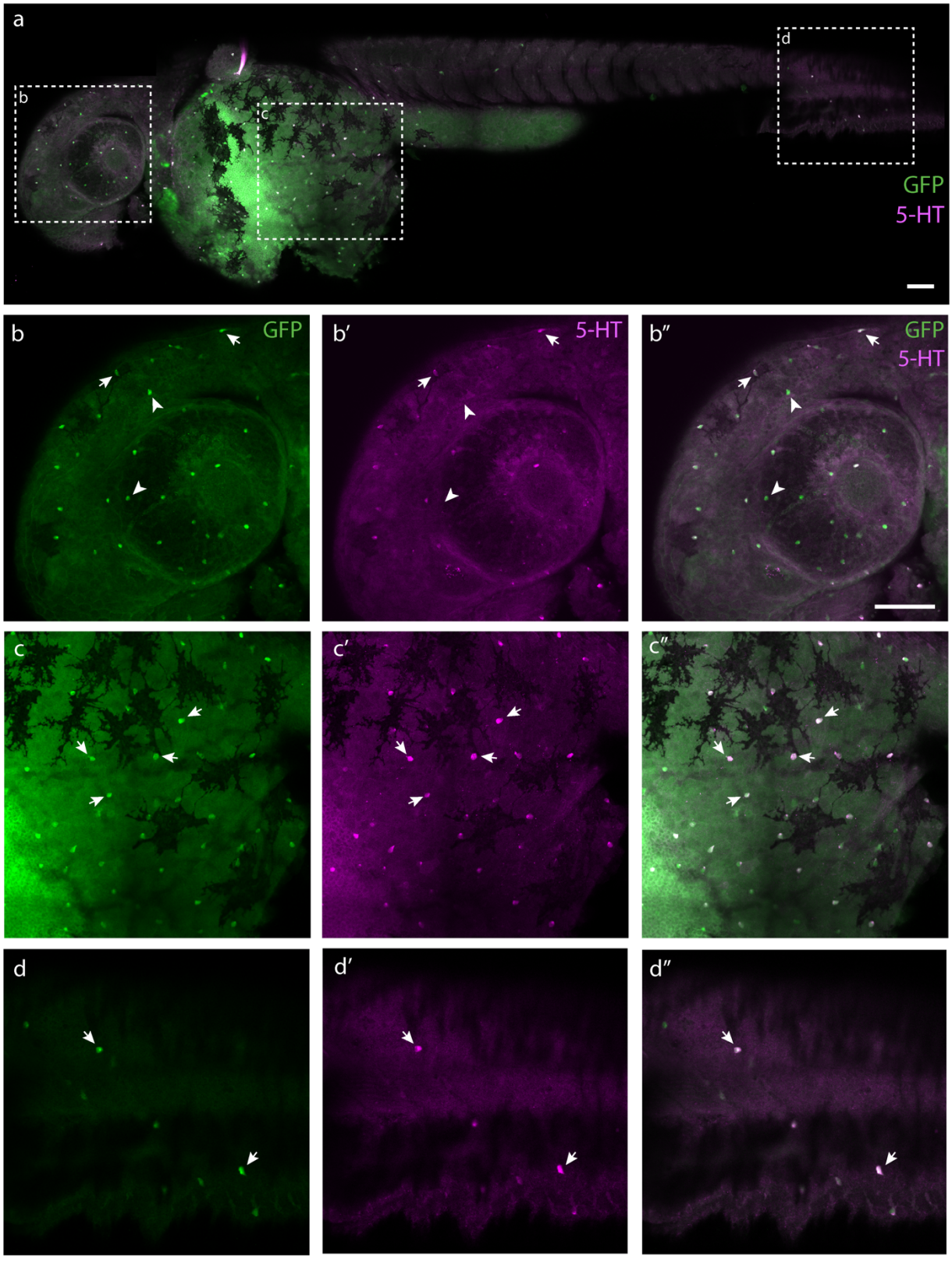
a
b
c
d
GFP
5-HT
b
GFP
b′
5-HT
b″
GFP
5-HT
c
c′
c″
d
d′
d″

Figure 2.2 Neuroepithelial cells (NECs) of the gills in adult *ETvmat2:GFP* were GFP-positive. a Whole-mount gill arch with endogenous GFP expression and anti-5-HT labelling. E, efferent side of filament of hemibranch facing the viewer; A, afferent side of filament of opposite hemibranch; GA, gill arch; GR, gill rakers; Scale bar = 200 μm. **b** A single gill filament with endogenous GFP and NECs stained with anti-5-HT (b'), anti-SV2 (b'') and these panels merged (b'''). Arrows point to stGFP-positive cells colabelled with 5-HT and SV2; double arrow shows a stGFP-positive cell negative for 5-HT but positive for SV2; arrowheads show weak GFP-expressing cells absent of 5-HT and SV2 labelling. b'''') Pseudocolour image of the endogenous GFP on a filament to show differential GFP expression over a gradient with a larger number indicating a stronger expression. F, filament; L, lamellae. Scale bar = 100 μm. **c** Distal end of a gill filament where NECs were abundant shows strong GFP cells colabelled with 5-HT (c' and c''). Double arrow shows a stGFP-positive cell negative for 5-HT in the filament. Scale bar = 30 μm.

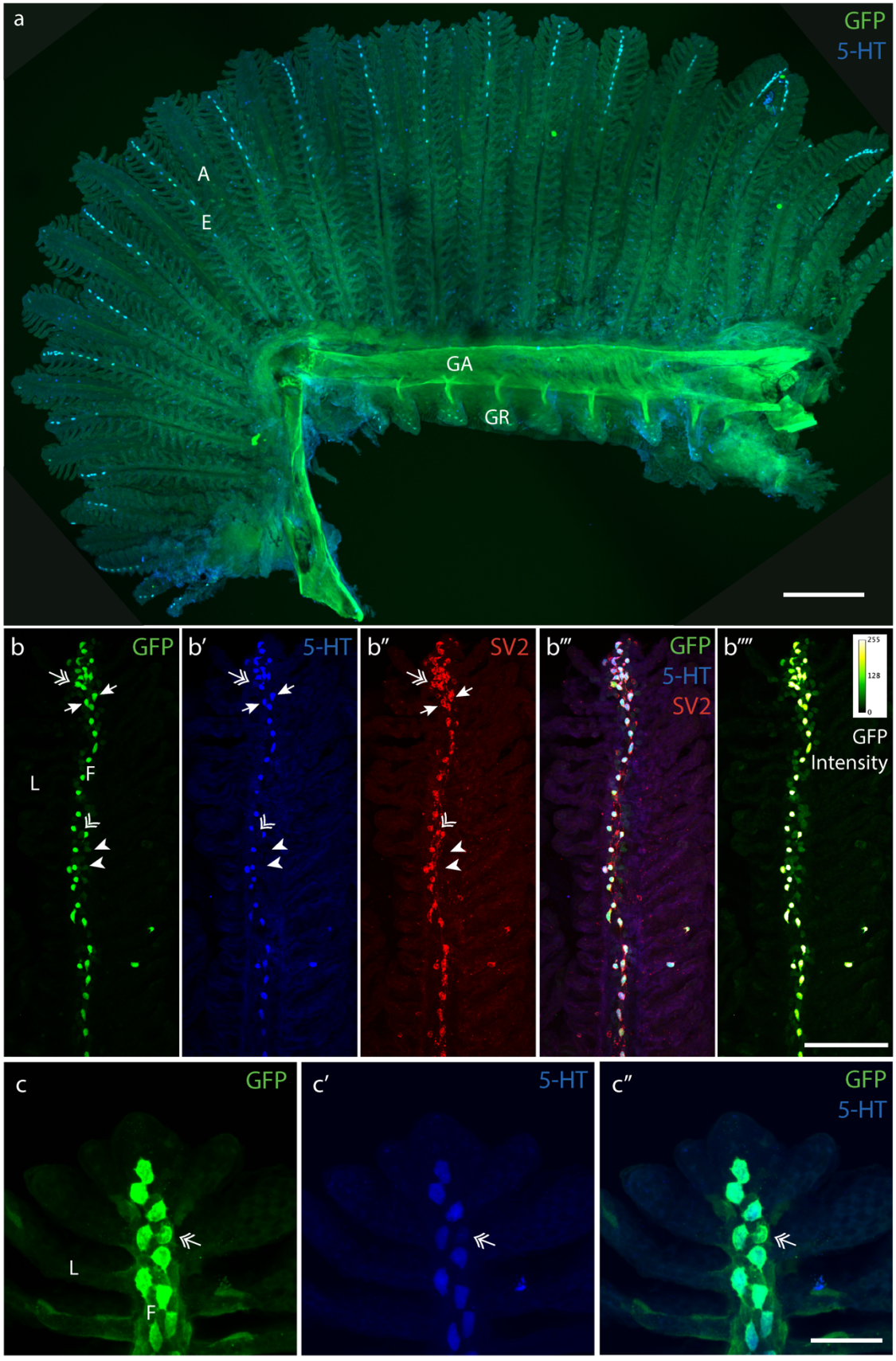
a
GFP
5-HT
A
E
GA
GR
b
GFP
L
F
b′
5-HT
b″
SV2
b‴
GFP
5-HT
SV2
b⁗
255
128
0
GFP
Intensity
c
GFP
L
F
c′
5-HT
c″
GFP
5-HT

Figure 2.3 GFP-positive cells in gill lamellae of *ETvmat2:GFP* fish. a Weak GFP-expressing cells were present throughout secondary gill lamellae. Round lamellar GFP-positive cells were colabelled with 5-HT (arrows, a' and a''). Regions within dashed boxes are enlarged in B. Scale bar = 100 μm. **b** Lamellar GFP-positive cells in A at a higher magnification. Scale bar = 20 μm.

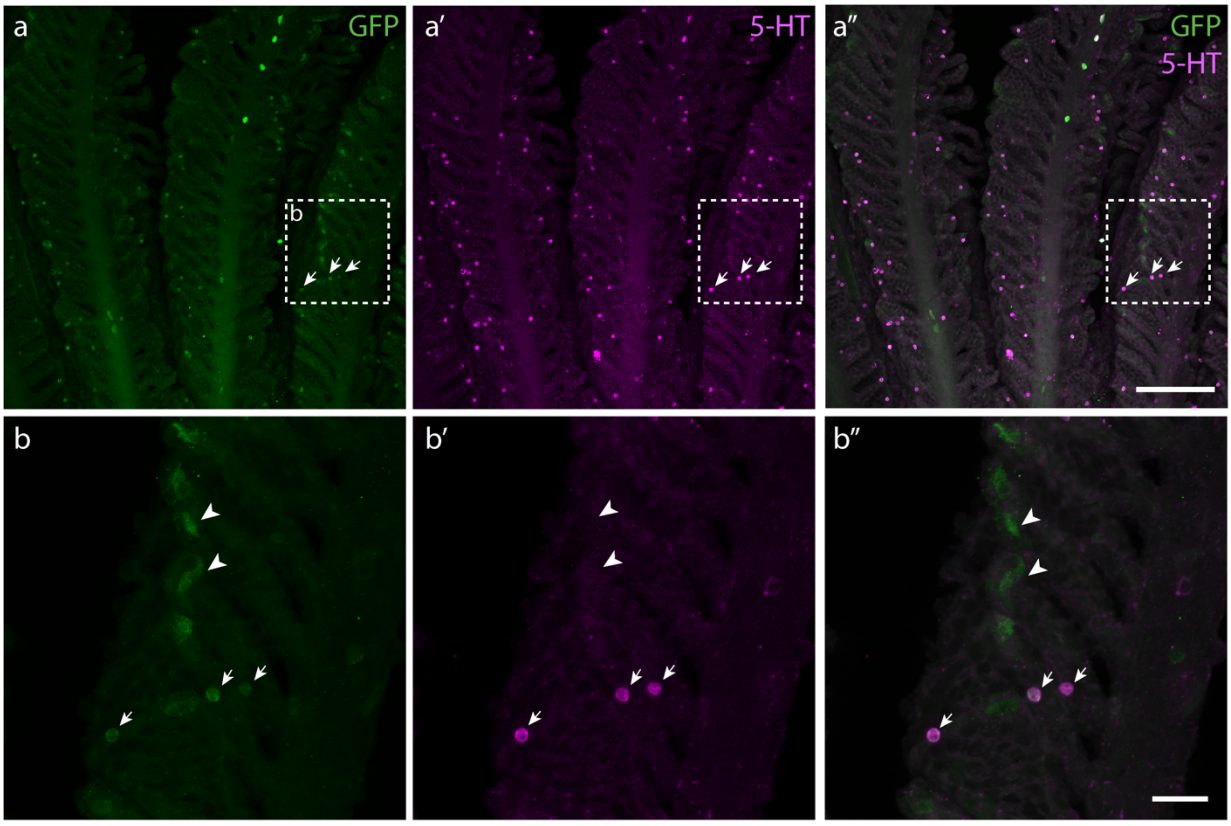
a
GFP
b
a′
5-HT
a″
GFP
5-HT
b
b′
b″

Figure 2.4 Endogenous GFP expression of *ETvmat2:GFP* labelled intrinsic neurons in gill filaments. a Chain neurons present in the filaments showed weak GFP expression and were colabelled with SV2 (arrows, a' and a''). Regions within dashed boxes are enlarged in b. Scale bar = 100 μm. **b** One chain neuron shown at higher magnification. Arrowheads in b' show puncta labelled by SV2. Scale bar = 20 μm.

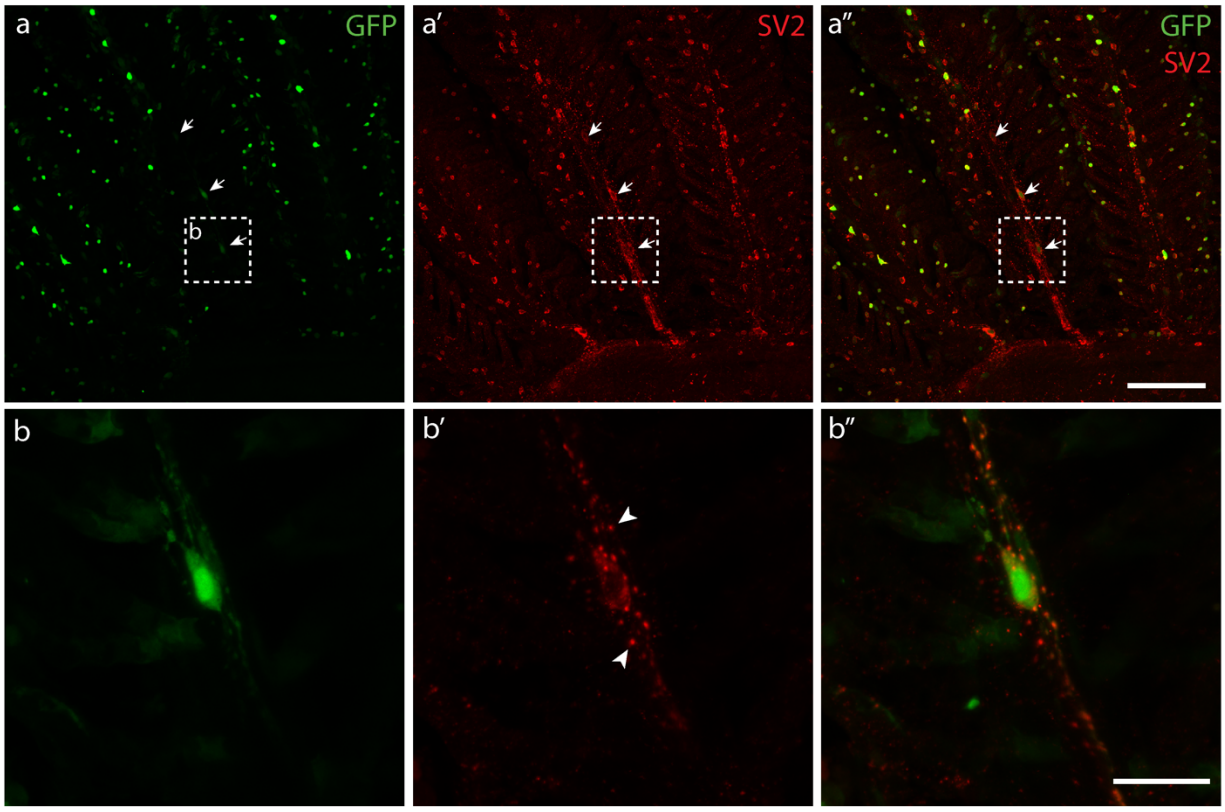
a
GFP
a′
SV2
a″
GFP
SV2
b
b
b′
b″

Figure 2.5 Endogenous GFP expression of *ETvmat2:GFP* labelled neurons in different tissue layers of gill filaments. a A GFP-positive chain neuron (arrowhead, a') was deeper in the filament tissue than a stGFP-positive NEC (arrow), as shown in two single optical sections (a and a'). XZ and YZ represent corresponding cross-sectional planes and yellow lines indicate points of intersection. F, filament; L, lamellae; GA, gill arch. Scale bar = 30 μm. **b** Superficial (arrows) and deep (arrowhead, b') proximal neurons present in different layers near the base of the filament showed weak endogenous GFP expression. Spatial-colour coded merged image (b'') shows the difference of these neurons in spatial orientation along the z-axis. Scale bar = 30 μm.

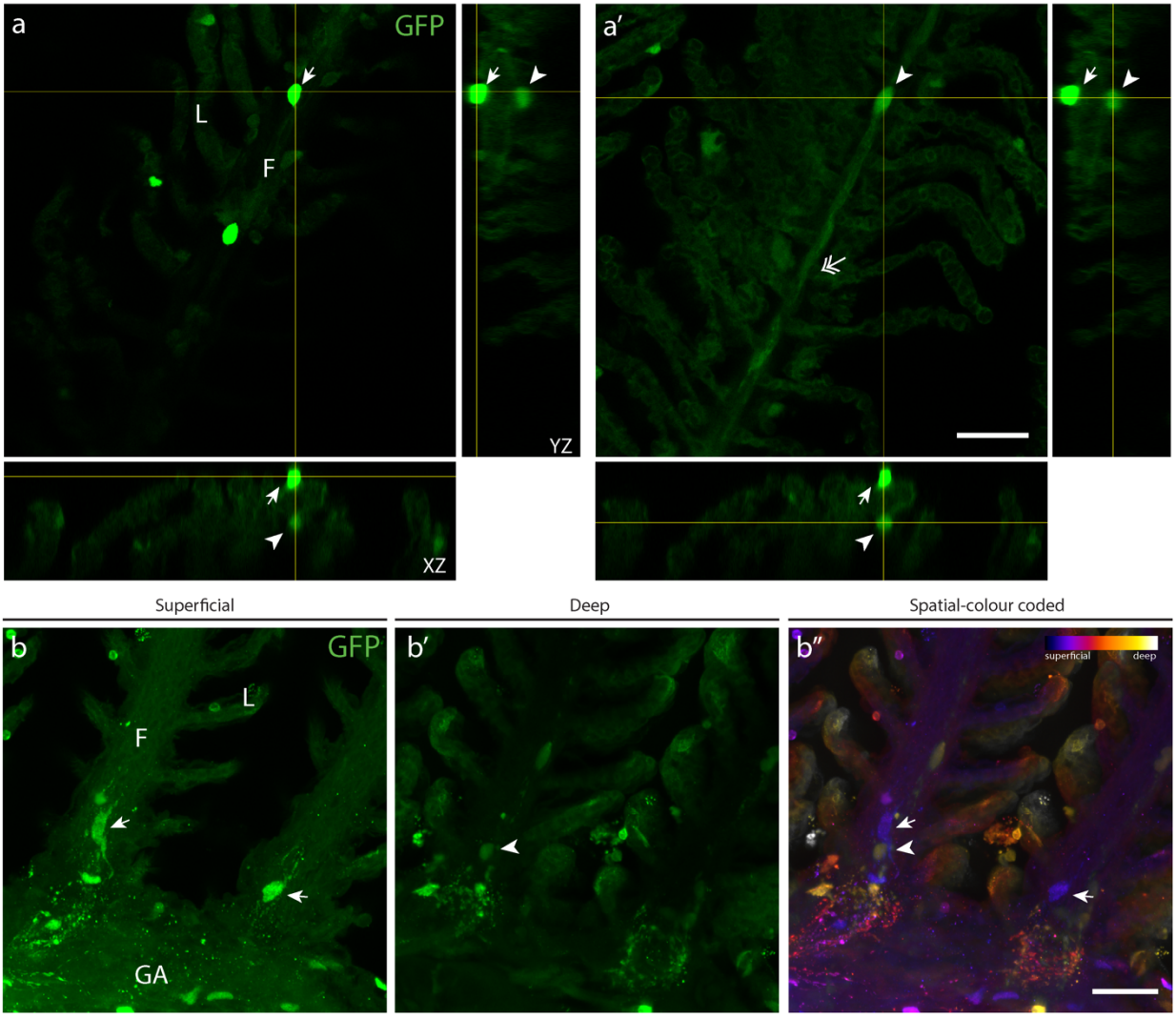
a
GFP
L
F
YZ
XZ
a′
Superficial
Deep
Spatial-colour coded
b
GFP
L
F
GA
b′
b″
superficial
deep

Figure 2.6 Identification of stGFP-positive NECs *in vitro*. a Phase-contrast image of gill cells dissociated from *ETvmat2:GFP* transgenic zebrafish. Arrows indicate stGFP-positive NECs. **b** Image showing GFP fluorescence (green). Scale bar = 50 μm and applies to both panels.

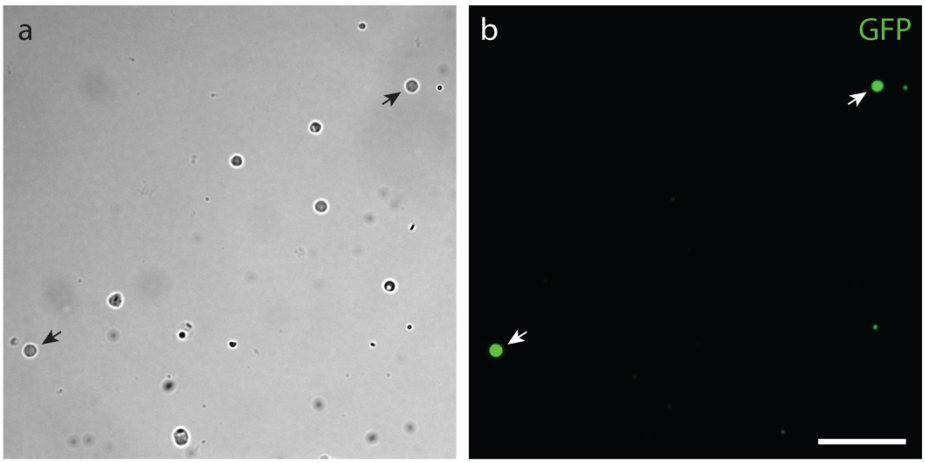
a
b
GFP

Figure 2.7 Representative gating strategy for isolated gill cells from *ETvmat2:GFP* transgenic zebrafish using flow cytometry. a Cells were gated to exclude debris based on forward and side scattering. **b** Doublet discrimination was performed to eliminate aggregates. **c** Unlabeled cells from wild type (WT) to gate the GFP-negative cell population. **d** Cells clustered into three populations based on GFP expression levels in *ETvmat2:GFP* fish in normoxia. **e** Three cell populations separated based on GFP expression in *ETvmat2:GFP* fish in chronic hypoxia.

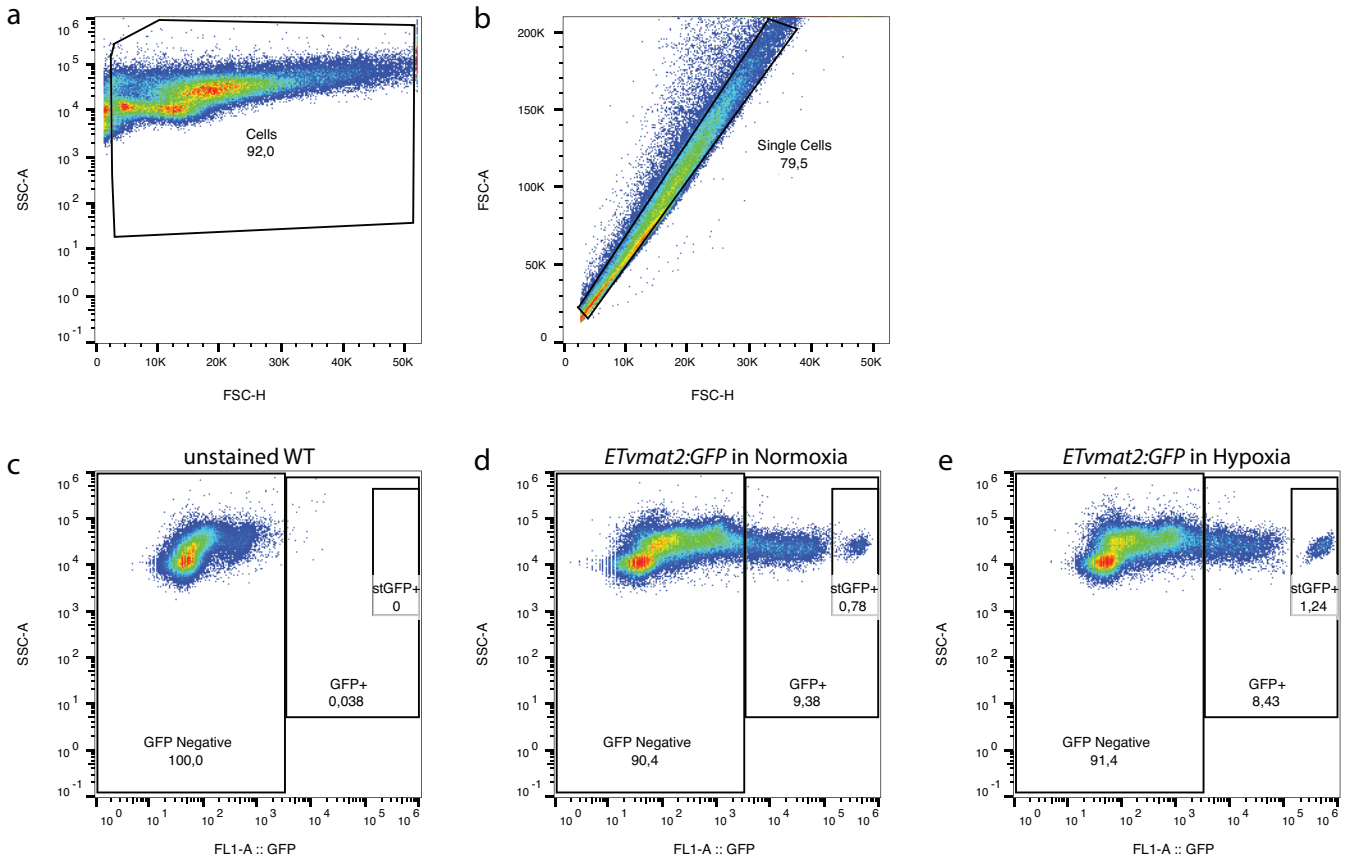
a
SSC-A
FSC-H
Cells
92,0
b
FSC-A
FSC-H
Single Cells
79,5
c
unstained WT
SSC-A
FL1-A :: GFP
stGFP+
0
GFP+
0,038
GFP Negative
100,0
d
ETvmat2:GFP in Normoxia
SSC-A
FL1-A :: GFP
stGFP+
0,78
GFP+
9,38
GFP Negative
90,4
e
ETvmat2:GFP in Hypoxia
SSC-A
FL1-A :: GFP
stGFP+
1,24
GFP+
8,43
GFP Negative
91,4

Figure 2.8 Flow cytometric analysis of stGFP-positive NECs from gills of adult *ETvmat2:GFP* transgenic fish in different O_2 conditions. a, **c** Histograms of stGFP-positive NECs from individual biological *ETvmat2:GFP* fish samples in normoxia (blue) and chronic hypoxia (red) displayed different GFP expression levels (a) and relative cell size distribution (a). **b**, **d** Cumulative cell distributions from three biological replicates shows changes of stGFP-positive NECs in GFP fluorescence intensity (b) and relative cell size (d) from normoxia to chronic hypoxia. The population comparison test verified that, in b, GFP fluorescence intensity in hypoxia was significantly different from normoxia (Chi-squared T(X) score of 97.22); and in d, showed that the difference in relative cell size between hypoxia and normoxia was significant (Chi-squared T(X) score of 25.40).

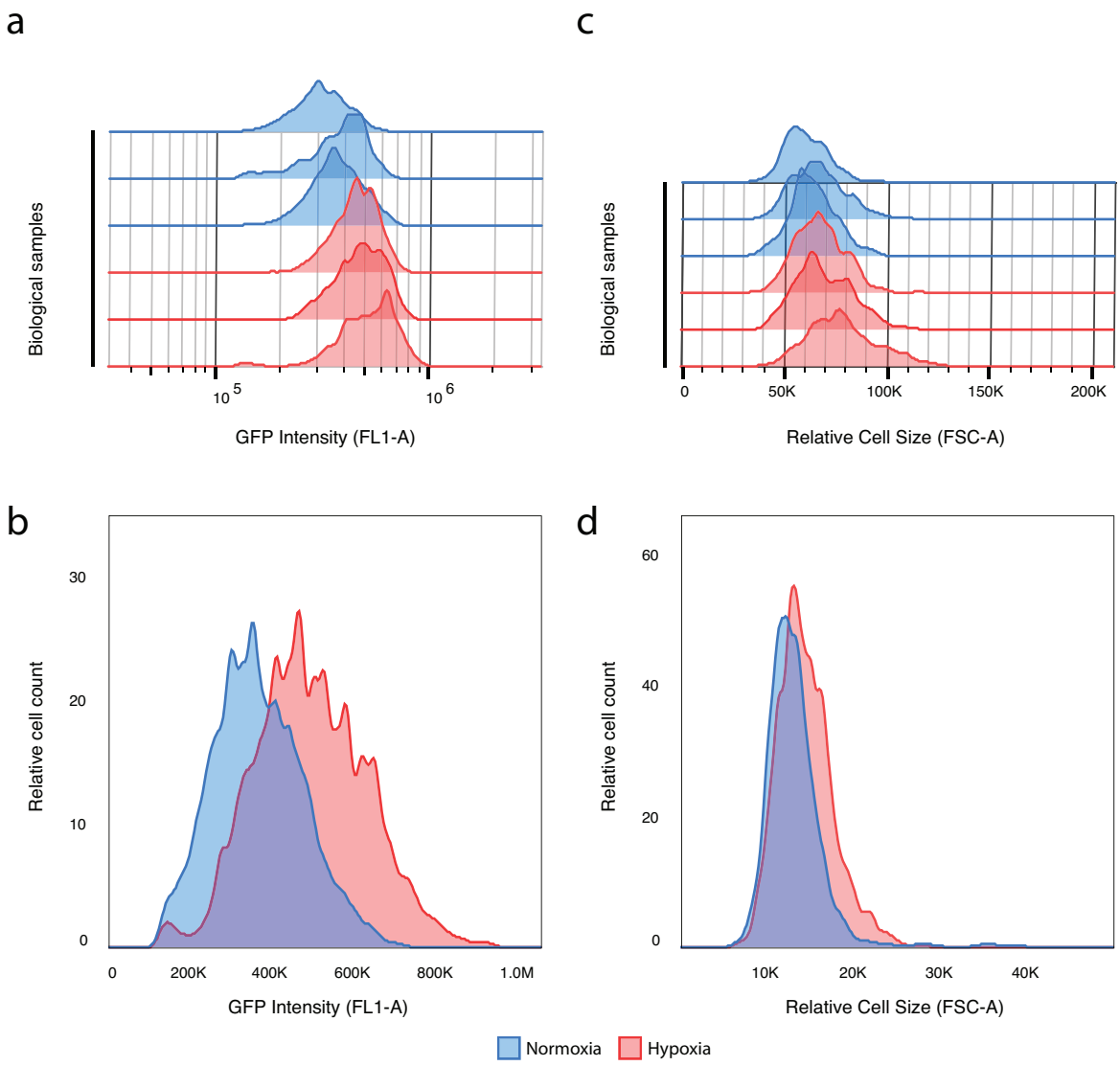
a
Biological samples
10 5
10 6
GFP Intensity (FL1-A)
c
Biological samples
0
50K
100K
150K
200K
Relative Cell Size (FSC-A)
b
Relative cell count
30
20
10
0
0
200K
400K
600K
800K
1.0M
GFP Intensity (FL1-A)
d
Relative cell count
60
40
20
0
10K
20K
30K
40K
Relative Cell Size (FSC-A)
Normoxia
Hypoxia

CHAPTER 3

Purinergic, cholinergic and dopaminergic controls in gills

Excerpted from: Rahbar S, Pan W, Jonz MG (2016) Purinergic and Cholinergic Drugs Mediate Hyperventilation in Zebrafish: Evidence from a Novel Chemical Screen. PLoS One 11:e0154261.

Zachar PC, Pan W, Jonz MG (2017) Distribution and morphology of cholinergic cells in the branchial epithelium of zebrafish (Danio rerio). Cell Tissue Res 367:169–179.

I performed all experiments and analyses presented in this chapter, some of which were published in articles mentioned above.

3.1 Introduction

Oxygen is essential to survival, and many vertebrate species have developed strategies to detect O_2 availability and make corrective changes in ventilation to maintain homeostasis (Perry et al. 2009; Palmer and Clegg 2014). Aquatic fish species are prone to O_2 fluctuation in their environment and respond through cardiorespiratory reflexes and changing systemic vascular resistance when facing hypoxia (Holeton and Randall 1967; Fritsche and Nilsson 1993; Perry et al. 1999). This type of response to hypoxia is dependent on O_2 chemoreception by neuroepithelial cells (NECs) present in the gill epithelium in teleost fish (Jonz et al. 2015). Gill NECs are serotonergic, homologous to type I cells of the carotid body (CB) in mammals, as they share similar mechanisms of chemoreception (Prabhakar 2000; Jonz and Nurse 2003; Jonz et al. 2004; López-Barneo et al. 2008). Much physiological evidence has indicated that NECs respond to hypoxia, through membrane depolarization and a possible release of neurotransmitters (Dunel-Erb et al. 1982; Jonz et al. 2004, 2015). NECs are innervated by nerve fibres and are in close proximity with nerve endings from afferent neurons (Jonz and Nurse 2003). Stimulation by hypoxia was previously shown to trigger vesicular recycling (Jonz et al. 2015); however, evidence regarding specific neurotransmitter release is lacking. In the mammalian carotid body, a number of neurotransmitters or modulators, including acetylcholine (ACh), adenosine-triphosphate (ATP) and dopamine (DA), have been determined to contribute to the chemosensory pathway (Nurse 2005). However in fish, the roles of these neurochemicals are less clear.

The neurotransmitter, ATP, which targets purinergic receptors, was previously shown to be involved in the hypoxic response in zebrafish. In ventilatory behavioural studies of 14 days post-fertilization (d.p.f) larvae, it was observed that suramin, a broad-spectrum P2 receptor

antagonist, decreased ventilation frequency and abolished the hyperventilatory response to hypoxia (Rahbar et al. 2016). PPADS, an antagonist to P2X2/3 receptors, was also found to inhibit the hyperventilatory response to hypoxia in larval zebrafish (Coe et al. 2017). On the other hand, application of ATPγS, a broad-spectrum purinergic P2X/Y agonist, elicited an increase in ventilation (Coe et al. 2017). Together, the evidence is suggestive of purinergic control in the hyperventilatory response in zebrafish. In mammalian CB, P2X2/3 receptors were localized to afferent nerve terminals apposed to type I chemoreceptors, and play an excitatory role in hypoxic signalling (Zhang et al. 2000; Zhang and Nurse 2004). A previous study in zebrafish also localized purinergic P2X3 receptors in a subpopulation of NECs and other cells in the lamellae (Jonz and Nurse 2003). However their presence in O_2 sensitive NECs in the filament and afferent nerve terminals needs to be further examined.

In the mammalian carotid body, ACh was identified as a main excitatory neurotransmitter co-released with ATP in hypoxic signalling (Nurse and Zhang 1999). In fish, the role of ACh was first revealed as Milsom and his colleague showed ACh and nicotine induced strong nerve activity in gills and increased ventilatory rate in rainbow trout (Burleson and Milsom 1995a, b). Later, it was shown that ACh induced hyperventilation in larval zebrafish and hexamethonium, a nicotinic ACh receptors antagonist, inhibited the hyperventilatory response to hypoxia at 12 d.p.f. (Shakarchi et al. 2013). Nicotine increased the ventilation frequency at 7 and 14 d.p.f zebrafish (Jonz et al. 2015), whereas atropine, the cholinergic antagonist, abolished the hypoxic ventilatory response at high concentrations (Rahbar et al. 2016). Results from these studies clearly indicate a role of ACh and cholinergic receptors in mediating the ventilatory response to hypoxia although the sites of ACh release remained uncertain. Cholinergic cells had been found in both larval and adult zebrafish through the presence of the vesicular acetylcholine transporter

(VAChT), which is responsible for loading ACh into secretory vesicles for secretion. These cells appeared to be of a distinct population from the serotonergic NECs (Shakarchi et al. 2013). The identity of these VAChT-positive cells requires further investigations to better understand their potential role in O_2 chemosensory pathways.

In addition to ATP and ACh, type I cells of the carotid body express predominantly dopamine and the synthetic enzyme, tyrosine hydroxylase (TH) (Prabhakar 2000; López-Barneo et al. 2008). DA has been recognized as an inhibitory neuromodulator in the carotid body through its actions on pre- and post-synaptic metabotropic receptors (Nurse 2014). In fish, serotonin (5-hydroxytryptamine, 5-HT) is the main neurotransmitter identified in gill NECs. TH had been localized in isolated serotonergic NECs in gills of channel catfish (Burleson et al. 2006); however, it was absent in gills of goldfish and trout through immunohistochemical labeling (Porteus et al. 2013). Nerve recordings from rainbow trout gills showed that DA induced weak nerve activity but had no effect on the ventilation rate (Burleson and Milsom 1995a, b). Zebrafish during larval stages, however, were sensitive to DA as it reduced the ventilation frequency in behavioural assays (Shakarchi et al. 2013). The above evidence suggests a possible modulating role of DA in ventilation responses in fish, depending on species and developmental stage. Its role in O_2 chemoreception in fish gills remains to be elucidated.

The main objective of the research presented in this chapter was to obtain evidence for the presence of potential purinergic, cholinergic and dopaminergic control mechanisms that may be involved in O_2 sensing in fish gills. Zebrafish present an ideal model organism due to the convenience in husbandry and manipulation, and available zebrafish transgenic lines. Through immunohistochemistry and confocal microscopy, we examined the presence of purinergic P2X3 receptors, and identified cholinergic and dopaminergic cells in zebrafish gills. More specifically,

we used antibodies targeting purinergic P2X3 receptors, VAChT, and choline acetyltransferase (ChAT), the rate-limiting enzyme in ACh production, to identify purinergic and cholinergic cells in wild type zebrafish gills. Lastly, the transgenic zebrafish lines Tg(*dat:tom20 MLS-mCherry*) with specific reporter genes recapitulating the expression of the dopamine active transporters (DAT), transporters responsible for the reuptake of DA from the synaptic cleft, were used to identify dopaminergic expression in the gills. The transgenic zebrafish ET*vmat2:GFP* was also adopted to visualize O_2-sensitive NECs.

3.2 Methods

3.2.1 Animals

Wild-type and transgenic adult zebrafish (*Danio rerio*) were raised to 12 months of age and held in a closed, re-circulated facility at the Laboratory for the Physiology and Genetics of Aquatic Organisms at the University of Ottawa. Larval fish were obtained by breeding from 12-month adult zebrafish and kept in 150 mm Petri dishes containing E3 embryo medium (5 mM NaCl, 0.17 mM KCl, 0.33 mM $CaCl_2 2H_2O$, 0.33 mM $MgSO_4 7H_2O$ and 0.3 mg l^{-1} of methylene blue at pH 7.8) for 5 days. At 5 d.p.f, larval fish were transferred to a small tank with 0.3 mg l^{-1} of methylene blue-treated system water until 16 d.p.f or adulthood. All fish were maintained at 28°C on a 14-10h light-dark cycle (Westerfield 2007). Animals were handled according to the institutional guidelines and protocol BL-1760, along with guidelines from Canadian Council on Animal Care (CCAC). For tissue harvest, adult zebrafish were euthanized by a blow to the head and decapitated. Larvae were euthanized by hypothermic shock via immersion in an ice bath for 20 min.

3.2.2 Immunohistochemistry and confocal microscopy

Techniques for tissue extraction and immunolabelling of adult gills were modified from those previously described by Jonz and Nurse (2003). Following decapitation, whole gill baskets were quickly removed from adult zebrafish heads by dissection in ice-cold phosphate-buffered solution (PBS) containing (mM): NaCl 137, Na_2HPO_4 15.2, KCl 2.7, and KH_2PO_4 1.5; pH 7.8 (Bradford et al. 1994). Gill tissues were rinsed in cold PBS to remove excessive mucous before overnight fixation in 4% paraformaldehyde in PBS at 4°C. Then tissues were rinsed in fresh PBS three times at 3 min before permeabilization in PBS-TX solution (2% Triton X-100 in PBS, pH 7.8) for 24 h at 4°C. After three more rinses in fresh PBS, tissues were separated into individual gill arches and treated with subsequent antisera. Whole larvae were fixed and permeabilized the same way without dissection.

For purinergic P2X3 receptor detection and co-labelling with 5-HT, fixed larval fish were placed in a solution containing polyclonal guinea pig anti-P2X3 diluted to 1:400-1:1000 (cat. no. GP10108; Neuromics, Edina, MN, USA; Antibody ID: AB_2283325) and polyclonal rabbit anti-5-HT at a dilution of 1:250 (cat. no. S5545, Sigma-Aldrich; Antibody ID: AB_477522) for 24 h at 4°C. The primary antibody solution was diluted in 0.5% Triton X-100 with PBS. Then tissue was rinsed three times with PBS and treated with secondary antibodies for 1-2 h at room temperature in the dark. The secondary antibody solution contained anti-rabbit fluorescein isothiocyanate (FITC, cat no. 111-095-003, Jackson Immuno Research Laboratories, West Grove, PA, USA) at a dilution of 1:50 and anti-guinea pig Alexa 594 (cat. no. A11076, Invitrogen) at a dilution of 1:400 in PBS. After three more rinses in PBS, gill complexes from larval fish tissue were removed and mounted on the glass slides for observation.

To identify cholinergic cells, adult gill tissue was treated with polyclonal guinea pig anti-VAChT antibody (1:50, cat. no. AB1588; EMD Millipore, Billerica, MA, USA) diluted in 0.5% PBS-TX for 24 h at 4°C. After three rinses in PBS, tissue was immersed in goat anti-guinea pig FITC secondary antibody (Molecular Probes) for 1 h at room temperature. Tissue was rinsed again and stained with nuclear dye, 4',6-diamidino-2-phenylindole (DAPI) before mounting onto glass slides. In addition, VAChT-positive cells were co-labeled with antibody targeting choline acetyltransferase (ChAT) to verify the site of ACh production. Prior to antibody binding, antigen retrieval and blocking were performed. Tissue was placed in buffer solution (10 mM sodium citrate and 0.05% tween 20, pH of 6.0) and incubated at 98°C for 10 min. After a thorough rinse in PBS, tissue was treated with 5% fetal bovine serum (cat. no. 10437-077; Invitrogen) for 2 h at room temperature. Then tissue was rinsed three times with PBS and incubated in goat anti-ChAT (cat. no. AB144P; EMD Millipore) at a dilution of 1:50 for 5 days at 4°C. It was subsequently treated with chicken anti-goat Alexa 594 secondary antibody (cat. no. A-21468; Invitrogen) at a dilution of 1:200 for 1 h at room temperature and mounted onto glass slides.

Transgenic zebrafish line Tg(*dat:tom20 MLS-mCherry*) acquired from the Laboratory for the Physiology and Genetics of Aquatic Organisms at the University of Ottawa was used to identify dopaminergic expression. To determine the distribution of dopaminergic expression relative to serotonergic NECs, adult homozygous Tg(*dat:tom20 MLS-mCherry*) fish was cross-bred with adult homozygous ET*vmat2:GFP* fish to generate double transgenic offspring containing both mCherry and GFP reporter genes. Double transgenic fish were raised to 3 months before harvesting for gill tissue. The transgenic line Tg(*dat:tom20 MLS-mCherry*) was generated using the regulatory elements of the dat gene to target a reporter, mCherry, after fusion with the mitochondrial localizing signal (MLS) of Tom20, to report dopaminergic expressing

cells with reporter genes confined to mitochondria (Noble et al. 2015). The reporter gene mCherry was proven to localize to mitochondria of dopaminergic neurons in the brain (Noble et al. 2015). GFP from ET*vmat2:GFP* was shown to label cells expressing vesicular monoamine transporter 2 (vmat2) and had been localized to the brain and gills (Wen et al. 2008; Pan et al. 2021a). In particular, O_2-sensitive NECs in the filaments were labeled with abundant GFP, termed strong expressing GFP (Pan et al. 2021a). Double transgenic fish containing both endogenous mCherry and GFP were euthanized and processed as described above. Then complete gill arches were mounted onto a microscopic slide without additional staining.

Mounted specimens were observed using an upright microscope platform (FN1, Nikon) with a Nikon Apo 25× water immersion objective lens, motorized XYZ control and a confocal scanning system (A1RsiMP, Nikon). Images were viewed and captured using the imaging software, NIS Elements (Nikon). Each specimen was scanned in optical sections that were 0.5-1.5 μm apart for up to 40 sections per z-stack. Images of multiple optical sections were presented in composite projections. Image processing was performed using open source software, Fiji (Schindelin et al. 2012) and Illustrator CS 6 (Adobe). Labelling by mCherry (red) in Tg(*dat:tom20 MLS-mCherry*) was changed to magenta to optimize contrast.

3.3 Results

3.3.1 P2X3 receptor distribution in larval gills

Immunohistochemistry localized purinergic P2X3 receptors in the gills of 16 d.p.f larval zebrafish. In 21 specimens, P2X3-immunoreactive cells were found throughout the gill complex. As in Figure 3.1A in ventral view, P2X3-positive cells were found on all four gill arches (I-IV). They were slightly larger in size, compared with serotonergic Merkel-like cells (arrows, Figure

3.1B) in the gill arch and NECs (arrowheads, Figure 3.1B) in the filament primordia. The colocalization of P2X3 and 5-HT was not clearly observable in the ventral view of the whole gill complex (Figure 3.1A-C); however, it could be seen in separated gill arches observed at a higher magnification (Figure 3.1D-I). In individual gill arches, P2X3 receptors were found in 5-HT-positive NECs (arrows) of the filament primordia, 5-HT-positive neurons (double arrow) in the arch, and nerve bundles in the arch and filament (Figure 3.1D-F). In addition, P2X3-immunoreactive cells negative for 5-HT (arrowhead, Figure 3.1D) were also present in the filament primordia, and some 5-HT-positive NECs (arrow, Figure 3.1G) were immunoreactive to P2X3 while others (arrowheads, Figure 3.1H) were negative.

3.3.2 Colocalization of vesicular acetylcholine transporter (VAChT) and choline acetyltransferase (ChAT) in adult gills

In adult zebrafish gills, cholinergic cells were identified based on their immunoreactivity to antibodies against VAChT. Cells positive for VAChT were present in the filament and some areas of lamellae (arrows, Figure 3.2a). The VAChT staining revealed cells of peculiar shape, with some extended processes. Colocalization of VAChT and the nuclear stain, 4',6-diamidino-2-phenylindole (DAPI), confirmed that VAChT labeled individual cells with single nuclei and the labeling was confined to the cytoplasm (Figure 3.2b,c).

To verify the cholinergic properties of cells labeled by antibodies against VAChT, we co-labeled cells with antibodies against ChAT. Cells immunoreactive to VAChT were also positive for ChAT (arrows, Figure 3.3a-c) in the filament. Most ChAT labeling appeared to be in the cytoplasm and generated a slightly different staining pattern than VAChT, the latter of which would be confined to vesicular membranes. In addition, another population of ChAT-positive

cells in the lamellae were found negative for VAChT (arrowhead, Figure 3.3b,c). These cells were greater in size and different in morphology than VAChT-positive cells.

3.3.3 Localization of dopamine transporters (DAT) in adult gills

Dopamine expression was visualized in gills of double transgenic zebrafish expressing both GFP under the control of *vmat2* in *ETvmat2:GFP* and mCherry under the control of *dat/slc6a3* in Tg(*dat:tom20 MLS-mCherry*). Owing to the construct design, the reporter gene mCherry in Tg(*dat:tom20 MLS-mCherry*) was localized to mitochondria and thus generated a granular labelling pattern which only partly labelled cells or nerve fibres. It could be seen in Figure 3.4A,B that expression of DAT, indicated by mCherry (magenta), was found predominantly along the midline and concentrated at the distal ends of efferent filaments, within which serotonergic NECs (arrows, Figure 3.4A,C) of the filament were located. In particular, prominent expression of DAT led to labelling of a nerve plexus located at the outer margins of the filament and lamellar junctions (arrowheads, Figure 3.4B). At low magnification, it appeared that VMAT2-positive NECs overlapped with DAT labelling in the filament (Figure 3.4A). However, at higher magnification, in the mid region of the filament, it was observed that DAT labelled what appeared to be bundles of nerve fibres at the midline (arrowheads, Figure 3.4D,E), in close proximity to filamental NECs (arrows, Figure 3.4D,F) and chain neuron (ChN, Figure 3.4F), but did not overlap. This feature was also observed when rotating the optical sections 45° and 90° (Figure 3.4G). In addition, DAT was found in parts of nerve fibres, some of which were VMAT2-positive, at interlamellar regions (arrowheads, Figure 3.4E), and the labelling of DAT resembled synapses. In a transverse view of the mid region of the filament, where images were rotated 90° along the long axis of the filament, the DAT expression at the filament midline and

interlamellar regions formed a network that wrapped around the efferent filamental artery (eFA), forming close associations with NECs of the filament and chain neurons (Figure 3.4G-I).

3.4 Discussion

In the present study, we investigated purinergic, cholinergic and dopaminergic pathways that may be involved in control of hypoxic responses by localizing relevant receptors or transporters. Purinergic P2X3 receptors were found on various cells in the filament and arch of larval fish gill. We also identified acetylcholine-producing cholinergic cells in the gills of adult zebrafish using antibodies against VAChT and ChAT. Lastly, dopaminergic nerve fibres were identified in adult gills based on their expression of reporter genes, mCherry, in transgenic zebrafish Tg(*dat:tom20 MLS-mCherry*). The current study has offered new details of the distribution of these receptors and transporters in zebrafish gills and furthered our understanding of the neurochemistry of O_2 sensing.

3.4.1 Purinergic P2X3 receptors in gills

Studies on ventilation behaviours have suggested a role of ATP as a potential neurotransmitter acting on P2X3 or other purinergic receptors in O_2 sensing in zebrafish gill (Rahbar et al. 2016; Coe et al. 2017). Antagonists for P2 and P2X2/3 receptors abolished the hyperventilatory response induced by hypoxia, whereas a broad-spectrum purinergic receptor agonist elicited a hyperventilatory response, suggesting that perhaps the release of ATP is the initiation of a hypoxic response. In the current study, we identified purinergic P2X3 receptors in gills of 16 d.p.f larval zebrafish. Abundant in the gill complex, P2X3 receptors labeled a few populations of cells. P2X3 receptors were found on some serotonergic NECs in the filament

primordia, which implicates a possible autocrine pathway to allow the potentiation of ATP release. This type of feedback mechanism has been observed in P2X receptors in taste receptor cells (Finger and Kinnamon 2013) and P2X3 receptors were found in rat carotid body type I cells following chronic hypoxia (He et al. 2006). P2X3 receptor expression found in other non-serotonergic cells in the gill may indicate a paracrine pathway in which NECs modulate chemosensory signal transmission. In the mammalian carotid body, such paracrine signalling has been observed and it was suggested that P2Y2-expressing glial-like cells may help boost the ATP signal by inducing more ATP release through opening of pannexin-1 channels (Nurse 2014).

In addition to cells in the filament, P2X3 receptors were also found in serotonergic neurons and nerve bundles in the larval gill arch. Serotonergic neurons were previously identified in the proximal filament of adult gills and they innervate chemoreceptive NECs in the filaments (Jonz and Nurse 2003; Pan et al. 2021a). In developing larvae, serotonergic neurons were observed in the gill arch and appeared to migrate to the filament base as gills matured (Jonz and Nurse 2005). The above findings suggest that serotonergic neurons in gill arches of developing larvae positive for P2X3 receptors could be innervating NECs and presented a possible afferent pathway which initiates the hyperventilatory reflex during hypoxic stimulation. In addition, P2X3-positive nerve bundles in the gill arch showed a labeling pattern consistent with previously observed innervation in developing zebrafish (Jonz and Nurse 2005).

3.4.2 Cholinergic cells in the gills produce and store ACh

The current study localized cholinergic cells in adult zebrafish gills through immunohistochemistry with antibodies targeting VAChT. Cells labeled by antibodies against

VAChT had a peculiar shape that were highly eccentric and smaller when compared with 5-HT-positive NECs (Zachar et al. 2017b). It was suggested that this labeling localized transporter vesicles, indicating sites of neurosecretion (Zachar et al. 2017b). This was supported with DAPI co-labeling in the present study, where VAChT labeling was found absent in the nuclear region labeled by DAPI. In addition, VAChT-positive cells were also found to be closely opposed to zn-12-immunoreactive nerve fibres, further suggesting that VAChT labeling may indicate sites of ACh storage and neurosecretion (Zachar et al. 2017b). This labeling pattern was not unique to VAChT, and had been observed with SV2 immunoreactivity in NECs, where synaptic vesicles were labeled, in zebrafish gills (Jonz and Nurse 2003).

In addition to storing ACh, colocalization of VAChT and the catalytic enzyme responsible for ACh synthesis, ChAT, revealed that these cholinergic cells also produce ACh. The labelling generated by antibodies against ChAT showed similar patterns but did not overlap completely with VAChT labelling, implicating a separation between production and storage sites. Moreover, a few VAChT-negative lamellar cells of different morphology were labeled with ChAT, possibly indicating anther population capable of ACh production. Overall, our observations showed that VAChT-positive cholinergic cells in the gills were neurosecretory cells that synthesize and store ACh.

3.4.3 Dopaminergic cells and innervation in the gills

Dopaminergic expression in fish gills are not well understood. Burleson and colleagues previously colocalized TH with 5-HT in chemoreceptive NECs *in vitro* in channel catfish (2006). By contrast, immunolabeling for TH failed to localize with NECs of trout and goldfish (Porteus et al. 2013). Through reporter gene expression in transgenic line Tg(*dat:tom20 MLS-mCherry*),

the present study localized dopaminergic innervation in zebrafish gills for the first time. Dopaminergic innervation, indicated by the expression of DAT through mCherry, was distributed throughout the gill filament, making contacts with multiple structures and cell populations. This diverse distribution of dopaminergic fibres could suggest that DA may be involved in multiple systems in the gill. DAT expression was abundant in the distal filaments and labelled nerve fibres that closely apposed NECs and chain neurons in the midline of the filament, indicating sites of synaptic transmission, where DA could affect sensory transduction. In addition, DAT expression labelled nerve fibres at interlamellar regions. The zebrafish gill with double transgenic markers revealed that DAT expression at the base of the lamellae colocalized with VMAT2 from *ETvmat2:GFP*. VMAT2 is a vesicular transporter that facilitates the uptake of monoamines, including DA; it is thus expected in dopaminergic cells or nerve fibres. This colocalization provided additional verification that synapses labelled by DAT at the interlamellar regions were dopaminergic. Moreover, the transverse view of confocal images showed that dopaminergic nerve fibres surrounded the filamental vasculature. Dopaminergic receptors have been localized in pulmonary vasculature in mammals and were suggested to have vasodilatory effects (Tanaka et al. 1990; Kobayashi et al. 1995). The specific role of DA in fish gill vasculature is not known but our results implicated a possible control of vascular activity.

3.4.4 Neurochemistry of O_2 sensing

The mechanism underlying O_2 sensing in fish gills is not completely understood. Putative O_2 chemoreceptive NECs were known to contain 5-HT; however, to date no direct evidence is available to demonstrate a hypoxia-stimulated neurotransmitter release. Ventilation studies revealed that hyperventilatory responses to hypoxia could be regulated by metabotropic 5-HT_2

and ionotropic 5-HT_3 receptors in zebrafish (Shakarchi et al. 2013; Jonz et al. 2015). In rainbow trout, 5-HT was also shown to induce a hyperventilatory response and gill nerve discharges; however, the effect was minor (Burleson and Milsom 1995a, b). In addition to 5-HT, the present study provided evidence to indicate the presence of neurotransmitters ATP, ACh and DA in zebrafish gills, and provided insights to their roles in O_2 sensing. Previously, purinergic P2X2/3 receptors were shown to facilitate hyperventilatory response to hypoxia in larval zebrafish (Rahbar et al. 2016; Coe et al. 2017). Our results showing the presence of P2X3 receptors in larval gills supports the excitatory role of ATP and suggest modulation through autocrine and paracrine mechanisms. Similarly, ACh receptors were shown to cause ventilation increases in larval zebrafish (Shakarchi et al. 2013; Rahbar et al. 2016). While in trout, ACh was found to produce pronounced nerve discharge and ventilatory responses to hypoxia (Burleson and Milsom 1995a, b). Cholinergic cells were found to be a separate population from serotonergic NECs which produce and store ACh. Their proximity to NECs and filamental arteries is suggestive of multiple functional roles. Cholinergic cells could be primary O_2 chemoreceptors aside from NECs and use ACh as the excitatory neurotransmitter to transmit hypoxic signals. On the other hand, cholinergic cells could play a secondary role and modulate the response of NECs to hypoxia via paracrine control. In addition, dopaminergic cells presented a distinct neuronal population that transports DA. Their close contact with NECs is also suggestive of a modulating role in the hypoxic response of NECs. Activation of dopaminergic receptors was previously shown to reduce ventilation (Shakarchi et al. 2013) so it is possible that dopaminergic nerve fibres surrounding NECs release DA to inhibit hypoxic signals. The present study suggested that multiple cell populations may be involved in the regulation of hypoxic signals. The interplay of these neurochemicals determines the output signal.

3.5 Conclusion

The present study investigated purinergic, cholinergic and dopaminergic control in O_2 sensing in zebrafish gills. For the first time, dopaminergic distribution was defined in fish gills. The study also characterized purinergic P2X3 receptors in larval zebrafish gills and ChAT-positive cholinergic cells in adult zebrafish gills, and their positions relative to serotonergic NECs. The study provided evidence for the presence of ATP, ACh and DA as neurotransmitters or modulators implicated in O_2 sensing.

Figure 3.1 Immunohistochemical localization of P2X3 receptors in larval zebrafish gill of 16 days post-fertilization (d.p.f). Co-labeling of antibodies against P2X3 receptors (red) and 5-HT (green) is shown at the whole gill complex in the ventral view (A-C) and at a higher magnification in an isolated gill arch (D-F) and protruding filament primordia (G-I). (A) P2X3-positive cells were found throughout four gill arches I-IV. (B) 5-HT immunoreactivity labeled serotonergic neuroepithelial cells (NECs, arrowheads) in the filament and Merkel-like cells in the gill arch (arrows). (C) Merge panel of A and B. (D-F) 5-HT-positive neuron (double arrow) in the gill arch (GA) was shown to be P2X3-immunoreactive along with cells in the filament primordia (F), including 5-HT-positive NECs (arrows) and 5-HT-negative cell (arrowhead). Panel F was a merge of D and E. (G-I) In protruding filament primordia (F), P2X3-immunoreactivity was shown in some 5-HT-positive NECs (arrow) but absent in others (arrowheads). Panel I was a merge of G and H. Scale bar in A = 50 μm, in D,G = 10 μm. Excerpted from: Rahbar S, Pan W, Jonz MG (2016) Purinergic and Cholinergic Drugs Mediate Hyperventilation in Zebrafish: Evidence from a Novel Chemical Screen. PLoS One 11:e0154261.

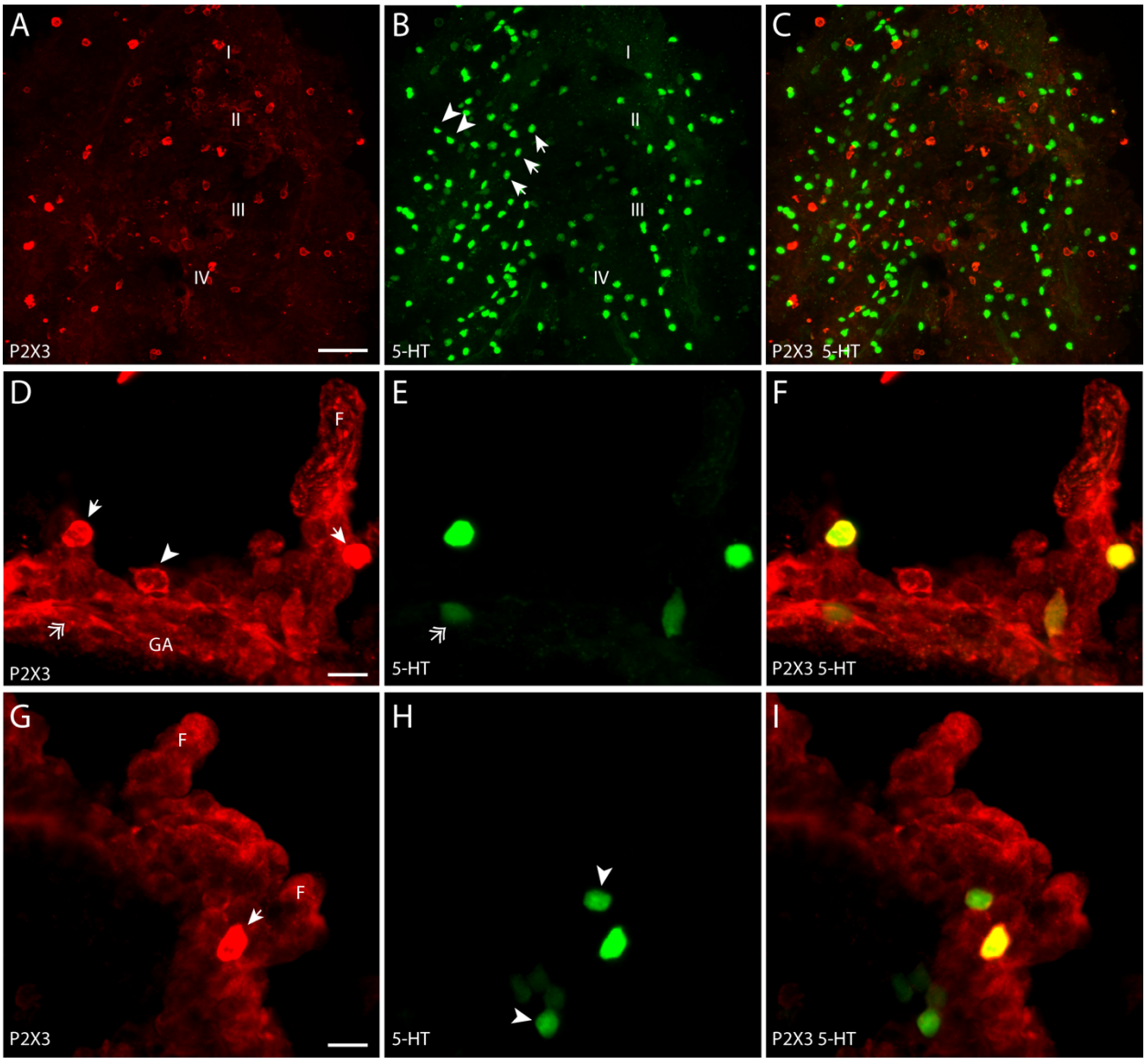
A
I
II
III
IV
P2X3
B
I
II
III
IV
5-HT
C
P2X3 5-HT
D
F
GA
P2X3
E
5-HT
F
P2X3 5-HT
G
F
F
P2X3
H
5-HT
I
P2X3 5-HT

Figure 3.2 Colocalization of vesicular acetylcholine transporter (VAChT) and the nuclear stain, 4′,6-diamidino-2-phenylindole (DAPI) in gills of adult zebrafish. (a) Cells positive for VAChT-immunoreactivity (green, indicated by arrows) were found in the filament (F) and lamellae (L). (b) These cells showed clear nuclear stain (blue, indicated by arrows). (c) Merged panel showed that area in the cell absent of VAChT labeling was filled with nuclear stain. Scale bar in a = 20 μm. Excerpted from: Zachar PC, Pan W, Jonz MG (2017) Distribution and morphology of cholinergic cells in the branchial epithelium of zebrafish (Danio rerio). Cell Tissue Res 367:169–179.

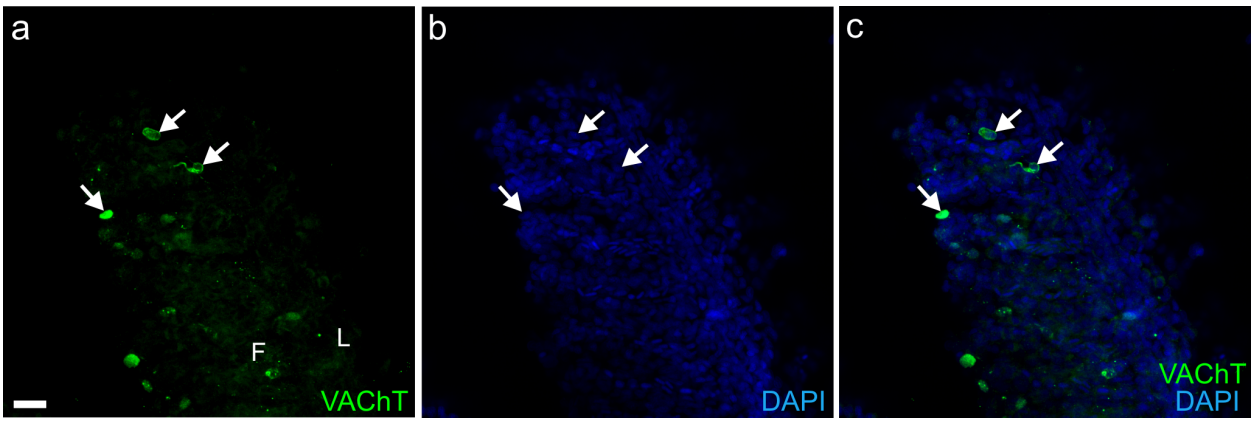
a
F
L
VAChT
b
DAPI
c
VAChT
DAPI

Figure 3.3 Colocalization of vesicular acetylcholine transporter (VAChT) and choline acetyltransferase (ChAT). (a) Antibodies against VAChT labeled VAChT-positive cells (green, arrows) at the distal end of the filament (F). L indicates lamellae (b) VAChT-positive cells were immunoreactive to ChAT (red, arrows) although some ChAT-positive cells were not VAChT-positive (arrowhead). (c) Merged panel showed that VAChT-positive cells colocalized with ChAT-positive cells but their labeling patterns only partly overlapped. Scale bar in a = 20 μm. Excerpted from: Zachar PC, Pan W, Jonz MG (2017) Distribution and morphology of cholinergic cells in the branchial epithelium of zebrafish (Danio rerio). Cell Tissue Res 367:169–179.

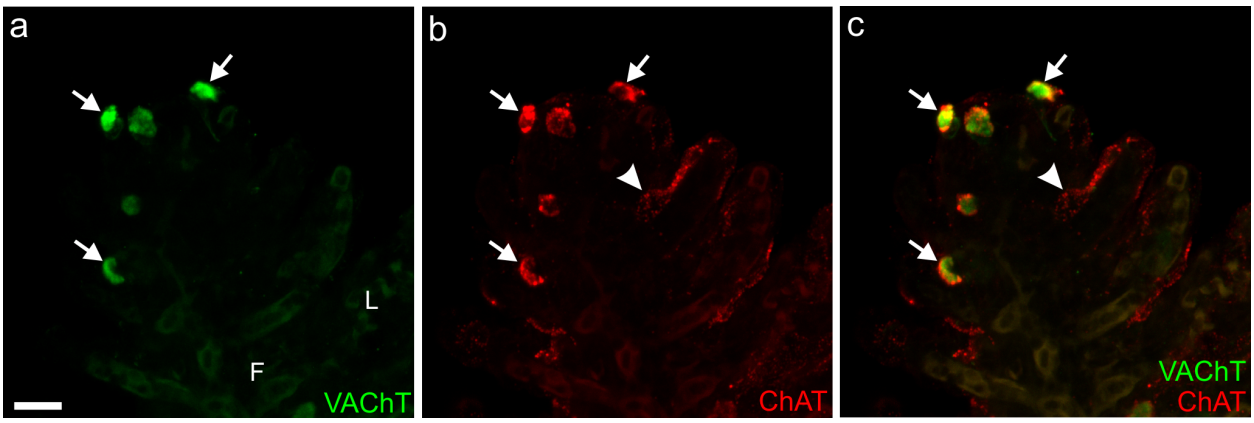
a
L
F
VAChT
b
ChAT
c
VAChT
ChAT

Figure 3.4 Localization of dopamine transporters (DAT) and vesicular monoamine transporters (VMAT2) in distal filaments. Endogenous reporter gene expression of Tg(*dat:tom20 MLS-mCherry*) and *ETvmat2:GFP* each indicating DAT and VMAT2 respectively was shown at low magnification (A-C) and higher magnification (D-I) in double transgenic zebrafish gill. (A) Merge panel showed that most of VMAT2 and DAT expression was present in the midline of the filament. Arrows point to neuroepithelial cells (NECs) in the filament and lamellae. Arrowheads indicate DAT expression. F, filament; L, lamella. (B) DAT expression only. (C) VMAT2 expression only. (D-F) At higher magnification, it was shown that VMAT2-positive NECs (arrows) and chain neuron (ChN) did not overlap with DAT-positive nerve fibres (arrowheads). (G-I) A rotation of the confocal image 45° and 90° along the long axis of the filament showed DAT-positive fibres were distributed around NECs and ChN, and formed nerve plexuses around the efferent filamental artery (eFA). Scale bar in A and D = 10 μm.

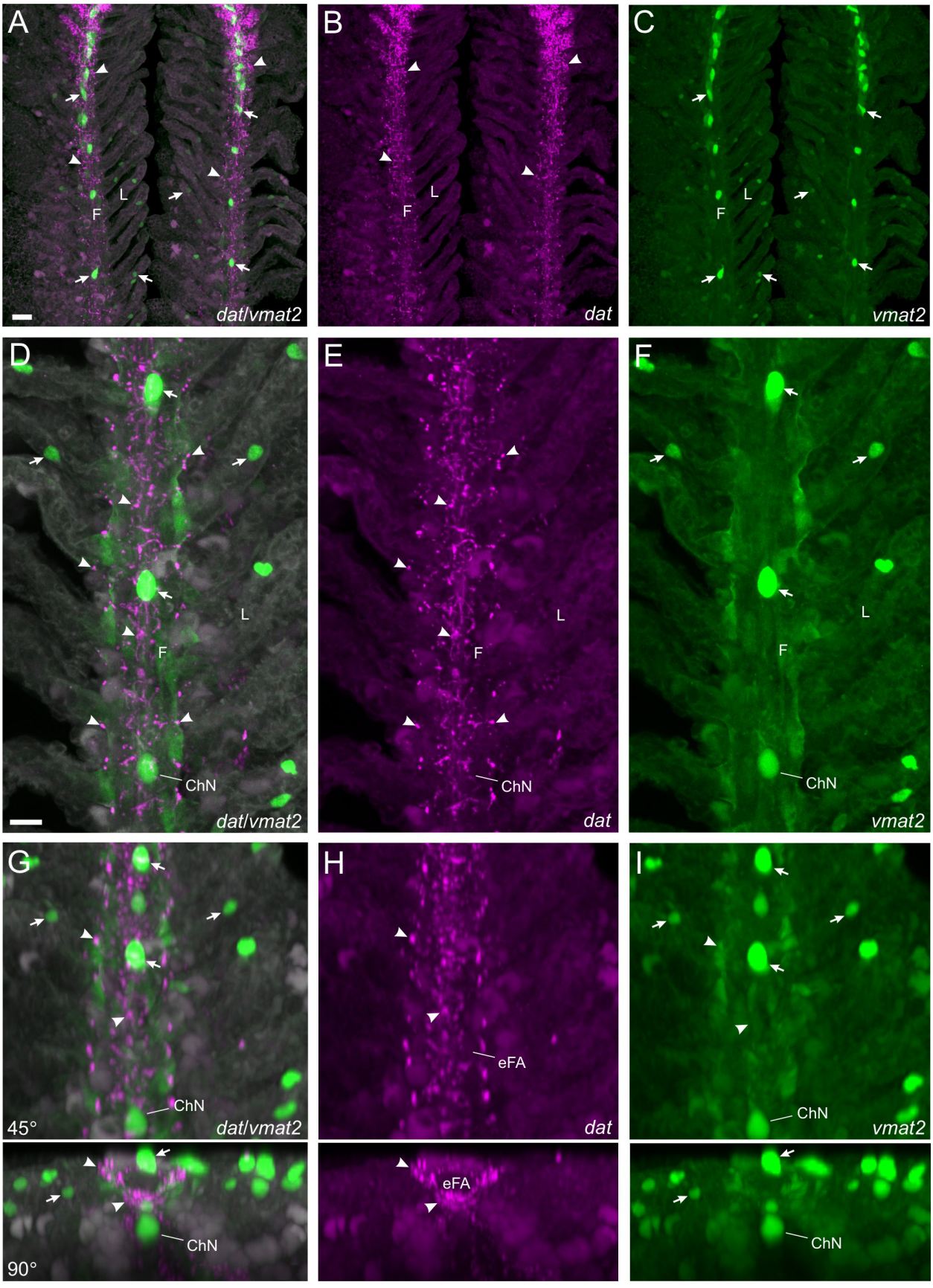
A
B
C
L
F
dat/vmat2
dat
vmat2
D
E
F
L
F
ChN
dat/vmat2
dat
vmat2
G
H
I
ChN
eFA
45°
dat/vmat2
dat
vmat2
ChN
eFA
ChN
90°

CHAPTER 4

Single cell transcriptomic analysis of NECs and gill cells

4.1 Introduction

It is vital for animals to readily detect O_2 availability in their environment and provide appropriate responses to maintain homeostasis. In the aquatic environment, teleost fish use gills to take up O_2 from water and initiate cardiorespiratory responses when encountering hypoxia to avoid the effects of O_2 deprivation on cells and tissues (Randall 1963; Holeton and Randall 1967; Perry et al. 2009). Such responses are suggested to be mediated by peripheral O_2 chemoreceptors, the neuroepithelial cells (NECs), in the gills (Jonz et al. 2004; Burleson et al. 2006; Porteus et al. 2014b; Jonz et al. 2015). NECs are found in the efferent epithelium of gill filaments (Jonz and Nurse 2003). They contain the neurotransmitter, serotonin (5-hydroxytryptamine, 5-HT) stored in dense-cored vesicles, and are highly innervated by afferent nerve fibres (Dunel-Erb et al. 1982; Bailly et al. 1992; Jonz and Nurse 2003). NECs are similar to O_2 chemoreceptors in mammals, such as those of the carotid body, and exhibit significant physiological responses to hypoxia (Jonz and Nurse 2003; Jonz et al. 2004, 2015). In addition, recent evidence suggests that NECs are homologues of O_2-sensitive pulmonary neuroepithelial bodies (Hockman et al. 2017). NECs express background K^+ channels that are inhibited by exposure to acute hypoxia, thus producing plasma membrane depolarization (Jonz et al. 2004; Burleson et al. 2006). Hypoxia was also shown to increase intracellular Ca^{2+} concentration and synaptic vesicle recycling in NECs, suggestive of Ca^{2+}-dependent neurotransmitter release (Jonz et al. 2015; Zachar et al. 2017a). These results indicate a pathway through which a hypoxic signal is generated by NECs.

Neuroepithelial cells also display pronounced plasticity when acclimated to low O_2 conditions. Chronic hypoxia induced significant morphological changes, such as hypertrophy, in NECs (Jonz et al. 2004; Regan et al. 2011; Porteus et al. 2014b). Flow cytometric study of NECs

labelled by green fluorescence protein (GFP) showed an increase in number, cell size and gene expression following two weeks of chronic hypoxia (Pan et al. 2021a). Fish acclimated to 1-4 weeks of hypoxia displayed increased ventilatory responses to subsequent, acute hypoxic exposure (Kerstens et al. 1979; Johnston et al. 1983; Burleson et al. 2002). It is unclear whether the change in hypoxic response was due to an altered O_2 sensitivity in NECs, although this appears to be the case in O_2 chemoreceptors of the carotid body follow chronic hypoxia (Powell 2007). The specific changes in gene expression in NECs that may occur during chronic hypoxia could indicate key components involved in the O_2 sensing mechanism.

Aside from serotonin, other neurotransmitters, such as, acetylcholine (ACh), adenosine triphosphate (ATP) and dopamine (DA), had previously been suggested to be involved in hypoxic signal regulation in the gill. Pharmacological studies on fish ventilation and their response to hypoxia have shown that serotonin and 5-HT_3 receptors contribute to the hypoxic response (Burleson and Milsom 1995a, b; Shakarchi et al. 2013). However, evidence for the release of serotonin or the presence of 5-HT receptors is still lacking. In addition, ACh and ATP, targeting nicotinic ACh receptors and purinergic P2X2/3 receptors, were suggested to elicit hyperventilatory responses (Rahbar et al. 2016; Coe et al. 2017). While P2X3 receptors have been localized to NECs and associated neurons in larval zebrafish gills (Rahbar et al. 2016), the presence of ACh receptors has not been determined. On the other hand, the role of DA is less clear. DA was shown to reduce ventilation frequency in larval zebrafish (Shakarchi et al. 2013) whereas in trout, application of DA induced a weak excitation followed by a weak inhibition in nerve discharge (Burleson and Milsom 1995a). The presence of DA receptors in the gills also remains to be elucidated.

Despite recent advances in delineating the role of gill NECs in the hypoxic response, specific mechanisms through which NECs sense, transduce and transmit hypoxic signals remain ambiguous. Conventional molecular approaches such as polymerase chain reaction (PCR) analysis allow only few gene candidates to be examined at a time, making it difficult to draw connections between different components of the signal pathway. Gao et al. (2017) recently revealed the metabolic profile of carotid body chemoreceptors using microarray analysis. A comprehensive transcriptomic analysis, such as RNA sequencing, would provide more specificity in gene detection, identify more protein-coding genes, and provide a wider range of gene expression changes when compared to microarrays (Rao et al. 2019). In addition, NECs make up only a small proportion of gill cells—about 0.79-1.17% of all dissociated cells from distal filaments, depending on whether animals are exposed to normal levels of O_2 or hypoxia (Pan et al. 2021a). The successful use of conventional RNA sequencing approaches to characterize the NEC transcriptome may therefore be limited by the collection of sufficient amounts of RNA from a relatively small cell population.

In the present study, we employed the droplet based single-cell RNA sequencing (scRNA-seq) approach to profile individual cells dissociated from distal gill filaments of zebrafish acclimated to 2 weeks of hypoxia (PO_2 = 35 mmHg) or normoxia. This shot-gun approach was adopted to capture transcriptomes of NECs and other cells involved in the hypoxia signalling pathway. NECs and other cell types were identified based on marker gene expression, and a gill cell atlas was generated from the dataset. Cross examination of different cell clusters uncovered genes highly differentially expressed in NECs, many of which are shared by the type I cells in mammalian carotid body. Our data provided evidence that NECs exhibit the machinery for chemosensory transduction of hypoxic signals. Our results also revealed the distribution of 5-

HT, ACh and DA receptors in the gills to indicate their potential roles in the regulation of hypoxic signals. Lastly, 2 weeks of chronic hypoxia had affected population sizes and transcriptomes of a few cell types including NECs. NECs had increased expression of ribosomal proteins after chronic hypoxia, suggesting cell growth and proliferation.

4.2 Materials and methods

4.2.1 Animals

Transgenic *ETvmat2:GFP* zebrafish (*Danio rerio*) used to identify O_2-sensitive NECs (Pan et al. 2021a) were bred and raised to 12 months before experiments. Fish were maintained at 28°C on a 14h-10h light-dark cycle (Westerfield 2007) at the Laboratory for the Physiology and Genetics of Aquatic Organisms at the University of Ottawa. All procedures on fish were performed according to protocol BL-1760 and according to guidelines provided by the Canadian Council on Animal Care (CCAC).

4.2.2 Chronic hypoxia

For chronic hypoxia treatment, adult fish were housed in closed, static 2 l aquaria for 14 days. Fish were fed and given water changes twice per day. To control the partial pressure of O_2 (PO_2) in water, a Pegas 4000 MF gas mixer (Columbus Instruments, Columbus, OH, USA) was used to mix compressed air and 100% N_2 to generate the appropriate O_2 tension to deliver to water in aquaria through suspended air stones. In the hypoxia group, 4 fish were acclimated to severe hypoxia through gradual decrease of PO_2 from 158 to 35 mmHg over the course of 1 week. Fish were then kept at 35 mmHg for one additional week. This PO_2 level was above the critical O_2 tension for zebrafish (Barrionuevo and Burggren 1999) and had been shown to induce

increases in cell size and population in NECs (Pan et al. 2021a), thus was chosen here to determine the transcriptomic changes associated with chronic hypoxia. As a control, the normoxia group had 4 fish kept in aquaria with continuously aerated water throughout the treatment period.

4.2.3 Tissue extraction and single cell sample preparation

After 14 days of hypoxia treatment, adult fish were stunned by a blow to the head and decapitated for tissue collection. Techniques for tissue extraction and cell dissociation were adapted from previous studies (Jonz et al. 2004; Pan et al. 2021a), and carried out in sterile conditions. In a laminar flow hood, whole gill baskets were removed from the head and quickly immersed in ice-cold phosphate-buffered solution (PBS) containing (mM): NaCl 137, Na_2HPO_4 15.2, KCl 2.7 and KH_2PO_4 1.5; pH 7.8 (Bradford et al. 1994). Then gill baskets were rinsed in wash solution containing 2% penicillin/streptomycin (cat. no. 15140122, Life Technologies Inc., Burlington, ON, Canada) in PBS for 10 min. Individual gill arches were separated to expose single filaments. For each gill arch, the distal region of gill filaments, where NECs are most abundant (Jonz and Nurse, 2003), was selectively removed and subjected to enzymatic dissociation in 0.25% trypsin/EDTA (cat. no. 25200072, Life Technologies Inc., Burlington, Canada) for 1 h at room temperature. Filament tissue in trypsin solution was minced with fine forceps and triturated with a 1-ml Pasteur pipette in a 15-ml centrifuge tube to facilitate further dissociation. To stop the trypsin reaction, 10% foetal bovine serum (FBS, cat. no. 10438018, Life Technologies Inc., Burlington, ON, Canada) was added to the solution containing cells. Cells were passed through a 40-μm Falcon cell strainer to remove clumps and tissue debris. After a 3

min centrifugation at 1300 rpm, the cell pellet was rinsed with fresh PBS. Cells were centrifuged again and dispersed in fresh PBS.

Cell samples of two treatments were individually "barcoded" to allow samples to be combined prior to library preparation and sequencing. The multiplexing procedure was carried out according to the MULTI-seq protocol (McGinnis et al. 2019b). Cells were first centrifuged to obtain the cell pellet. Then 150 µl of 200 nM anchor/200 nM barcode solution was added to cells and cells were resuspended. The lipid-modified DNA oligonucleotide anchor and unique oligonucleotides served as barcodes and bound to cells during this process. Each sample received a different barcode sequence which allowed computational demultiplexing later on. After 10 min of incubation at room temperature, 200 nM of co-anchor was supplemented to stabilize anchoring of barcodes at the membrane. Cells were incubated on ice for 5 min, then centrifuged at 1300 rpm for 3 min. The cell pellet was washed twice with PBS containing 1% FBS before resuspension in PBS. Cells were counted manually with a hemocytometer and samples were pooled with a 1:1 ratio to reach a final concentration of 500-1000 cells/µl.

4.2.4 10X genomics single-cell library preparation and sequencing

Samples of dissociated cells with a viability above 89% were submitted to the StemCore Laboratories at the Ottawa Hospital Research Institute (OHRI) for preparation and sequencing. For single-cell cDNA library preparation, 3 samples of 15,000 cells mixed from hypoxia and normoxia treatments were processed with the Chromium Single Cell 3' Assay (10X Genomics, San Francisco, CA, USA). cDNA synthesis and library construction were carried out according to the manufacturer's protocol and the resulting cDNA libraries were amplified using PCR.

Samples were sequenced on NextSeq 500 sequencing system (Illumina, San Diego, USA) with a target read of 18,000 per cell.

4.2.5 Bioinformatic analysis of scRNA-seq data

The resulting sequencing data was first analyzed using the Cell Ranger pipeline (10X Genomics) to demultiplex raw base cell files, perform alignment, aggregate outputs and generate feature-barcode matrices. The reference genome used in alignment was constructed using the Ensembl release 101 *Danio* genome annotation (Yates et al. 2020) and the EGFP sequence. Matrices containing gene features and counts of single cells were further analyzed using deMULTIplex software package (McGinnis et al. 2019b) to demultiplex sample barcodes in order to differentiate samples of different treatment groups.

4.2.5.1 Seurat unsupervised analysis

Bioinformatic analysis of the data was carried out using the Seurat package v3.2.1(Stuart et al. 2019) within R v4.0.2. Cell quality was assessed through a combination of quality control metrics including total number of expressed genes, number of unique genes and mitochondrial gene content. Outlier cells were defined if they were found outside of three absolute deviations from the median for any metric and excluded from subsequent analyses. Data was normalized and scaled using the built-in functions in Seurat. Principal component analysis (PCA) was performed on the scaled data and the first 30 principal components were used in the "FindNeighbors" function to determine the Shared Nearest Neighbour (SNN). Using the "FindClusters" function with a resolution of 0.2, cells showing similar expressions were clustered.

The multidimensional dataset was visualized in the Uniform Manifold Approximation Projection (UMAP) graph generated with the first 30 principal components. UMAPs allowed graphical presentation of cell clusters with identity labels and visualization of marker gene expression. To determine unique marker genes of each cluster, Wilcoxon sum tests were performed using the "FindAllMarkers" function. Positive markers from the analysis were used to determine cell identity and new cluster identities were assigned using the "RenameIdents" function. In addition, cells were assigned a score for cell cycle using the "CellCycleScoring" function to determine their mitotic state. Heatmaps and dotplots showing gene expression were generated using built-in functions in Seurat.

4.2.5.2 Doublet Removal

An additional doublet removal was performed using the DoubletFinder package (McGinnis et al. 2019a), after the quality control was performed in Seurat. DoubletFinder performed PCA and used the principal component distance matrix to find each cell's proportion of k nearest neighbors to predict doublets. Predicted doublet cells were removed to reduce aggregated cells in the dataset. The returned output was used in subsequent analyses with Seurat.

4.2.5.3 Differential expression analysis using DEsingle

The Bioconductor package DEsingle v1.10.0 was used to infer transcriptomic changes in hypoxia treatment in comparison to normoxia. DEsingle uses the zero-inflated negative binomial model to discriminate dropout zeros to detect differentially expressed genes with high accuracy (Miao et al. 2018). For each cell cluster examined, an expression matrix containing gene counts and a group vector containing group information were created. These two inputs were passed to

the “DEsingle” function to conduct the differential gene expression analysis. Only genes with statistical significance (adjusted p-value below 0.05) between hypoxia and normoxia were selected to be presented in heatmaps.

4.3 Results

4.3.1 Gill cell atlas

To investigate expression of genes involved in the O_2 sensing pathway, a gill cell atlas with 16 cell identities was generated using the single cell sequencing data. This atlas served as a tool to demonstrate relationships between cell clusters and visualize relative gene expression. After initial filtering and quality control, a total of 12,819 cells were obtained from 8 animals between two conditions (4 fish in hypoxia and 4 fish in normoxia). The data had mean reads of 27,312 per cell, median genes of 485 per cell and 2,844 median unique transcript molecules per cell. Following demultiplexing of sample barcodes, the multidimensional dataset was mapped onto a two-dimensional graph using the uniform manifold approximation projection (UMAP) method.

The cell atlas was built with aggregated data from both treatment conditions to ensure consistent clustering and cell identifications between conditions. The Seurat unsupervised clustering analysis compared cells based on transcriptomic similarities and returned 22 computationally identified clusters. Due to the interest of current research and our knowledge of gill cells, certain cell clusters were annotated with a broader identity without further specification. For example, two computationally defined cell clusters expressing endothelial cell markers could not be further specified based on their gene expression, therefore were both given the identity of endothelial cells. The resulting cell atlas contained 16 cell identities, including

NECs, neurons and other cell types, as shown in Figure 4.1A. These annotated cell populations had a dynamic number of unique genes and mitochondrial gene contents (Figure 4.1C,D); some of these features contributed to the verification of cell identities. Moreover, the 16 cell identities differed greatly in gene expression and their highly differentially expressed genes were depicted in the heatmap in Figure 4.1E.

The annotation of cell clusters was mostly based on previously established molecular markers and known functional characteristics of gill cells. For example, NECs displayed particularly high expression for *tph1a* (Figure 4.1E). Endothelial cells were identified based on their high expression of endothelial PAS domain protein (*epas1a* and *epas1b*), basal cell adhesion molecule (*bcam*) and endothelin 1 (*edn1*) (Yanagisawa et al. 1988; Takeda et al. 2004). The gene *ptprc* encoding protein tyrosine phosphatase receptor type C or cd45 antigen was used to identify the broad leukocyte population (Bertrand et al. 2007). The cluster of mucous cells did not have high expression of specific cell markers but were identified based on expression of mucins (*muc5.1* and *muc13a*). For clusters without established gene markers, the top 30 significantly enriched genes were examined in more detail to reveal identity. For instance, respiratory pavement cells were identified by their high expressions of *cldna, cldnb,* and *cldne* (Figure 4.1E). These genes are orthologous to human gene *CLDN4* which is highly expressed in respiratory type I and type II alveolar cells in lung epithelium (Wang et al. 2003). Immune cells were assigned this identity due to their high expression of lymphocyte antigen *ly6m5* (Figure 4.1E) and chemokines, such as *ccl19b* (Figure 4.1E), *cxcl8a* and *ccl25b.* In addition, proliferating cells were identified based on their high expression of proliferative markers, such as *mki67* and *top2a* (Figure 4.1E). Results from cell cycle scoring confirmed that cells in the proliferating cell cluster were in growth phase 2 or metaphase (G2M) of the cell cycle (Figure

4.1B). Moreover, two stem and progenitor cell populations were identified in our data. They are the cluster of hematopoietic stem and progenitor cells (HSPC), identified by their expression of *grn1* (Figure 4.1E), *grn2* and *thy1/*cd90 (Belcourt et al. 1993; Craig et al. 1993), and the cluster of epidermal neural progenitor cells (ENPC) identified by the expression of *lfng* (Figure 4.1E)*, notch 1b, grhl1, foxi3b* (Jänicke et al. 2007, 2010).

The population of ionocytes was identified in our dataset through their expression of *foxi3a* and *foxi3b* (Figure 4.1E). Aside from the cluster of ENPC, these genes were present in two computationally defined clusters. Close examination of the top differentially expressed genes in these two cell clusters showed that one expressed a high level of *atp6v1c1b* and *atp6v1aa* encoding H^+-ATPase subunits. These cells were further identified as H^+-ATPase-rich cells (HR cells) (Horng et al. 2007). The other cluster expressed a high level of *atp1b1b* and *atp1a1a.1* for Na^+/K^+ ATPase subunits, markers for Na^+/K^+ ATPase-rich cells (NaR cells) (Hsiao et al. 2007) and were annotated as such. Moreover, NaR cells showed high mitochondrial gene content as shown in Figure 4.1D and this feature is consistent with the high mitochondrial content of mitochondria-rich ionocytes.

Furthermore, we have identified novel cell populations in the gills. Two cell clusters expressing significant levels of the transcription factor, *pou2f3*, and advillin (*avil*) and villin 1 (*vil1*) were annotated with identities “Tuft cells I” and “Tuft cells II”. These cells were given such identities due to their resemblance in gene expressions to the mammalian tuft cells (O’leary et al. 2018). Genes orthologous to mammalian tuft cell markers, such as *mydgf, ptgs2b,* and *gng13a* were also highly expressed in tuft cells I, whereas *mydgf*, *ptgs2b*, *trpm4a* and *alox5a* were highly expressed in tuft cells II. Both clusters shared distinctly high expression of *plcg2*.

4.3.2 Neuroepithelial cells and neurons

Neuroepithelial cells of the gills were identified based on expression of the reporter genes, *EGFP* and *slc18a2/vmat2*. *EGFP* recapitulates the expression of vesicular monoamine transporter 2 (*vmat2*/*slc18a2*) in the *ETvmat2:GFP* transgenic line. Although not prominent, *EGFP* and *vmat2*/*slc18a2* colocalized in the cluster annotated as NECs (black arrowheads, Figure 4.2A). The identity of cells in this cluster was verified as NECs by confocal microscopy. In whole-mount gill filaments removed from *ETvmat2:GFP* zebrafish, NECs were co-labelled by EGFP and antibodies against 5-HT (Figure 2.2 in Chapter 2), consistent with previous characterization of these cells (Jonz and Nurse 2003; Pan et al. 2021a). Moreover, high expression of the serotonin synthesizing enzymes, tryptophan hydroxylase (*tph1a*), and dopa decarboxylase (*ddc*) indicate serotonin expression in these cells. *tph1a* and *ddc* were expressed predominantly in the NEC cluster (Figure 4.2A) with an average log-fold increase of 3.42 and 1.29, respectively, in NECs in comparison with other gill cells. In addition, some cells in the neuron cluster next to NECs also expressed low levels of *tph1a* (red arrowhead, Figure 4.2A), consistent with serotonergic neurons of the gill filaments (Jonz and Nurse, 2003). Moreover, synaptic vesicle glycoprotein 2A (*sv2a*) and serotonin transporter (*slc6a4a*) were highly differentially expressed in NECs, providing additional verification for serotonin-containing NECs.

In the cell atlas, NECs were positioned distant from other cell clusters as they exhibit a unique transcriptomic profile. Differential gene expression (DE) analysis of NECs against all other gill cells in the dataset indicated that 617 genes were significantly differentially expressed (adjusted p-value <0.05) in NECs. The most highly expressed genes in NECs are listed in Table 4.1. Among these, regulators of G protein signaling, such as *si:ch211-196h16.12* (encoding

rgs5al), *rgs5a* and *rgs4*, were among the most differentially expressed and were up to a 6-log fold-increase from the global average. A few G protein genes, such as *si:dkey-27j5.5* and *rasd1*, were also highly expressed in NECs. NECs also had exclusively high expression of gastrin releasing peptide, *grp*, and retinaldehyde dehydrogenase 2, *aldh1a2*, for neuropeptide signaling and retinoic acid production, respectively. In addition, a few transcription factors, *zgc:56628*, *pbx1a*, *meis2a.1*, *ascl1a* and *tbx1*, were uniquely expressed in NECs. Moreover, the glial cell-line derived neurotrophic factor receptor, *gfra3*, was found to be highly expressed.

NECs are known for their O_2 sensing properties (Jonz et al. 2004). To investigate potential O_2 sensors within NECs, we examined top expressing mitochondrial genes in the NEC cluster. We found the NADH dehydrogenase (ubiquinone) subunit (*ndufa4l2a*) and the cytochrome c oxidase subunit 8A like (*si:dkey-85n7.8*) to be highly expressed in NECs (Table 4.1). *ndufa4l2a* was ranked as the 5th differentially expressed gene with an average log-fold increase of 3.34, and *si:dkey-85n7.8* was ranked 7th with an average log fold increase of 2.79 in NECs. These high expression values were unique to NECs, as their expression in a few other cell clusters were much lower (Figure 4.2B). Moreover, NECs also showed high expression of hypoxia inducible factor genes, *epas1a*/*hif-2aa* and *epas1b/hif-2a*. In particular, *epas1a*/*hif-2aa* was highly differentially expressed in NECs and endothelial cells cluster, and was found at lower levels of expression in other cell types (Figure 4.2B).

The cell cluster adjacent to NECs expressed high levels of neuronal markers, such as *CR759836.1*(arrowhead, Figure 4.5A), *pvalb8* and *nrxn2a*, and were assigned as neurons (arrowhead, Figure 4.3). *CR759836.1* and *pvalb8* encode 5-HT_3-like receptor subunits and parvalbumin 8, respectively, and they are markers that are highly expressed in GABAergic interneurons in the brain (Rudy et al. 2011). However, we did not detect significant expression of

genes involved in gamma-aminobutyric acid (GABA) synthesis or uptake in the neuron cluster. Neurons also showed high expression of transcription factors, *lmx1bb* and *lmx1ba*, and their mammalian orthologues had been shown to be important to the survival of dopaminergic neurons in mammals (Doucet-Beaupré et al. 2016). In addition, voltage-gated K^+ channels (*kcnc1a*), GDNF family receptor alpha-like (*gfral*) and secretogranin III (*scg3*) were among the top differentially expressed genes in neurons (Figure 4.3). GFRAL and SCG3 were shown to be widely expressed in neuronal cells (Taupenot et al. 2003; Worth et al. 2020). DE analysis of neurons against all other gill cells showed 501 genes, whose expression was significantly higher (adjusted p-value <0.05) in neurons. The top differentially expressed genes in neurons are listed in Table 4.2. Other genes that were highly expressed in neurons include *prr15la, vill* and *stom.* Neurons also uniquely express transcription factors, *foxa, foxa1* and *foxa3.* In addition, genes encoding Ca^{2+} binding proteins, *ano2b* and *anxa5b*, were highly differentially expressed in neurons.

The NEC and neuron clusters were positioned closely in the UMAP reduction and had overlapping gene expression. To examine this in detail, the two clusters were extracted for comparison (Figure 4.4A). Close examination of the subset data containing only NECs and neurons showed that they shared some gene expression characteristic of neurons. Although more prevalent in NECs, both cell clusters exhibit profound expression of membrane transporters, such as *atp1a3b, atp1b2a* and *atp1a3a* (Figure 4.4B). Genes encoding the calcium binding protein, synaptotagmins *syt1a* and *syt11a*, were expressed highly in NECs and neurons (Figure 4.4C). In addition, synaptosomal-associated protein (*snap25a*) for exocytotic neurotransmitter release was exclusively found in the two clusters, while the expression level was significantly higher in

NECs. Furthermore, a number of genes involved in neurotransmission, including *stx1b, vamp2* and *cplx2*, were also highly expressed in the two clusters (Figure 4.4D).

As NECs and neurons showed resemblance with their high gene expression of neuronal genes, we compared the transcriptomes of both clusters to further investigate unique expression in NECs. DE analysis between the two clusters revealed genes differentially expressed in either cluster and the top 20 genes were presented in a heatmap (Figure 4.4E). The results showed that, when compared to neurons, the top expressing genes found in NECs were consistent with previous DE analysis against all other cells. These genes include *rgs5a*, *rgs5al*, *tph1a, ndufa4l2a,* and *grp*. It was also revealed that *epas1a* and *epas1b* were significantly highly expressed in NECs compared to neurons. Moreover, secretagogin (*scgn*) was highly differentially expressed in NECs. On the other hand, neurons had high expression of epithelial cell adhesion molecule (*epcam*), claudins, *cldnh, cldnb* and *cldn7b,* delayed rectifier K^+ channel subunit *kcnc1a,* and plac8 related protein 6, *ponzr6*. When compared to neurons, these genes were down-regulated in NECs.

4.3.3 5-HT, ACh and DA receptor distributions

In addition to profiling chemoreceptors, the present study also mapped the distribution of genes encoding various neurotransmitter receptors in gills on UMAPs. Only receptors showing significant expression were selected to be shown in Figure 4.5A-C. 5-HT receptors were found throughout many clusters. In particular, *CR759836.1* (encoding 5-hydroxytryptamine receptor 3A-like or 5-HT_3-like) was highly expressed in neurons, occupying more than 90% of the cells in that cluster (arrowhead, Figure 4.5A). The average expression of *CR759836.1* in neurons was also significantly higher than in other gill cells, with a difference of more than a 4 log-fold

change (Table 4.2). On the other hand, *htr3a* was found in some endothelial cells, tuft cells and pavement cells. Moreover, *htr2b* was expressed in many endothelial cells, pavement cells and tuft cells. The high expression of *htr2b* appeared to concentrate in the endothelial cell cluster (arrow, Figure 4.5A). The gene for inhibitory 5-HT_{1A} receptor, *htr1ab* was found most abundant in NECs (arrow, Figure 4.5A) and platelets, but nearly absent in other clusters.

In contrast to 5-HT receptors, expression of cholinergic receptors, targets of acetylcholine, were less abundant in gills. The nicotinic ACh receptor α subunit gene, *chrna2b*, was limited to NECs, neurons and two tuft cell clusters (arrows, Figure 4.5B). The other subtype, *chrna6*, showed expression primarily in NECs (arrow, Figure 4.5B). The β subunit genes, *chrnb4* and *chrnb3a*, were present mainly in neurons and NECs, respectively.

The presence of all dopamine receptors was investigated; however, only genes for receptors in the D2-like family were detected. The expression of D4 receptor *drd4a* was found in a few cell clusters including NECs, endothelial cells, and NaR cells (arrows, Figure 4.5C). In addition, *drd3* was highly expressed only in neurons and HR cells clusters (arrows, Figure 4.5C).

The dotplot in Figure 4.5D summarizes the expression of various 5-HT, ACh, DA and P2X3 receptor genes. It could be observed from the graph that *CR759836.1*/*htr3al* was the most abundant receptor gene in terms of average expression level and percent of cells showing such expression in the cluster. Other neurotransmitter receptors were less abundant but present in various cell populations. NECs and neurons were among the top clusters showing the greatest number of different receptors.

4.3.4 Changes of cell proportion and transcription in chronic hypoxia

The aggregated data contained cells from animals acclimated to both hypoxia and normoxia. After demultiplexing the attached MultiSeq barcodes, cells from different treatments could be distinguished. Results showed that the 16 cell identities were present in both treatment conditions. However, cells from fish acclimated to hypoxia had different proportions of cell identities compared to fish in normoxia. As shown in the stacked bar plot in Figure 4.6A, endothelial cells and pavement cells were the two largest cell populations in both treatment groups. When compared to normoxia, the hypoxia group had greater proportions of endothelial cells and pavement cells that, when combined, accounted for more than 50% of the overall cell population. However, in normoxia, endothelial cells and pavement cells together accounted for less than 50% of the overall cell population. The proportions of individual cell identities are presented in the bar plots in Figure 4.6B. Results indicated that 3 cell identities showed an increase in cell proportion in hypoxia. These cells types were NECs, endothelial cells and platelets. In contrast, cell identities, such as leukocytes, immune cells, HR cells, HSPC, proliferating cells, tuft cells II and fibroblasts, showed a decrease in relative frequency in hypoxia. In addition, mucous cells, tuft cells I, neurons and ENPC remained largely unchanged in their relative frequency.

To determine the effects of chronic hypoxia at the transcriptional level, we conducted a differential gene expression analysis between hypoxia and normoxia with all cells in the dataset. The top 30 differentially expressed genes between these two conditions were selected and their expression in each cell identity was shown in the heatmap in Figure 4.6C. Among the top differentially expressed genes in hypoxia, many were directly involved in regulation of the cell cycle, such as *gadd45bb, gadd45ba,* and *gadd45ga.* Other genes are expected to contribute to the

structure or growth of cells, including *cldni, tmsb1, cfl1l, apoeb,* and *socs3a*. The HIF genes, *epas1a* and *epas1b*, and the G-protein signaling regulator, *si:ch211-196h16.12*, were also among the top differentially expressed genes in hypoxia. It could be observed that top 30 differentially expressed genes in hypoxia were mostly expressed in the endothelial cell cluster. On the other hand, NECs also showed high expression of a few genes that were upregulated by hypoxia. These include *si:ch211-196h16.12, bcam, epas1b, epas1a* and *gadd45ga.*

4.3.5 Differential gene expression analysis of chronic hypoxia in NECs

To further examine the effects of chronic hypoxia on transcription in NECs, differential gene expression analysis was conducted using DEsingle with the subset data containing only NECs. The result revealed that 30 genes were significantly differentially expressed in cells from hypoxia compared to normoxia (adjusted p-value < 0.05). Among these genes, 21 were upregulated (within red bracket, Figure 4.7) and 9 were down regulated (within blue bracket, Figure 4.7) in hypoxia. The top highly regulated genes in hypoxia included *apoeb, krt91, cfd, phlda2, junba*; ribosomal proteins, such as *rp7, rpl10a, rpl6, rps6*; and elongation factors, *eef1g* and *eef1b2.* In particular, *phlda2* was believed to be involved in the positive regulation of apoptosis (Jin et al. 2016), whereas *junba* was a proto oncogene, which could contribute to cell proliferation (Bise et al. 2019). Most of the genes that were highly upregulated were encoding ribosomal proteins or elongation factors. On the other hand, genes that were down regulated in hypoxia included *lgals17, isg15, zgc:152791, dnase1l4.1, irf1b, vil1, rasd1, scgn* and *hist2h2l.* Aside from *rasd1* and *scgn,* no other genes involved in the chemosensory transduction of O_2 signalling were found to be differentially regulated.

4.4 Discussion

Investigating the mechanisms of O_2 sensing and chemotransduction in the fish gill has been limited mostly due to our lack of understanding of the cell types involved, and the molecular basis of these processes. Using a transgenic zebrafish, the present study employed single-cell RNA sequencing and developed a transcriptomic atlas of cells from the distal gill filaments, where chemoreceptive NECs reside. The single cell atlas presented information regarding gene expression, cell identification, and transcriptomic similarities between different cell populations. In the atlas, we broadly identified 16 cell populations, including NECs, neurons, endothelial cells and ionocytes, using unbiased clustering analysis and determined their unique gene expression profiles. We were able to identify expression of numerous genes implicated in O_2 sensing and chemotransduction in vertebrates, including those involved in neurotransmission, neurosecretion, ion channels, and mitochondrial proteins. Moreover, we demonstrated transcriptional changes in gill cells following exposure to chronic hypoxia.

In the cell atlas, chemoreceptive NECs were found next to the neuron cluster, away from other gill cells. NECs of the fish gill are considered to be neuron-like, or paraneurons (Zaccone et al. 1997), and their positioning in the UMAP indicated significant transcriptomic differences from other cells. NECs showed a unique transcriptome and genes involved in 5-HT production, such as *tph1a*, were among those highly expressed. In zebrafish, three paralogs of *tph* genes are present in the central nervous system: *tph1a*, *tph1b* and *tph2* (Lillesaar 2011). In a recent report, *tph1a* expression was described in cutaneous NECs and cells of the pharyngeal arch in zebrafish (Pan et al. 2021b). The present results of *tph1a* expression in O_2-sensitive NECs of the gill filaments provide evidence that 5-HT is produced within NECs, and support accumulating evidence that 5-HT is an important neurotransmitter involved in O_2 sensing in the gill (Dunel-

Erb et al. 1982; Burleson and Milsom, 1995a,b; Shakarchi et al. 2013; Jonz et al. 2015). In addition, the high expression of *slc6a4a*, which encodes the serotonin transporter (SERT) and displays broad expression in the zebrafish brain (Norton et al. 2008), may indicate reuptake of 5-HT by NECs from the synaptic cleft after the release of 5-HT during signal transmission. Furthermore, the gill cell atlas recapitulated expression of *vmat2* in the NEC cluster, confirming the identity of these cells. The *vmat2* gene has previously been characterized in gill NECs in zebrafish (Pan et al. 2021a; See also Chapter 2) and encodes a vesicular monoamine transporter involved in storage of 5-HT.

NECs also showed high expression of mitochondrial genes, *ndufa4l2a* and *si:dkey-85n7.8* or *cox8al* (cox8a-like subunit). The corresponding mitochondrial electron transport chain (ETC) subunits, Ndufa4l2, Cox4i2 and Cox8b, were highly expressing genes found in mammalian chemoreceptive type I cells (Zhou et al. 2016; Gao et al. 2017). Cox4i2 and Cox8b subunits were suggested to interact to regulate O_2 diffusion across the mitochondrial inner membrane, a process that can be highly sensitive to a decrease in PO_2, marking a potential site of acute O_2 sensing (Gao et al. 2017). The highly expressed cox8a like subunit in NECs in zebrafish could pose a potential site of O_2 sensing. In mouse, the Cox8b gene contained Hif binding sites in the promoter region and was proposed to be overexpressed due to high expression of Hif2a genes (Gao et al. 2017). In our dataset, we observed concurrent high expressions of the hif2a genes, *epas1a, epas1b* in NECs.

DE analyses showed that NECs had high expression of genes involved in membrane potential regulation, Ca^{2+} signals and neurosecretion. These observations are aligned with the putative O_2 sensory and neurosecretory roles of NECs (Jonz et al. 2004). Many highly differentially expressed genes in NECs overlapped with those found in the mammalian O_2-

chemoreceptive type I cells (Zhou et al. 2016), and supported the functional homology between these chemoreceptors. Mammalian type I cells expressed high levels of G proteins (such as *Gnas* and *Gnb2l1*), and G protein regulator (*Rgs4*). In NECs, pronounced expression of G proteins (*gng13b, rasd1*) and G protein regulators (*rgs5a*, *rgs4*) were observed. G-protein subunits and coupled receptors have been found in NECs of the obligate air-breathing fish, *Arapaima gigas* (Zaccone et al. 2020), though G-protein-mediated signaling in fish species remains poorly studied. In the mammalian carotid body, G-proteins were observed to modulate hypoxic sensory transduction or transmission (Prabhakar et al. 1995; Cachera 1996). Our observations of high expression of G-protein regulators could suggest sensory modulation by G-proteins in NECs. In addition, NECs had an exclusively high expression of retinaldehyde dehydrogenase (*aldh1a2*). Retinaldehyde dehydrogenase catalyzes the chemical reaction to produce retinoic acid, which is important for the growth and development of many cells (Niederreither and Dollé 2008). The retinoic acid receptor gene, *rarga*, was found in all clusters in our dataset. The specific role of retinaldehyde dehydrogenase in NECs is unclear but its high expression could indicate a potential retinoic acid signaling pathway through which NECs communicate with other cells.

Our data did not show any significant changes in expression of genes involved in chemosensory transduction or transmission in NECs after 2 weeks of chronic hypoxia. Genes that were upregulated in hypoxia mostly encoded ribosomal proteins or elongation factors. An increase in expression of these genes could indicate ongoing cell growth or proliferation, as we observed with the increased proportion of NECs in the hypoxia group. Two weeks of chronic hypoxia was previously shown to increase the proportion of GFP-labeled NECs, cell size and GFP expression (Pan et al. 2021a). Although the increase in EGFP expression, which reflects an increase in *vmat2/slc18a2,* could not be detected in our data possibly due to the lack of

sequencing depth, our results of increased proliferation agreed with previous findings. The transcriptional changes in genes expected to be involved in chemotransduction could have occurred before the end of the 2 week hypoxic treatment, possibly even during the first few days, as 36 h of hypoxic exposure had previously caused changes in the HIF pathway (Robertson et al. 2014). Nevertheless, chronic hypoxia induced changes in cell composition in gills. Our results revealed that endothelial cells were most affected by hypoxia. Endothelial cells have long been recognized as part of a vascular oxygen-sensing system (Pohl 1990). Their high expressions of HIF genes, *epas1a* and *epas1b*, also indicated their ability to respond to hypoxia. Chronic hypoxia induces proliferation and vascular remodeling (Voelkel and Tuder 2000), and our results of increased expressions of cell cycle regulator genes and cell structural components support this notion.

Our analysis revealed a distinct neuron population, whose transcriptome was similar to NECs. Their high expression of membrane Na^+/K^+ pumps, Ca^{2+} binding proteins and synaptic proteins are indicators of critical processes involved in neuronal function, such as regulation of transmembrane ionic gradients, and Ca^{2+}-dependent neurotransmission. This cluster of cells may include serotonergic neurons that have been described previously in the zebrafish gill filaments (Jonz and Nurse 2003; Pan et al. 2021a), as some cells within the neuron cluster showed expression of 5-HT synthesizing enzyme genes, *tph1a* and *ddc.* However, the specific function and role of the whole cluster would require further investigation. Despite their ambiguous identity, these neurons are candidates for involvement in post-synaptic, hypoxic signal regulation, as they express a variety of neurotransmitter receptors. The most highly differentially expressed gene in neurons was *CR759836.1* encoding 5-HT_3-like receptors, which presents a notable target of 5-HT secretion from NECs. The 5-HT_3 receptor is a ligand-gated ion channel

mediating fast synaptic excitation (Férézou et al. 2002). Previous studies showed that application of the 5-HT_3 receptor agonist, 2-methyl-5-HT, or the antagonist, tropanyl 3,5-dichlorobenzoate, accordingly increased or decreased ventilation frequency in zebrafish (Jonz et al. 2015). An excitatory signal from NECs to neurons could therefore be mediated via 5-HT_3 receptors. In addition, a few other populations, such as endothelial cells, were also found to express *CR759836.1, htr3a* and 5-HT_2 receptors (*htr2b*) but to a lesser degree. Whether chemosensory information, such as hypoxia, could also be transmitted from NECs to these cells types through such receptors has yet to be confirmed. The inhibitory 5-HT_1 receptor (*htr1ab*) was found to be mainly expressed in NECs and could present a pathway for negative feedback regulation.

In addition to 5-HT, receptors for ACh were found in the atlas. ACh receptors with significant expression found in our data were mostly nicotinic and located in NECs and neurons. ACh and ACh receptor agonists were previously found to induce nerve discharge and changes in ventilation via nicotinic receptors in rainbow trout and zebrafish (Burleson and Milsom 1995a, b; Shakarchi et al. 2013; Rahbar et al. 2016), indicating an excitatory role. ACh is the main excitatory neurotransmitter released by mammalian type I cells (Nurse 2005). In zebrafish, the presence of ACh in a distinct cell population was determined by immunolabelling with antibodies against VAChT (Zachar et al 2017). These cholinergic cells were found in close proximity to NECs and nerve fibres, and were suggested to modulate the NEC response to hypoxia through release of ACh. Furthermore, in zebrafish, application of nicotine or hexamethonium (agonist or antagonist of nicotinic receptors) led to an increase or decrease of ventilation frequency, respectively (Shakarchi et al. 2013; Rahbar et al. 2016). Our finding of nicotinic receptors in NECs and neurons has provided evidence to support a model, in which

VAChT-positive cells release ACh during hypoxic stimulation, leading to subsequent post-synaptic effects on ACh receptors of neurons, and paracrine effects on NECs.

DA receptor expression was less prominent but present in NECs and neurons. The two DA receptor genes, *drd3* and *drd4a*, present in neurons and NECs respectively, belong to the D2-like receptor family that mediates inhibitory neurotransmission. D2 receptors are found in the carotid body in type I cells, where they serve as autoreceptors, and on afferent nerve terminals; and in both cases, they are involved in inhibitory neuromodulation (Mir et al. 1984; Gonzalez et al. 1994; Carroll et al. 2005; Nurse 2010). The presence of D2-like receptors in NECs and neurons, in the present study, appears to support an inhibitory role of DA in O_2 sensing in zebrafish. DA was shown to suppress ventilation when applied exogenously in zebrafish (Shakarchi et al. 2013).

In the present study, we discovered two novel cell populations, named "Tuft cells I" and "Tuft cells II" which had not been described previously in gills. Tuft cells in the mammalian system were identified based on their signature 'tuft-like' brush of microvilli and are present at various locations covering a range of functions, from taste sensing to type II immunity (O'leary et al. 2018; Pan et al. 2020). Tuft cells found in the respiratory tract, in close proximity to pulmonary neuroendocrine cells in lungs, represent an epithelial cell type with both sensory and secretory properties (Xu et al. 2020). Tuft cells I and II in our dataset shared expression of many marker genes with these cells, including the lineage defining transcription factor, *pou2f3*. Respiratory tuft cells found in rodents were cholinergic and expressed VAChT (Pan et al. 2020). Cholinergic cells were previously identified in zebrafish distal gill filaments through their expressions of VAChT and ChAT (Zachar et al. 2017b). In our dataset, we did not detect expression of cholinergic markers, *slc18a3a*, *slc18a3b* (VAChT), *chata*, or *chatb* (choline O-

acetyltransferase, ChAT). While this may have been due to the lack of sequencing depth, it is possible that tuft cells I and II in our dataset may be part of the cholinergic cell population in the gills. However, verification of this would require further investigation.

4.5 Conclusion

The current study has presented the transcriptomic profiles of NECs, neurons and other important cell types of the zebrafish gill using single cell RNA sequencing. We confirmed the identity of NECs in our data by using a transgenic line in which *vmat2* expression could be identified and matched with expression of other genes that were not previously identified in NECs. In addition, we revealed potential pathways of hypoxic signal transduction and neurotransmission through analysis of differential gene expression in NECs and neurons. Identification of the expression of neurotransmitter receptors found in different cell populations provided evidence for putative synaptic or paracrine signalling. The gill cell atlas generated in this chapter presents a valuable resource for future studies on O_2 sensing in zebrafish and other aspects of the biology of fish gills.

Table 4.1 Top 25 most abundant genes in the NEC cluster.

Rank	Gene symbol	Gene name or encoding protein	Avg_logfc	P_val_adj
1	si:ch211-196h16.12	Regulator of G-protein signaling 5-like	6.66819094	0
2	rgs5a	Regulator of G protein signaling 5a	4.22770298	0
3	grp	Gastrin-releasing peptide	3.47543212	0
4	tph1a	Tryptophan hydroxylase 1 (tryptophan 5-monooxygenase) a	3.4249251	0
5	ndufa4l2a	NADH dehydrogenase [ubiquinone] 1α subcomplex subunit 4-like 2a	3.33965647	0
6	aldh1a2	Retinal Dehydrogenase 2	2.81710862	0
7	si:dkey-85n7.8	Cytochrome c oxidase subunit 8A, mitochondrial-like	2.79363448	0
8	si:dkey-27j5.5	GTP-binding protein Rhes	2.62995357	0
9	scgn	Secretagogin, EF-hand calcium binding protein	2.61615044	0
10	CABZ01030107.1	CABZ01030107.1 (Clone-based (Ensembl) gene)	2.40748274	0
11	atp1a3b	ATPase Na+/K+ transporting subunit alpha 3b	2.36620908	0
12	col18a1a	Collagen type XVIII alpha 1 chain a	2.36239711	0
13	atp1b2a	ATPase Na+/K+ transporting subunit beta 2a	2.25801307	0
14	rgs4	Regulator of G protein signaling 4	2.15894663	0
15	zgc:56628	LIM domain transcription factor LMO4	2.158902	0
16	vamp2	Vesicle-associated membrane protein 2	2.02345599	0
17	syt1a	Synaptotagmin Ia	1.96952853	0
18	pbx1a	Pre-B-cell leukemia homeobox 1a	1.93824599	0
19	rasd1	RAS, dexamethasone-induced 1	1.92882428	0
20	scg3	Secretogranin III	1.85782806	0
21	gfra3	GDNF family receptor alpha 3	1.82981327	0
22	cplx2	Complexin 2	1.822202	0
23	tnnc1b	troponin C type 1b (slow)	1.8103739	0
24	meis2a.1	Meis homeobox 2a	1.77830566	0
25	qdpra	quinoid dihydropteridine reductase a	1.75669179	0

Avg_logfc, average log-fold change; P_val_adj, adjusted p-value

Table 4.2 Top 25 most abundant genes in the neuron cluster.

Rank	Gene symbol	Gene name or encoding protein	Avg_logfc	P_val_adj
1	CR759836.1	5-hydroxytryptamine receptor 3A-like	4.056190208	0
2	pvalb8	parvalbumin 8	3.740667793	0
3	si:ch211-152c2.3	si:ch211-152c2.3	3.137073958	0
4	scg3	secretogranin III	2.979105524	0
5	kcnc1a	potassium voltage-gated channel, Shaw-related subfamily, member 1a	2.562373094	0
6	prr15la	proline rich 15 like a	2.293900808	0
7	lmx1bb	LIM homeobox transcription factor 1, beta b	2.244647571	0
8	vill	villin-like	2.132083264	0
9	stom	stomatin	1.985328071	0
10	ano2b	anoctamin 2b	1.957043858	0
11	si:ch211-207j7.2	protein IWS1 homolog A-like	1.899318745	0
12	syt1a	Synaptotagmin Ia	1.885554566	0
13	zgc:112408	zgc:112408	1.846226482	0
14	hepacam2	HEPACAM family member 2	1.793285052	0
15	gfral	GDNF family receptor alpha like	1.767965884	0
16	nrxn2a	neurexin 2a	1.655585901	0
17	rbfox1	RNA binding fox-1 homolog 1	1.649833606	0
18	zgc:101731	SNARE_SNAP25N and SNARE_SNAP23C domain-containing protein; synaptosomal-associated protein 25	1.619684792	0
19	anks4b	ankyrin repeat and sterile alpha motif domain containing 4B	1.609309744	0
20	itpkca	inositol-trisphosphate 3-kinase Ca	1.599939548	0
21	ret	ret proto-oncogene receptor tyrosine kinase	1.585006516	0
22	foxa	forkhead box A sequence	1.576191965	0
23	si:ch211-56a11.2	protein phosphatase 1 regulatory subunit 17	1.538358988	0
24	pclob	piccolo presynaptic cytomatrix protein b	1.523143163	0
25	ggctb	gamma-glutamylcyclotransferase b	1.426595285	0

Avg_logfc, average log-fold change; P_val_adj, adjusted p-value

Figure 4.1 Transcriptomic atlas of gill cells dissociated from the distal gill filaments of *ETvmat2:GFP* zebrafish. (A) Unsupervised uniform manifold approximation projection (UMAP) plot in which gill cells are subdivided into 16 clusters. Colours correspond to separate cell clusters whose identities are defined by the major cell type present within the cluster. Identified cell clusters include endothelial cells, pavement cells, immune cells, mucous cells, proliferating cells, H^+-ATPase-rich cells (HR cells), Na^+/K^+ ATPase-rich cells (NaR cells), epidermal neural progenitor cells (ENPC), hematopoietic stem and progenitor cells (HSPC), leukocytes, platelets, fibroblast, tuft cells I, tuft cells II, neurons and neuroepithelial cells (NECs). (B) UMAP visualization of cell-cycle phases of the aforementioned clusters. G1, G1 phase; G2M, G2 and metaphase; S, synthesis phase. (C) Violin plot showing the number of unique genes in each cell cluster. (D) Violin plot showing the proportion of mitochondrial genes present within each cell cluster. (E) Heatmap of the top 30 genes that were differentially enriched in each cell cluster. Two representative genes from each cluster are highlighted and shown close to the cluster. Scaled gene expression is shown by colours where yellow indicates relative high expression and purple indicates relative low expression.

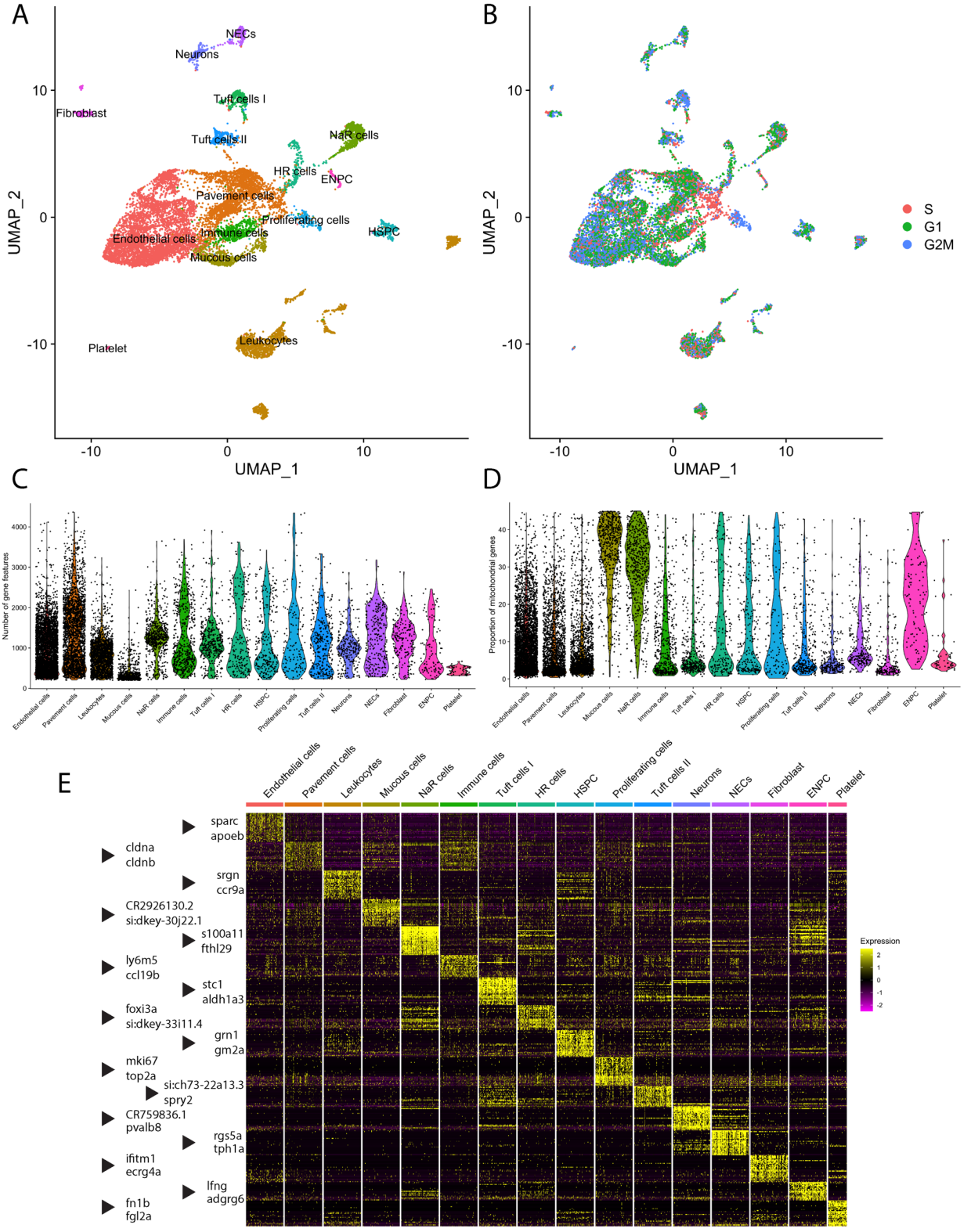
A
NECs
Neurons
Fibroblast
Tuft cells I
Tuft cells II
NaR cells
HR cells
ENPC
Pavement cells
Proliferating cells
HSPC
Immune cells
Endothelial cells
Mucous cells
Leukocytes
Platelet
UMAP_1
UMAP_2
B
S
G1
G2M
C
Number of gene features
D
Proportion of mitochondrial genes
E
Endothelial cells
Pavement cells
Leukocytes
Mucous cells
NaR cells
Immune cells
Tuft cells I
HR cells
HSPC
Proliferating cells
Tuft cells II
Neurons
NECs
Fibroblast
ENPC
Platelet
sparc
apoeb
cldna
cldnb
srgn
ccr9a
CR2926130.2
si:dkey-30j22.1
s100a11
fthl29
ly6m5
ccl19b
stc1
aldh1a3
foxi3a
si:dkey-33i11.4
grn1
gm2a
mki67
top2a
si:ch73-22a13.3
spry2
CR759836.1
pvalb8
rgs5a
tph1a
ifitm1
ecrg4a
lfng
adgrg6
fn1b
fgl2a
Expression

Figure 4.2 Expression of signature genes found in neuroepithelial cells (NECs). (A) UMAP plots showing the log normalized counts of selective genes involved in identification of NECs. Colour intensity is proportional to the expression level of a given gene. Scales indicate relative gene expression. Black arrowheads indicate high expression in the NEC cluster; red arrowhead indicates expression in the neuron cluster. (B) UMAP plots showing the normalized counts of representative genes that may be involved in O_2 sensing in NECs. See text and Table 4.1 for gene description.

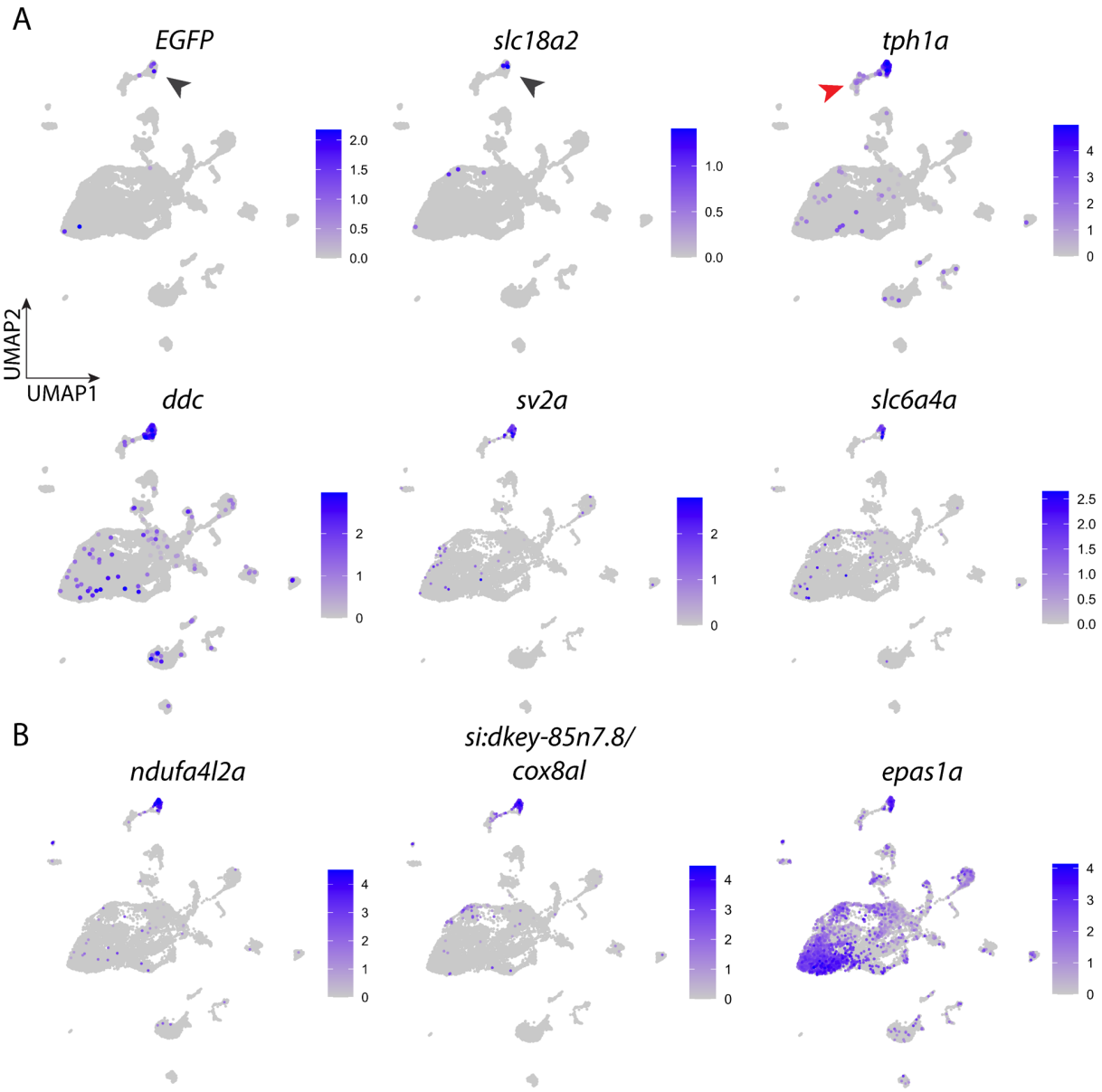
A
EGFP
slc18a2
tph1a
UMAP2
UMAP1
ddc
sv2a
slc6a4a
B
ndufa4l2a
si:dkey-85n7.8/
cox8al
epas1a

Figure 4.3 Expression of signature genes found in the neuron cluster. UMAP plots showing the log normalized counts of selective genes that were highly differentially expressed in neurons. Colour intensity is proportional to the expression level of a given gene. Scales indicate relative gene expression. Arrowhead indicates significant expression in the neuron cluster. See text and Table 4.2 for gene description.

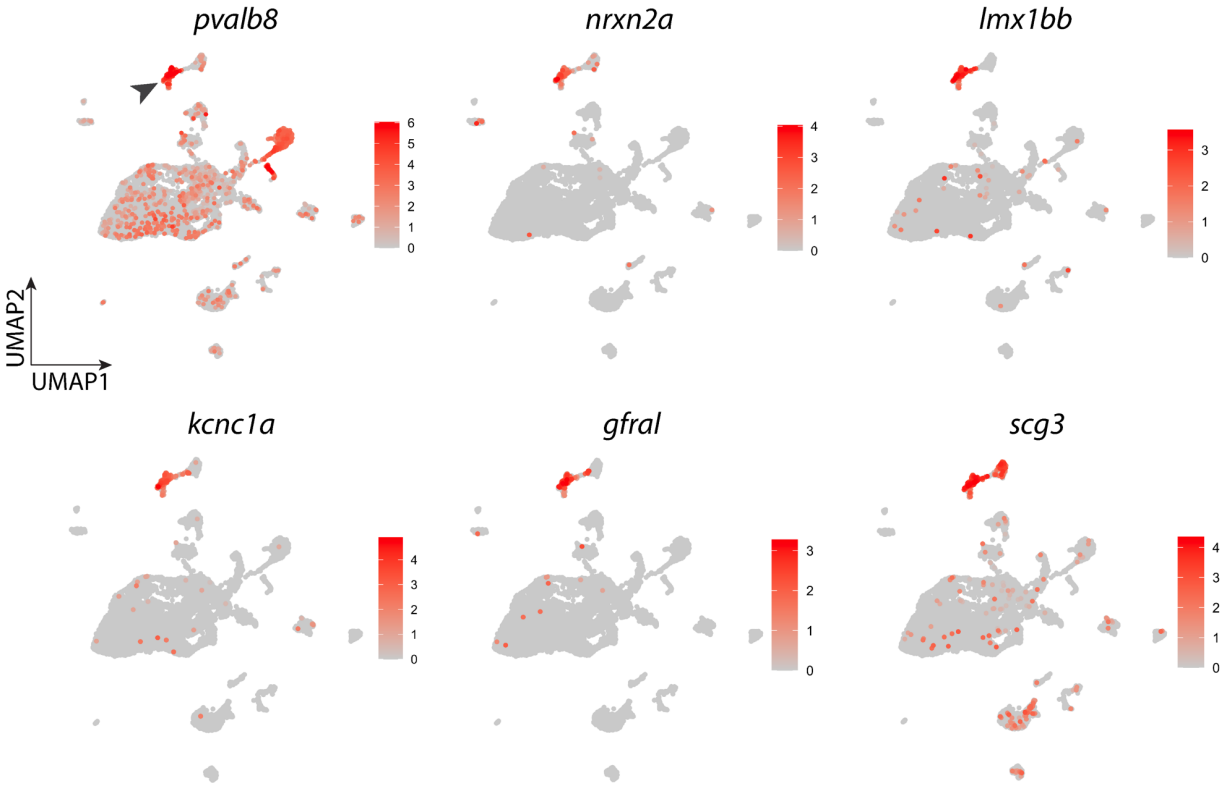
pvalb8
nrxn2a
lmx1bb
kcnc1a
gfral
scg3
UMAP2
UMAP1

Figure 4.4 Comparison of gene expression between the NEC and neuron clusters. (A) UMAP plot showing the subset of the cell population containing NECs and neurons only. (B) UMAP plots showing the log normalized expression of genes encoding membrane transporters. (C) UMAP plots showing the log normalized expression of genes involved in Ca^{2+}-mediated signals. (D) UMAP plots showing the log normalized expression of genes involved in neurotransmitter release. (E) Heatmap of the top 20 highly differentially expressed genes in NECs and neurons. Scaled gene expression is shown by colours where yellow indicates relative high expression and purple indicates relative low expression. See text and Tables 4.1 and 4.2 for gene description.

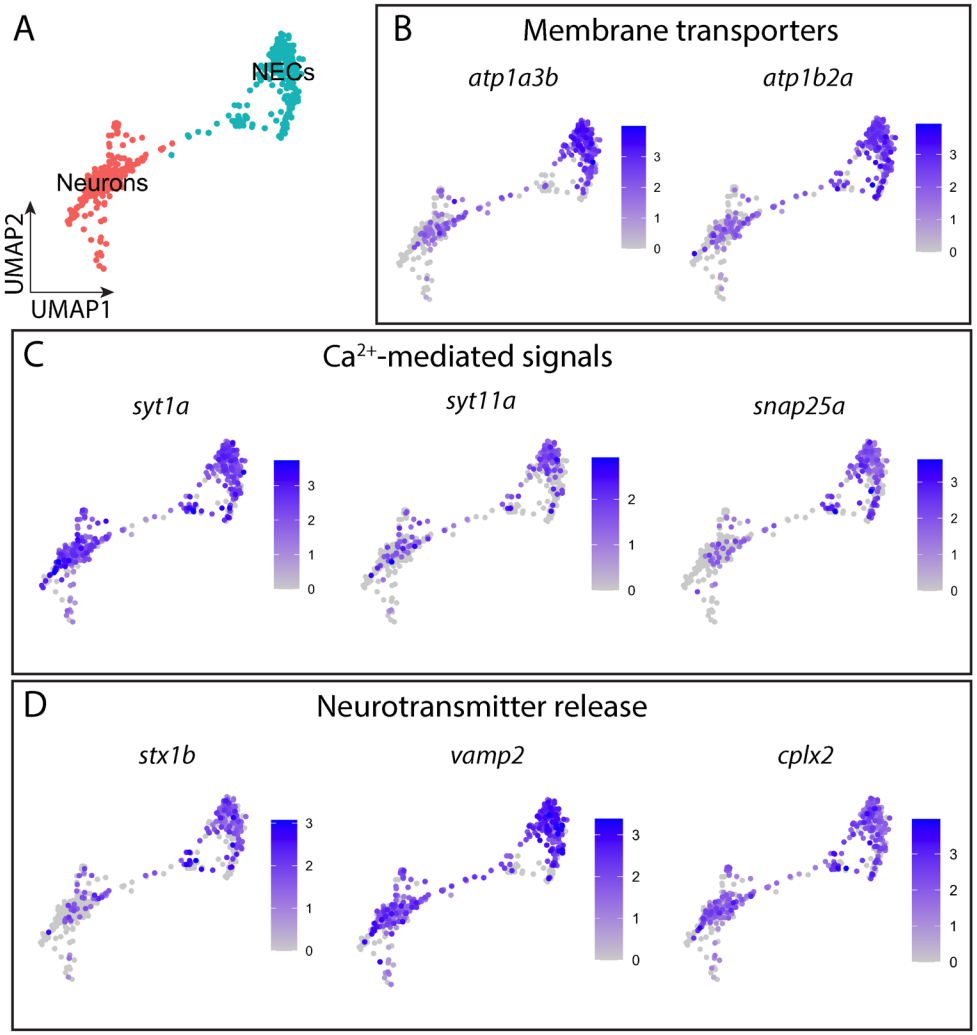
A
NECs
Neurons
UMAP2
UMAP1
B
Membrane transporters
atp1a3b
atp1b2a
C
Ca2+-mediated signals
syt1a
syt11a
snap25a
D
Neurotransmitter release
stx1b
vamp2
cplx2
E
Neurons
NECs
si:ch211-196h16.12
rgs5a
scgn
col18a1a
tph1a
aldh1a2
ndufa4l2a
grp
si:dkey-27j5.5
rnd3a
epas1a
epas1b
si:dkey-85n7.8
rgs4
meis2a.1
gfra3
zgc:56628
mt2
ppdpfb
CABZ01030107.1
pvalb8
CR759836.1
epcam
cldnh
kcnc1a
cldnb
ponzr6
tob1a
lmx1bb
elf3
fthl27
si:ch211-195b11.3
si:ch211-152c2.3
vil1
gstp1
prr15la
cldn7b
stom
anxa5b
foxq1a
Expression
2
1
0
-1
-2

Figure 4.5 Expression of neurotransmitter receptors in the gill cell atlas. (A) UMAP plots showing the distribution of selective 5-HT receptor subunits in all cell populations. Arrowheads indicate cell clusters with significant gene expression. (B) UMAP plots showing distribution of selective cholinergic receptor subunits in all cell populations. (C) UMAP plots showing distribution of selective dopamine receptors in all cell populations. (D) Dotplot of various neurotransmitter receptor subunit expression in 16 gill cell clusters. Colour intensity is proportional to the level of expression; the size of dot indicates the percent of cells showing gene expression in the cell cluster. See text and Tables 4.1 and 4.2 for gene description.

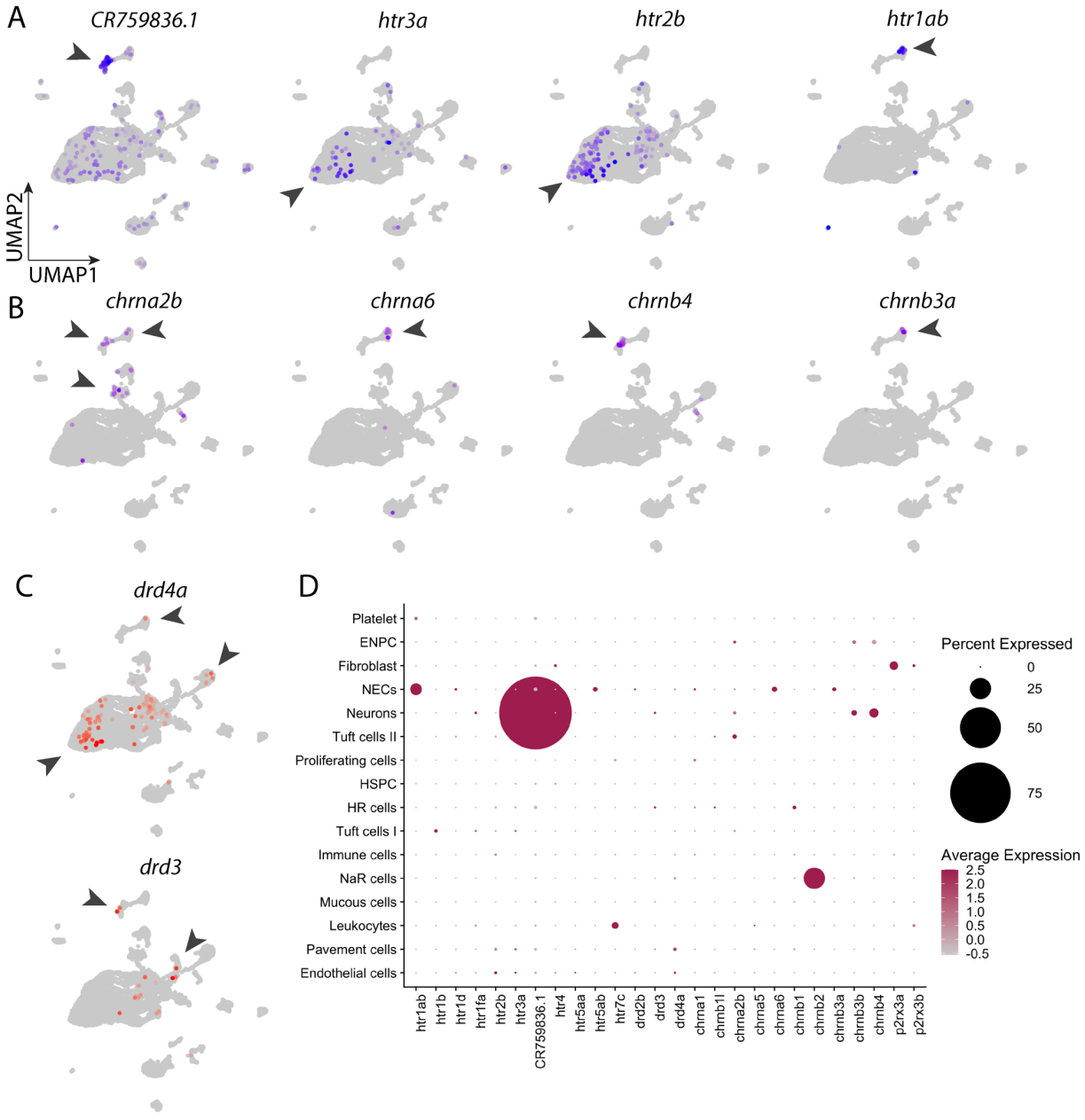
A
CR759836.1
htr3a
htr2b
htr1ab
UMAP2
UMAP1
B
chrna2b
chrna6
chrnb4
chrnb3a
C
drd4a
drd3
D
Platelet
ENPC
Fibroblast
NECs
Neurons
Tuft cells II
Proliferating cells
HSPC
HR cells
Tuft cells I
Immune cells
NaR cells
Mucous cells
Leukocytes
Pavement cells
Endothelial cells
htr1ab
htr1b
htr1d
htr1fa
htr2b
htr3a
CR759836.1
htr4
htr5aa
htr5ab
htr7c
drd2b
drd3
drd4a
chrna1
chrnb1l
chrna2b
chrna5
chrna6
chrnb1
chrnb2
chrnb3a
chrnb3b
chrnb4
p2rx3a
p2rx3b
Percent Expressed
0
25
50
75
Average Expression
2.5
2.0
1.5
1.0
0.5
0.0
-0.5

Figure 4.6 Effects of chronic hypoxia on gill cell composition and global gene expression. (A) Stacked bar graph shows the relative difference in % cell composition between normoxic and hypoxic conditions. Cell types are coded by colour and are indicated at the right. (B) Bar graphs showing changes in relative cell frequency in normoxia (green) vs. hypoxia (orange) in each cell cluster. (C) Heatmap showing the distribution of the top 40 highly differentially expressed genes in chronic hypoxia. Scaled gene expression is shown by colours where yellow indicates relative high expression and purple indicates relative low expression.

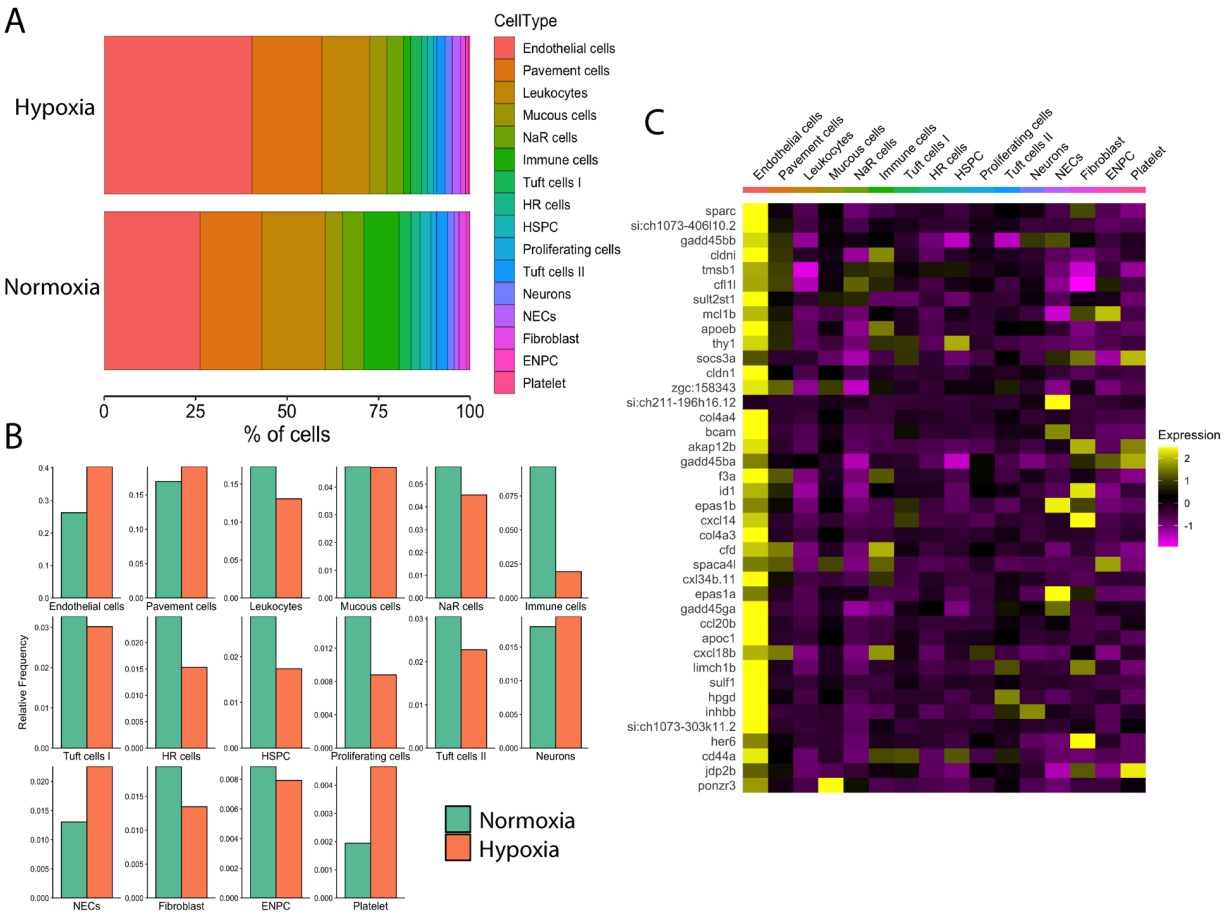
A
Hypoxia
Normoxia
0
25
50
75
100
% of cells
CellType
Endothelial cells
Pavement cells
Leukocytes
Mucous cells
NaR cells
Immune cells
Tuft cells I
HR cells
HSPC
Proliferating cells
Tuft cells II
Neurons
NECs
Fibroblast
ENPC
Platelet
B
Relative Frequency
Endothelial cells
Pavement cells
Leukocytes
Mucous cells
NaR cells
Immune cells
Tuft cells I
HR cells
HSPC
Proliferating cells
Tuft cells II
Neurons
NECs
Fibroblast
ENPC
Platelet
Normoxia
Hypoxia
C
Endothelial cells
Pavement cells
Leukocytes
Mucous cells
NaR cells
Immune cells
Tuft cells I
HR cells
HSPC
Proliferating cells
Tuft cells II
Neurons
NECs
Fibroblast
ENPC
Platelet
sparc
si:ch1073-406l10.2
gadd45bb
cldni
tmsb1
cfl1l
sult2st1
mcl1b
apoeb
thy1
socs3a
cldn1
zgc:158343
si:ch211-196h16.12
col4a4
bcam
akap12b
gadd45ba
f3a
id1
epas1b
cxcl14
col4a3
cfd
spaca4l
cxl34b.11
epas1a
gadd45ga
ccl20b
apoc1
cxcl18b
limch1b
sulf1
hpgd
inhbb
si:ch1073-303k11.2
her6
cd44a
jdp2b
ponzr3
Expression
2
1
0
-1

Figure 4.7 Differential gene expression analysis of NECs between normoxic and hypoxic conditions. Heatmap of highly enriched genes that were statistically significant ($p<0.05$) in both normoxic and hypoxic conditions in the NEC cluster. Genes enclosed in the red bracket were significantly expressed in hypoxia. Genes enclosed in the blue bracket were significantly expressed in normoxia.

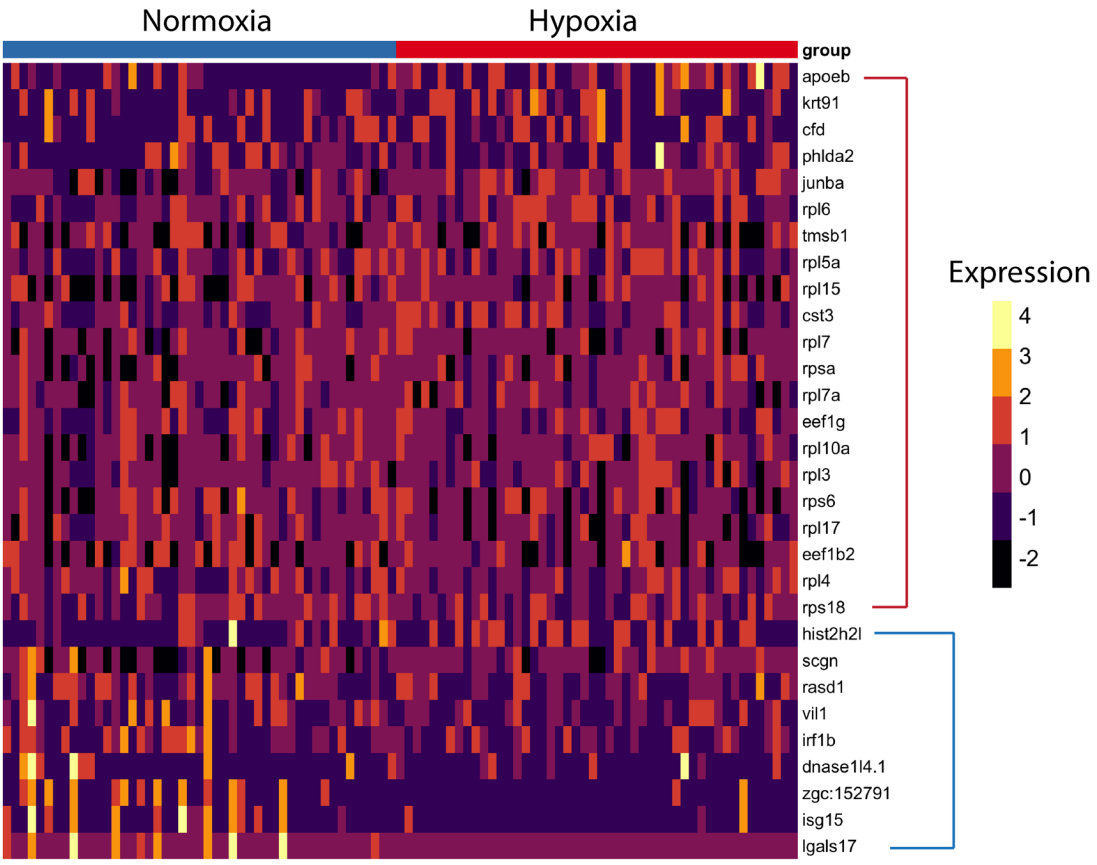
Normoxia
Hypoxia
group
apoeb
krt91
cfd
phlda2
junba
rpl6
tmsb1
rpl5a
rpl15
cst3
rpl7
rpsa
rpl7a
eef1g
rpl10a
rpl3
rps6
rpl17
eef1b2
rpl4
rps18
hist2h2l
scgn
rasd1
vil1
irf1b
dnase1l4.1
zgc:152791
isg15
lgals17
Expression
4
3
2
1
0
-1
-2

CHAPTER 5

General discussion and perspectives

5.1 Introduction

The goal of my Ph.D. studies was to investigate the cellular and molecular basis of O_2 sensing in NECs of gills. In Chapter 2, I characterized reporter gene expression in gills of the transgenic line, *ETvmat2:GFP*, to be used to identify serotonergic NECs. This method allowed for consistent and reliable identification of NECs, compared to previous, conventional approaches involving vital dyes. In addition, the use of vmat2 expression as an indicator for serotonergic NECs in gills could prove to be another important cell marker for NECs. In Chapter 3, I presented evidence of purinergic, cholinergic and dopaminergic control in gills, providing potential pathways in which neurotransmitters could contribute to hypoxic signaling. In Chapter 4, I discussed the transcriptomic profile of NECs and uncovered genes potentially involved in O_2 sensing and chemotransduction. Genes uniquely expressed in NECs composed a "transcriptomic signature" and inferred homology with O_2 chemoreceptors found in the mammalian system. Moreover, using the cell atlas generated with the gill sequencing data, I localized expression of various neurotransmitter receptors in different gill cells, and provided evidence for autocrine and paracrine control in hypoxic signaling.

Findings of my Ph.D. studies will greatly contribute to our understanding of O_2 sensing and signal regulation in gills. In the present chapter, I will integrate my findings with current knowledge of O_2 sensing from the fish and mammalian literature to construct an O_2 sensing model in NECs. In addition, I will discuss the autocrine and paracrine control of the hypoxic signal with evidence from my studies and other systems of O_2 chemoreception.

5.2 Proposed model of O_2 sensing

The identity of the molecular O_2 sensor responsible for initiating membrane depolarization in NECs has remained controversial. Two separate hypotheses had been proposed (Perry et al. 2009). The membrane-delimited mechanism, adapted from carotid body (López-Barneo et al. 1988), hypothesized that O_2 was detected at the plasma membrane. The mitochondrial hypothesis, however, proposed that hypoxia was detected through mitochondrial dysfunction, linked to changes in oxidative phosphorylation and the production of reactive oxygen species (ROS) (Perry et al. 2009). My findings of high expression of mitochondrial electron transport chain (ETC) subunits, *ndufa4l2a* and *si:dkey-85n7.8/cox8al*, in NECs appear to support the mitochondrial hypothesis. In mice, *Ndufa4l2*, *Cox4i2* and *Cox8b* were found to be highly differentially expressed in specialized O_2 chemoreceptors in carotid body and adrenal medulla (Zhou et al. 2016; Gao et al. 2017). The presence of these subunits was suggested to make cytochrome c oxidase highly sensitive to drops in PO_2 as an excessive amount of reduced ubiquinone accumulates, leading to a reduction in mitochondrial complex I activity and production of molecules which could signal ion channels in the plasma membrane (Gao et al. 2017). In mammalian O_2 chemoreceptors, the expression of NDUFA4L2 and COX4I2 was shown to be strongly regulated by HIF-1 (Fukuda et al. 2007; Tello et al. 2011; Aras et al. 2013), whereas high expression of COX8B was linked to HIF2α expression (Gao et al. 2017). In my studies, Cox4i2 was not found to be highly expressed in NECs. However, the concurrent high expression of the other two ETC subunits, and Hif1 and Hif2a (*epas1a*, *epas1b*) genes, still conferred functional homology between NECs and O_2 chemoreceptors found in mammals. Fish in an aquatic environment may be sensitive to a different range of PO_2 changes when compared to mammals on land. As observed within the aquatic environment, different fish species display

different levels of sensitivity to PO_2 changes in chemoreceptor activation (Jonz et al. 2004; Burleson et al. 2006; Zachar and Jonz 2012a; Zachar et al. 2017a). Thus, the combination of cytochrome c subunits (*i.e.* high expression of Cox8al and low expression of Cox4i2) present in zebrafish NECs may indicate a different mitochondrial sensitivity to changes in PO_2 compared to mammalian O_2 chemoreceptors.

A drop in PO_2, possibly detected at mitochondria, leads to background K^+ (K_B) channel inhibition and subsequent membrane depolarization (Jonz et al. 2004). The depolarization is believed to activate voltage-gated Ca^{2+} channels to permit Ca^{2+} influx (Jonz et al. 2004). Such Ca^{2+} channels were shown to be present in NECs in goldfish and mediated an increase in intracellular Ca^{2+} concentration ($[Ca^{2+}]_i$) with acute hypoxic exposure (Zachar et al. 2017a). In zebrafish NECs, an increase in $[Ca^{2+}]_i$ was observed in response to elevated CO_2 and extracellular H^+, even in the absence of external Ca^{2+} (Abdallah et al. 2015a). It was shown that under hypoxia, Ca^{2+} influx triggers release of Ca^{2+} from intracellular stores to further increase $[Ca^{2+}]_i$. In my study, I showed that NECs express high levels of Ca^{2+} binding proteins and components of the SNARE complex, providing evidence for Ca^{2+}-mediated neurosecretion. An increase in $[Ca^{2+}]_i$ in response to hypoxia can lead to potential synaptic vesicle docking and release of neurotransmitters, as observation of vesicular degranulation and recycling in previous studies suggested (Dunel-Erb et al. 1982; Jonz et al. 2015). Moreover, through differential gene expression analysis, I showed that 5-HT synthesizing enzymes were among the top expressed genes in NECs. Together with immunohistochemical observations of abundant 5-HT in NECs (Jonz and Nurse 2003; Pan et al. 2021a), we can infer that 5-HT is a major neurotransmitter present in NECs. Furthermore, the high expression of 5-HT receptor 3A-like subunits in a neuron population shown in my study suggests that 5-HT released from NECs may bind to neurons,

including afferent nerves. To a lesser degree, 5-HT receptor 3A subunits were found in other gill cell populations, including endothelial cells and newly discovered tuft cells. 5-HT3 receptors are ligand-gated ion channels capable of mediating fast excitatory neurotransmission in the central and peripheral nervous system (Sugita et al. 1992). Taken together, 5-HT is likely the main excitatory neurotransmitter released by NECs, targeting neurons and vascular endothelial cells to transmit excitatory signals during hypoxic signaling.

5.3 Autocrine and paracrine modulation of hypoxic signals

The regulation of hypoxic signals involves a number of neurotransmitters. Pharmacological studies on ventilation behaviours of zebrafish revealed that 5-HT, ACh, ATP and DA all contribute to the ventilatory response to hypoxia (Burleson and Milsom 1995b; Shakarchi et al. 2013; Rahbar et al. 2016; Coe et al. 2017). In my thesis, I have localized cells that are putative sources of neurosecretion, and relevant receptor types which may modulate the hypoxia signal.

Using the gill cell atlas, I localized 5-HT_1 autoreceptors through the high expression of *htr1ab* in NECs. 5-HT_1 receptors are G protein-coupled receptors typically mediating inhibitory signaling pathways in most neurons (Albert and Vahid-Ansari 2019). The presence of these receptors suggests negative feedback regulation of chemosensory signalling by NECs, a potential autocrine modulation pathway of the hypoxic signal. Similar autoreceptor inhibition had been shown in mammalian carotid body type I cells, where DA functions via inhibitory D2 autoreceptors (Mir et al. 1984; Gonzalez et al. 1994; Carroll et al. 2005).

In addition, the role of ACh was investigated. ACh is one of the main excitatory neurotransmitters mediating hypoxic signals in the mammalian carotid body (Zhang et al. 2000;

Shirahata et al. 2007) and its production is localized to type I cells (Wang et al. 1989). In fish, ACh was shown as a stimulant in both afferent nerve activity in gills of trout (Burleson and Milsom 1995a) and to trigger pronounced hyperventilation in trout and larval zebrafish (Burleson and Milsom 1995b; Shakarchi et al. 2013). Through immunohistochemistry, I showed that cholinergic cells present in gills contained choline acetyltransferase (ChAT), indicating ACh synthesis within these cells. These cells are distinct from serotonergic NECs. Their expression of vesicular acetylcholine transporters (VAChT) and proximity to afferent nerve fibres and NECs indicate potential ACh secretion by these cells (Zachar et al. 2017b). This notion was further supported by the localization of nicotinic ACh receptors in NECs and neurons in the gill cell atlas. It is also noteworthy that neuronal-type nicotinic receptors were the most abundant cholinergic receptors in gills, predominately found in NECs and neurons. Nicotinic ACh receptors are ligand-gated cation channels, and their activation enables rapid cation flow and membrane depolarization. It is then proposed that ACh released by cholinergic cells, possibly from direct O_2 sensing, binds to nicotinic receptors in afferent nerves to induce depolarization and initiation of action potentials. Binding of ACh to nicotinic receptors in presynaptic NECs, however, may induce additional neurotransmitter release, as seen in previous studies on presynaptic ionotropic receptors (reviewed by MacDermott et al. 1999). This mechanism offers paracrine control in signal transmission.

Moreover, ATP was also determined to be involved in signal modulation. In mammalian carotid body, ATP is an excitatory neurotransmitter co-released with ACh during chemotransduction (Zhang et al. 2000). In larval zebrafish, purinergic P2X2/3 receptors were found to regulate the hyperventilatory responses to hypoxia (Rahbar et al. 2016; Coe et al. 2017). In my study, I localized P2X3 purinoreceptors in gills of larval fish. I showed that P2X3

receptors were present in some NECs, branchial serotonergic neurons and neurons within filamental primordia. Like nicotinic receptors, P2X3 receptors are ligand-gated ion channels. Binding of ATP to P2X3 receptors in neurons could contribute to the sensory discharge leading to the ventilatory response to hypoxia, as observed in a previous study in which broad-spectrum agonist application elicited hyperventilation (Coe et al. 2017). P2X3 receptor activation in the subset of NECs could modulate the response of these cells to potentiate signal transduction. However, it should also be noted that in the single cell RNA sequencing preparation, P2X3 receptor subunit expression levels were lowly detected, whereas receptors for 5-HT and ACh were prominently expressed. This may indicate a sub-dominant role of P2X3 transmission in signal regulation. Nevertheless, the above evidence supports paracrine modulation by ATP via P2X3 receptors.

In mammalian carotid body, DA is the predominant neurotransmitter found in type I cells and has inhibitory effects via dopaminergic D2 receptors (Nurse 2005). The role of DA in hypoxic signaling in gills of fish is less clear. DA was shown to decrease ventilation in larval zebrafish, and induce weak excitation followed by a weak inhibition of nerve discharge in trout (Burleson and Milsom 1995b; Shakarchi et al. 2013). These findings suggest DA affects chemosensory signaling, possibly through DA receptors present in afferent nerve endings. In my studies, I identified dopaminergic nerve fibres in gill filaments, which formed close associations with serotonergic NECs and the efferent filamental artery. These nerve fibres expressed dopamine transporters (dat), were part of the nerve plexus of the gill filaments, and possibly originated from neuronal cell bodies intrinsic to the gills. Localization of DA receptors (*drd3* and *drd4a*) in neuron and NEC clusters in the gill cell atlas further implicated the functional relationship between these cells. The mammalian orthologs D3 and D4 receptors belong to the

D2-like receptor family which mediates inhibitory neurotransmission (Missale et al. 1998). It is implicated that DA receptors found in gills also mediate inhibitory modulation of the hypoxic response through paracrine signaling.

5.4 Future directions

My Ph.D. studies have identified a number of cells and molecular candidates potentially involved in hypoxic sensing and signal modulation. More work is still required to confirm specific signaling pathways. First, investigation of the role of two mitochondrial subunits, Ndufa4l2 and Cox8b-like, could reveal the mechanism of O_2 sensing in NECs. Pharmacological inhibition of mitochondrial subunits combined with physiological experimentation can be used to determine their O_2 sensitivity. The relationship between mitochondrial by-products under hypoxic conditions and membrane channel regulation can also be investigated, as that may be a part of hypoxic signal transduction.

Moreover, the role of cholinergic cells and dopaminergic fibres requires further investigation. Cholinergic cells found in gills present another neurosecretory cell population, yet they could not be identified in the gill cell atlas due to low detection of cholinergic markers. Although we speculated that newly identified tuft cells could include cholinergic cells, this requires verification. Identification of cholinergic cells in the gill cell atlas will grant access to the transcriptomic profile, which will allow us to study their function as a potential chemosensory cell population. In addition, low expression of various 5-HT and ACh receptors found in tuft cells could indicate another level of regulation by these neurotransmitters and may be an interesting topic for future research. While DA appears to mediate inhibitory signals in O_2 sensing, identifying origins of dopaminergic fibres shown in gills will help us to understand their

role. Like cholinergic cells, the presence of dopaminergic cells could not be detected based on dopaminergic markers alone in the gill cell atlas. However, through immunohistochemistry or *in situ* hybridization, identification can be achieved using marker genes of candidate cell populations, such as the neuron cluster in the gill cell atlas. This also allows gene expression analysis of cells giving rise to dopaminergic fibres, to determine their specific function in O_2 signal regulation.

Furthermore, a number of neurotransmitter receptors have been localized in my studies. The types of receptors identified in NECs and neurons have functional implications that are consistent with previous literature. However, future physiological studies will be needed to validate these functions. For example, in isolated NECs identified using the reporter gene GFP in *ETvmat2:GFP*, measurements of 5-HT release in response to hypoxia can verify 5-HT transmission. In addition, ACh-mediated neurotransmitter release in NECs can also be investigated. Other studies can examine the effects on hyperventilatory responses through pharmacological inhibition of identified receptors to verify their roles. The gill cell atlas generated using the single cell RNA sequencing data contained gene expression information from identified cell populations and can be used in future research regarding interactions between NECs and other cells. The atlas also allows cross reference between physiological observations and expression at the molecular level.

5.5 Summary

Overall, findings of my studies greatly supported the role of NECs as the primary O_2 chemoreceptor in gills and furthered our understanding in O_2 sensing in fish. From molecular O_2 sensors to major neurotransmitters and modulators, I found a number of molecular components

involved in the O_2 sensing pathway. Together with knowledge derived from previous research, I was able to construct an updated putative O_2 sensing model. The current research provided compelling evidence for chemosensory transduction and transmission in NECs, information that was lacking previously. In addition, my findings of neurotransmitters and receptors in different cell populations provided a molecular basis for hypoxic signal regulation and modulation. Furthermore, these studies have provided two useful tools for future research regarding O_2 sensing in gills. The first is the use *ETvmat2:GFP* for reliable identification of NECs across various experimental techniques. The second is the gill cell atlas which can serve as a reference for investigations on gene expressions in relevant cell populations.

REFERENCES

Abdallah SJ, Jonz MG, Perry SF (2015a) Extracellular H^+ induces Ca^{2+} signals in respiratory chemoreceptors of zebrafish. Pflugers Arch Eur J Physiol 467:399–413.

Abdallah SJ, Thomas BS, Jonz MG (2015b) Aquatic surface respiration and swimming behaviour in adult and developing zebrafish exposed to hypoxia. J Exp Biol 218:1777–1786.

Acker H, Dufau E, Huber J, Sylvester D (1989) Indications to an NADPH oxidase as a possible pO2 sensor in the rat carotid body. FEBS Lett. 256(1-2):75-8

Albert PR, Vahid-Ansari F (2019) The 5-HT1A receptor: Signaling to behavior. Biochimie. 161:34-45.

Annese V, Navarro-Guerrero E, Rodríguez-Prieto I, Pardal R (2017) Physiological Plasticity of Neural-Crest-Derived Stem Cells in the Adult Mammalian Carotid Body. Cell Rep. 19(3):471-478.

Aras S, Pak O, Sommer N, Finley R Jr, Hüttemann M, Weissmann N, Grossman LI (2013) Oxygen-dependent expression of cytochrome c oxidase subunit 4-2 gene expression is mediated by transcription factors RBPJ, CXXC5 and CHCHD2. Nucleic Acids Res. 41(4):2255-66.

Archer SL, Reeve HL, Michelakis E, et al (1999) O_2 sensing is preserved in mice lacking the gp91 phox subunit of NADPH oxidase. Proc Natl Acad Sci U S A. 96(14):7944-9.

Arias-Stella J, Valcarcel J (1976) Chief cell hyperplasia in the human carotid body at high altitudes: Physiologic and pathologic significance. Hum Pathol. 7(4):361-73.

Bailly Y, Dunel-Erb S, Laurent P (1992) The neuroepithelial cells of the fish gill filament: Indolamine-immunocytochemistry and innervation. Anat Rec 233:143–161.

Barrionuevo WR, Burggren WW (1999) O_2 consumption and heart rate in developing zebrafish (*Danio rerio*): Influence of temperature and ambient O_2. Am J Physiol 276(2):R505-13.

Belcourt DR, Lazure C, Bennett HPJ (1993) Isolation and primary structure of the three major forms of granulin-like peptides from hematopoietic tissues of a teleost fish (*Cyprinus carpio*). J Biol Chem. 268(13):9230-7.

Bertrand JY, Kim AD, Violette EP, et al (2007) Definitive hematopoiesis initiates through a committed erythromyeloid progenitor in the zebrafish embryo. Development. 134(23):4147-56.

Biscoe TJ, Duchen MR, Eisner DA, et al (1989) Measurements of intracellular Ca^{2+} in dissociated type I cells of the rabbit carotid body. J Physiol. 416:421-34.

Bise T, de Preux Charles AS, Jaźwińska A (2019) Ciliary neurotrophic factor stimulates cardioprotection and the proliferative activity in the adult zebrafish heart. NPJ Regen Med. 24;4:2.

Bradford CS, Sun L, Collodi P, Barnes DW (1994) Cell cultures from zebrafish embryos and adult tissues. J Tissue Cult Methods. 16:99–107.

Buckler KJ (1997) A novel oxygen-sensitive potassium current in rat carotid body type I cells. J Physiol. 1;498 (Pt 3)(Pt 3):649-62.

Buckler KJ (2007) TASK-like potassium channels and oxygen sensing in the carotid body. Respir Physiol Neurobiol 157:55–64.

Buckler KJ, Vaughan-Jones RD (1998) Effects of mitochondrial uncouplers on intracellular calcium, pH and membrane potential in rat carotid body type I cells. J Physiol. 15;513 (Pt 3)(Pt 3):819-33.

Buerk DG, Iturriaga R, Lahiri S (1994) Testing the metabolic hypothesis of O_2 chemoreception in the cat carotid body in vitro. J Appl Physiol. 76(3):1317-23.

Burleson M, Milsom W (2003) Comparative Aspects of O_2 Chemoreception. In: Oxygen Sensing. CRC Press, pp 702–725

Burleson ML, Carlton AL, Silva PE (2002) Cardioventilatory effects of acclimatization to aquatic hypoxia in channel catfish. Respir Physiol Neurobiol 131:223–232.

Burleson ML, Mercer SE, Wilk-Blaszczak MA (2006) Isolation and characterization of putative O2 chemoreceptor cells from the gills of channel catfish (*Ictalurus punctatus*). Brain Res 1092:100–107.

Burleson ML, Milsom WK (1993) Sensory receptors in the first gill arch of rainbow trout. Respir Physiol. 93(1):97-110.

Burleson ML, Milsom WK (1995a) Cardio-ventilatory control in rainbow trout: I. Pharmacology of branchial, oxygen-sensitive chemoreceptors. Respir Physiol. 100(3):231-8.

Burleson ML, Milsom WK (1995b) Cardio-ventilatory control in rainbow trout: II. Reflex effects of exogenous neurochemicals. Respir Physiol. 101(3):289-99.

Cachera TG (1996) Cholera and pertussis toxins reveal multiple regulation of cAMP levels in the rabbit carotid body. Eur J Neurosci. 8(11):2320-7.

Campanucci VA, Zhang M, Vollmer C, Nurse CA (2006) Expression of multiple P2X receptors by glossopharyngeal neurons projecting to rat carotid body O_2-chemoreceptors: Role in nitric oxide-mediated efferent inhibition. J Neurosci. 26(37):9482-93.

Carroll JL, Boyle KM, Wasicko MJ, Sterni LM (2005) Dopamine D2 receptor modulation of carotid body type 1 cell intracellular calcium in developing rats. Am J Physiol - Lung Cell Mol Physiol. 288(5):L910-6.

Chen J, He L, Dinger B, Fidone S (2000) Cellular mechanisms involved in rabbit carotid body excitation elicited by endothelin peptides. Respir Physiol. 121(1):13-23.

Chou CL, Shirahata M (1996) Two types of voltage-gated K channels in carotid body cells of adult cats. Brain Res. 742(1-2):34-42.

Coccimiglio ML, Jonz MG (2012) Serotonergic neuroepithelial cells of the skin in developing zebrafish: morphology, innervation and oxygen-sensitive properties. J Exp Biol 215:3881–3894.

Coe AJ, Picard AJ, Jonz MG (2017) Purinergic and adenosine receptors contribute to hypoxic hyperventilation in zebrafish (*Danio rerio*). Comp Biochem Physiol -Part A Mol Integr Physiol 214:50–57.

Coolidge EH, Ciuhandu CS, Milsom WK (2008) A comparative analysis of putative oxygen-sensing cells in the fish gill. J Exp Biol 211:1231–42.

Craig W, Kay R, Cutler RL, Lansdorp PM (1993) Expression of Thy-1 on human hematopoietic progenitor cells. J Exp Med. 177(5):1331-42.

Cross AR, Henderson L, Jones OTG, et al (1990) Involvement of an NAD(P)H oxidase as a pO_2 sensor protein in the rat carotid body. Biochem J. 272(3):743-7.

Cutz E, Jackson A (1999) Neuroepithelial bodies as airway oxygen sensors. Respir Physiol 115:201–214.

Dasso LLT, Buckler KJ, Vaughan-Jones RD (2000) Interactions between hypoxia and hypercapnic acidosis on calcium signaling in carotid body type I cells. Am J Physiol - Lung Cell Mol Physiol. 279(1):L36-42.

Dean BW, Rashid TJ, Jonz MG (2017) Mitogenic action of hypoxia upon cutaneous neuroepithelial cells in developing zebrafish. Dev Neurobiol 77:789–801.

Delpiano MA, Hescheler J (1989) Evidence for a PO_2-sensitive K^+ channel in the type-I cell of the rabbit carotid body. FEBS Lett. 249(2):195-8.

Donnelly DF (1996) Chemoreceptor nerve excitation may not be proportional to catecholamine secretion. J Appl Physiol. 81(2):657-64.

Donnelly DF, Kim I, Yang D, Carroll JL (2011) Role of MaxiK-type calcium dependent K^+ channels in rat carotid body hypoxia transduction during postnatal development. Respir

Physiol Neurobiol. 177(1):1-8.

Doucet-Beaupré H, Gilbert C, Profes MS, et al (2016) Lmx1a and Lmx1b regulate mitochondrial functions and survival of adult midbrain dopaminergic neurons. Proc Natl Acad Sci U S A. 113(30):E4387-96.

Douglas WW (1954) Is there chemical transmission at chemoreceptors? Pharmacol Rev 6:81–83

Duchen MR, Biscoe TJ (1992) Relative mitochondrial membrane potential and $[Ca^{2+}]_i$ in type I cells isolated from the rabbit carotid body. J Physiol. 450:33-61.

Duchen MR, Caddy KW, Kirby GC, et al (1988) Biophysical studies of the cellular elements of the rabbit carotid body. Neuroscience 26:291–311

Dunel-Erb S, Bailly Y, Laurent P (1982) Neuroepithelial cells in fish gill primary lamellae. J Appl Physiol 53:1342–1353

Edwards C, Heath D, Harris P (1971) The carotid body in emphysema and left ventricular hypertrophy. J Pathol. 104(1):1-13.

Eyzaguirre C, Zapata P (1984) Perspectives in carotid body research. J. Appl. Physiol. Respir. Environ. Exerc. Physiol. 57(4):931-57.

Fearon IM, Zhang M, Vollmer C, Nurse CA (2003) GABA mediates autoreceptor feedback inhibition in the rat carotid body via presynaptic GABAB receptors and TASK-1. J Physiol. 553(Pt 1):83-94.

Férézou I, Cauli B, Hill EL, et al (2002) 5-HT3 receptors mediate serotonergic fast synaptic excitation of neocortical vasoactive intestinal peptide/cholecystokinin interneurons. J Neurosci. 22(17):7389-97.

Fidone S, Gonzalez C, Yoshizaki K (1982a) Effects of hypoxia on catecholamine synthesis in rabbit carotid body in vitro. J Physiol. 333:81-91.

Fidone S, Gonzalez C, Yoshizaki K (1982b) Effects of low oxygen on the release of dopamine from the rabbit carotid body in vitro. J Physiol. 333:93-110.

Finger T, Kinnamon S (2013) A taste for ATP: neurotransmission in taste buds. Front. Cell. Neurosci. 7:264

Finkel T, Holbrook NJ (2000) Oxidants, oxidative stress and the biology of ageing. Nature 408:239–247.

Fitzgerald RS (2000) Oxygen and carotid body chemotransduction: The cholinergic hypothesis - A brief history and new evaluation. Respir Physiol 120:89–104.

Fritsche R, Nilsson S (1993) Cardiovascular and ventilatory control during hypoxia BT - Fish Ecophysiology. In: Rankin JC, Jensen FB (eds). Springer Netherlands, Dordrecht, pp 180–206

Fu XW, Nurse CA, Wong V, Cutz E (2002) Hypoxia-induced secretion of serotonin from intact pulmonary neuroepithelial bodies in neonatal rabbit. J Physiol. 539(Pt 2):503-10.

Fu XW, Wang D, Nurse CA, et al (2000) NADPH oxidase is an O2 sensor in airway chemoreceptors: Evidence from K+ current modulation in wild-type and oxidase-deficient mice. Proc Natl Acad Sci U S A. 97(8):4374-9.

Fukuda R, Zhang H, Kim J whan, et al (2007) HIF-1 Regulates Cytochrome Oxidase Subunits to Optimize Efficiency of Respiration in Hypoxic Cells. Cell. 129(1):111-22.

Ganfornina MD, López-Barneo J (1992a) Potassium channel types in arterial chemoreceptor cells and their selective modulation by oxygen. J Gen Physiol. 100(3):401-26.

Ganfornina MD, López-Barneo J (1992b) Gating of O_2-sensitive K^+ Channels of arterial chemoreceptor cells and kinetic modifications induced by low PO_2. J Gen Physiol. 100(3):427-55.

Gao L, Bonilla-Henao V, García-Flores P, et al (2017) Gene expression analyses reveal metabolic specifications in acute O2-sensing chemoreceptor cells. J Physiol 595:6091–6120.

García-Fernández M, Ortega-Sáenz P, Castellano A, López-Barneo J (2007) Mechanisms of low-glucose sensitivity in carotid body glomus cells. Diabetes. 56(12):2893-900.

Gauda EB, Cooper R, Johnson SM, et al (2004) Autonomic microganglion cells: A source of acetylcholine in the rat carotid body. J. Appl. Physiol. 96(1):384-91.

Gomez-Niño A, Obeso A, Baranda JA, et al (2009) MaxiK potassium channels in the function of chemoreceptor cells of the rat carotid body. Am J Physiol - Cell Physiol. 297(3):C715-22.

Gonzalez C, Almaraz L, Obeso A, Rigual R (1994) Carotid body chemoreceptors: From natural stimuli to sensory discharges. Physiol. Rev. 74(4):829-98.

González C, Almaraz L, Obeso A, Rigual R (1992) Oxygen and acid chemoreception in the carotid body chemoreceptors. Trends Neurosci 15:146–153.

Gracey AY, Troll J V., Somero GN (2001) Hypoxia-induced gene expression profiling in the euryoxic fish Gillichthys mirabilis. Proc Natl Acad Sci 98:1993–1998.

He L, Chen J, Dinger B, et al (2002) Characteristics of carotid body chemosensitivity in NADPH oxidase-deficient mice. Am J Physiol - Cell Physiol. 282(1):C27-33.

He L, Chen J, Dinger B, et al (2006) Effect of chronic hypoxia on purinergic synaptic transmission in rat carotid body. J Appl Physiol. 100(1):157-62.

Heath D, Smith P, Jago R (1982) Hyperplasia of the carotid body. J Pathol. 138(2):115-27.

Hempleman SC (1996) Increased calcium current in carotid body glomus cells following in vivo acclimatization to chronic hypoxia. J Neurophysiol 76:1880–1886.

Hempleman SC (1995) Sodium and potassium current in neonatal rat carotid body cells following chronic in vivo hypoxia. Brain Res 699:42–50

Herman JK, O'Halloran KD, Janssen PL, Bisgard GE (2003) Dopaminergic excitation of the goat carotid body is mediated by the serotonin type 3 receptor subtype. Respir Physiol Neurobiol 136(1):1-12.

Hockman D, Burns AJ, Schlosser G, et al (2017) Evolution of the hypoxia-sensitive cells involved in amniote respiratory reflexes. Elife 6:e21231.

Holeton GF, Randall DJ (1967) Changes in blood pressure in the rainbow trout during hypoxia. J Exp Biol 46:297–305

Horng JL, Lin LY, Huang CJ, et al (2007) Knockdown of V-ATPase subunit A (atp6v1a) impairs acid secretion and ion balance in zebrafish (*Danio rerio*). Am J Physiol - Regul Integr Comp Physiol. 292(5):R2068-76.

Hsiao C Der, You MS, Guh YJ, et al (2007) A positive regulatory loop between foxi3a and foxi3b is essential for specification and differentiation of zebrafish epidermal ionocytes. PLoS One. 2(3):e302.

Jacono FJ, Peng YJ, Kumar GK, Prabhakar NR (2005) Modulation of the hypoxic sensory response of the carotid body by 5-hydroxytryptamine: Role of the 5-HT2 receptor. Respir Physiol Neurobiol. 145(2-3):135-42.

Jänicke M, Carney TJ, Hammerschmidt M (2007) Foxi3 transcription factors and Notch signaling control the formation of skin ionocytes from epidermal precursors of the zebrafish embryo. Dev Biol. 307(2):258-71.

Jänicke M, Renisch B, Hammerschmidt M (2010) Zebrafish grainyhead-like1 is a common marker of different non-keratinocyte epidermal cell lineages, which segregate from each other in a Foxi3-dependent manner. Int J Dev Biol. 54(5):837-50.

Jin F, Qiao C, Luan N, Li H (2016) Lentivirus-mediated PHLDA2 overexpression inhibits trophoblast proliferation, migration and invasion, and induces apoptosis. Int J Mol Med. 37(4):949-57.

Johnston IA, Bernard LM, Maloiy GM (1983) Aquatic and Aerial Respiration Rates, Muscle

Capillary Supply and Mitochondrial Volume Density in the Airbreathing Catfish (*Clarias Mossambigus*) Acclimated to Either Aerated or Hypoxic Water. J Exp Biol 105 (1): 317–338.

Jonz MG (2018) Insights into the evolution of polymodal chemoreceptors. Acta Histochem 120:623–629.

Jonz MG, Fearon IM, Nurse CA (2004) Neuroepithelial oxygen chemoreceptors of the zebrafish gill. J Physiol 560:737–752.

Jonz MG, Nurse CA (2005) Development of oxygen sensing in the gills of zebrafish. J Exp Biol 208:1537–1549.

Jonz MG, Nurse CA (2003) Neuroepithelial cells and associated innervation of the zebrafish gill: A confocal immunofluorescence study. J Comp Neurol 461:1–17.

Jonz MG, Zachar PC, Da Fonte DF, Mierzwa AS (2015) Peripheral chemoreceptors in fish: A brief history and a look ahead. Comp. Biochem. Physiol. -Part A Mol. Integr. Physiol. 186:27–38.

Karlsson L(1983) Gill morphology in the zebrafish, Brachydanio rerio (Hamilton- Buchanan). J. Fish Biol. 23(5): 511-524.

Kerstens A, Lomholt JP, Johansen AK (1979) the Ventilation, Extraction and Uptake of Oxygen in Undisturbed Flounders, *Platichthys Flesus*: Responses To Hypoxia Acclimation. J exp Bid 83:169–179

Kim D (2013) K^+ channels in O_2 sensing and postnatal development of carotid body glomus cell response to hypoxia. Respir. Physiol. Neurobiol. 185(1):44-56.

Kim D, Cavanaugh EJ, Kim I, Carroll JL (2009) Heteromeric TASK-1/TASK-3 is the major oxygen-sensitive background K^+ channel in rat carotid body glomus cells. J Physiol. 587(Pt 12):2963-75.

Kim DK, Prabhakar NR, Kumar GK (2004) Acetylcholine release from the carotid body by hypoxia: Evidence for the involvement of autoinhibitory receptors. J Appl Physiol 96:376–383.

Kimmel CB, Ballard WW, Kimmel SR, et al (1995) Stages of embryonic development of the zebrafish. Dev Dyn. 203(3):253-310.

Kobayashi Y, Ricci A, Amenta F, et al (1995) Localization of dopamine receptors in the rabbit lung vasculature. J Vasc Res. 32(3):200-6.

Koerner P, Hesslinger C, Schaefermeyer A, et al (2004) Evidence for histamine as a transmitter in rat carotid body sensor cells. J Neurochem. 91(2):493-500.

Kumar P (2009) Systemic effects resulting from carotid body stimulation. Adv Exp Med Biol. 648:223-33.

Lillesaar C (2011) The serotonergic system in fish. J Chem Neuroanat. 41(4):294-308.

Lomholt JP, Johansen K (1979) Hypoxia Acclimation in Carp: How It Affects O_2 Uptake, Ventilation, and O_2 Extraction from Water. Physiol. Zool. 52:38–49

López-Barneo J (1994) Oxygen-sensitive ion channels: how ubiquitous are they? Trends Neurosci. 17(4):133-5.

López-Barneo J, López-López JR, Ureña J, González C (1988) Chemotransduction in the carotid body: K+ current modulated by PO2 in type I chemoreceptor cells. Science 241:580–582.

López-Barneo J, Ortega-Sáenz P, Molina A, et al (1997) Oxygen sensing by ion channels. Kidney Int 51(2):454-61.

López-Barneo J, Ortega-Sáenz P, Pardal R, et al (2008) Carotid body oxygen sensing. Eur Respir J 32:1386–1398.

López-Barneo J, Ortega-Sáenz P, Pardal R, et al (2009) Oxygen sensing in the carotid body. Ann N Y Acad Sci 1177:119–131.

Lopez-Barneo J, Pardal R, Ortega-Sáenz P (2001) Cellular mechanism of oxygen sensing. Annu Rev Physiol 63:259–87.

López-López JR, Pérez-García MT (2007) Oxygen sensitive Kv channels in the carotid body. Respir Physiol Neurobiol. 157(1):65-74.

MacDermott AB, Role LW, Siegelbaum SA (1999) Presynaptic ionotropic receptors and the control of transmitter release. Annu. Rev. Neurosci. 22:443-85.

McGinnis CS, Murrow LM, Gartner ZJ (2019a) DoubletFinder: Doublet Detection in Single-Cell RNA Sequencing Data Using Artificial Nearest Neighbors. Cell Syst. 8(4):329-337.e4.

McGinnis CS, Patterson DM, Winkler J, et al (2019b) MULTI-seq: sample multiplexing for single-cell RNA sequencing using lipid-tagged indices. Nat Methods 16:619–626.

McGregor KH, Gil J, Lahiri S (1984) A morphometric study of the carotid body in chronically hypoxic rats. J Appl Physiol Respir Environ Exerc Physiol. 57(5):1430-8.

Mendelsohn BA, Kassebaum BL, Gitlin JD (2008) The zebrafish embryo as a dynamic model of anoxia tolerance. Dev Dyn. 237(7):1780-8.

Miao Z, Deng K, Wang X, Zhang X (2018) DEsingle for detecting three types of differential expression in single-cell RNA-seq data. Bioinformatics. 34(18):3223-3224.

Miller S, Pollack J, Bradshaw J, et al (2014) Cardiac responses to hypercapnia in larval zebrafish (*Danio rerio*): The links between CO_2 chemoreception, catecholamines and carbonic anhydrase. J Exp Biol 217:3569–3578.

Mills E, Jöbsis FF (1972) Mitochondrial respiratory chain of carotid body and chemoreceptor response to changes in oxygen tension. J Neurophysiol. 35(4):405-28.

Milsom WK, Brill RW (1986) Oxygen sensitive afferent information arising from the first gill arch of yellowfin tuna. Respir Physiol. 66(2):193-203.

Milsom WK, Burleson ML (2007) Peripheral arterial chemoreceptors and the evolution of the carotid body. Respir Physiol Neurobiol 157:4–11.

Mir AK, McQueen DS, Pallot DJ, Nahorski SR (1984) Direct biochemical and neuropharmacological identification of dopamine D2-receptors in the rabbit carotid body. Brain Res. 291(2):273-83.

Missale C, Russel Nash S, Robinson SW, et al (1998) Dopamine receptors: From structure to function. Physiol. Rev. 78(1):189-225.

Monteiro SM, Garcia-Santos S, Fontaínhas-Fernandes A, Sousa M (2009) An immunohistochemical study of gill epithelium cells in the Nile tilapia, *Oreochromis niloticus*. Comp Biochem Physiol Part A Mol Integr Physiol 153:S111.

Montoro RJ, Ureña J, Fernández-Chacón R, et al (1996) Oxygen sensing by ion channels and chemotransduction in single glomus cells. J Gen Physiol 107:133–143.

Mulligan E, Lahiri S (1982) Separation of carotid body chemoreceptor responses to O_2 and CO_2 by oligomycin and by antimycin A. Am J Physiol - Cell Physiol. 242(3):C200-6.

Navarro-Guerrero E, Platero-Luengo A, Linares-Clemente P, et al (2016) Gene Expression Profiling Supports the Neural Crest Origin of Adult Rodent Carotid Body Stem Cells and Identifies CD10 as a Marker for Mesectoderm-Committed Progenitors. Stem Cells. 34(6):1637-50.

Niederreither K, Dollé P (2008) Retinoic acid in development: towards an integrated view. Nat Rev Genet. 9:541–553.

Noble S, Godoy R, Affaticati P, Ekker M (2015) Transgenic Zebrafish Expressing mCherry in the Mitochondria of Dopaminergic Neurons. Zebrafish 12:349–356.

Norton WH, Folchert A, Bally-Cuif L (2008) Comparative analysis of serotonin receptor (HTR1A/HTR1B families) and transporter (slc6a4a/b) gene expression in the zebrafish brain. J Comp Neurol. 511(4):521-42.

Nurse CA (2005) Neurotransmission and neuromodulation in the chemosensory carotid body. Auton Neurosci Basic Clin 120:1–9.

Nurse CA (2010) Neurotransmitter and neuromodulatory mechanisms at peripheral arterial chemoreceptors. Exp Physiol. 95(6):657-67.

Nurse CA (2014) Synaptic and paracrine mechanisms at carotid body arterial chemoreceptors. J Physiol 16:3419–3426.

Nurse CA, Buttigieg J, Brown S, Holloway AC (2009) Regulation of oxygen sensitivity in adrenal chromaffin cells. Ann N Y Acad Sci 1177:132-9.

Nurse CA, Piskuric NA (2013) Signal processing at mammalian carotid body chemoreceptors. Semin. Cell Dev. Biol. 24(1):22-30.

Nurse CA, Zhang M (1999) Acetylcholine contributes to hypoxic chemotransmission in co-cultures of rat type 1 cells and petrosal neurons. Respir Physiol 115:189–199.

O'leary CE, Schneider C, Locksley RM (2018) Tuft Cells-Systemically Dispersed Sensory Epithelia Integrating Immune and Neural Circuitry. Annu Rev Immunol. 37:47-72.

Olson KR, Healy MJ, Qin Z, et al (2008) Hydrogen sulfide as an oxygen sensor in trout gill chemoreceptors. Am J Physiol Regul Integr Comp Physiol 295(2):R669-80.

Oomori Y, Nakaya K, Tanaka H, et al (1994) Immunohistochemical and histochemical evidence for the presence of noradrenaline, serotonin and gamma-aminobutyric acid in chief cells of the mouse carotid body. Cell Tissue Res. 278(2):249-54.

Ortega-Sáenz P, Levitsky KL, Marcos-Almaraz MT, et al (2010) Carotid body chemosensory responses in mice deficient of TASK channels. J. Gen. Physiol. 135(4):379-92.

Ortega-Saenz P, Pardal R, Garcia-Fernandez M, Lopez-Barneo J (2003) Rotenone selectively occludes sensitivity to hypoxia in rat carotid body glomus cells. J Physiol. 548(Pt 3):789-800.

Padilla PA, Roth MB (2001) Oxygen deprivation causes suspended animation in the zebrafish embryo. Proc Natl Acad Sci U S A. 98(13):7331-5.

Palmer BF, Clegg DJ (2014) Oxygen sensing and metabolic homeostasis. Mol. Cell. Endocrinol. 397(1-2):51-8.

Pan J, Zhang L, Shao X, Huang J (2020) Acetylcholine From Tuft Cells: The Updated Insights Beyond Its Immune and Chemosensory Functions. Front. Cell Dev. Biol. 8:606

Pan W, Scott AL, Nurse CA, Jonz MG (2021a) Identification of oxygen-sensitive neuroepithelial cells through an endogenous reporter gene in larval and adult transgenic zebrafish. Cell

Tissue Res. 384(1):35-47.

Pan YK, Jensen G, Perry SF (2021b) Disruption of tph1 genes demonstrates the importance of serotonin in regulating ventilation in larval zebrafish (*Danio rerio*). Respir Physiol Neurobiol. 285:103594.

Pardal R, López-Barneo J (2002) Low glucose-sensing cells in the carotid body. Nat Neurosci. 5(3):197-8.

Pardal R, Ortega-Sáenz P, Durán R, López-Barneo J (2007) Glia-like Stem Cells Sustain Physiologic Neurogenesis in the Adult Mammalian Carotid Body. Cell. 131(2):364-77.

Peers C, Buckler KJ (1995) Transduction of chemostimuli by the type I carotid body cell. J. Membr. Biol. 144(1):1-9.

Perry SF, Fritsche R, Hoagland TM, et al (1999) The control of blood pressure during external hypercapnia in the rainbow trout (*Oncorhynchus mykiss*). J Exp Biol 202(Pt 16):2177-2190.

Perry SF, Jonz MG, Gilmour KM (2009a) Chapter 5 Oxygen Sensing And The Hypoxic Ventilatory Response, 1st edn. Elsevier Inc. 27:193-253.

Pohl U (1990) Endothelial cells as part of a vascular oxygen-sensing system: Hypoxia-induced release of autacoids. Experientia 46(11-12):1175-9.

Ponte J, Sadler CL (1989) Studies on the regenerated carotid sinus nerve of the rabbit. J Physiol. 410:411-24.

Porteus CS, Abdallah SJ, Pollack J, et al (2014a) The role of hydrogen sulphide in the control of breathing in hypoxic zebrafish (*Danio rerio*). J Physiol. 592(14):3075-88.

Porteus CS, Brink DL, Coolidge EH, et al (2013) Distribution of acetylcholine and catecholamines in fish gills and their potential roles in the hypoxic ventilatory response. Acta Histochem. 115(2):158-69.

Porteus CS, Brink DL, Milsom WK (2012) Neurotransmitter profiles in fish gills: Putative gill oxygen chemoreceptors. Respir Physiol Neurobiol 184:316–325.

Porteus CS, Pollack J, Tzaneva V, et al (2015) A role for nitric oxide in the control of breathing in zebrafish (*Danio rerio*). J Exp Biol. 218(Pt 23):3746-53.

Porteus CS, Wright PA, Milsom WK (2014b) Characterisation of putative oxygen chemoreceptors in bowfin (*Amia calva*). J Exp Biol. 217(Pt 8):1269-77.

Powell F., Milsom W., Mitchell G. (1998) Time domains of the hypoxic ventilatory response. Respir Physiol 112:123–134.

Powell FL (2007) The influence of chronic hypoxia upon chemoreception. Respir Physiol Neurobiol. 157(1):154-61.

Prabhakar NR (2000) Oxygen sensing by the carotid body chemoreceptors. J Appl Physiol 88:2287–2295.

Prabhakar NR, Kou YR, Kumar GK (1995) G proteins in carotid body chemoreception. NeuroSignals. 4(5):271-6.

Prabhakar NR, Overholt JL (2000) Cellular mechanisms of oxygen sensing at the carotid body: Heme proteins and ion channels. Respir Physiol. 122(2-3):209-21.

Prasad M, Fearon IM, Zhang M, et al (2001) Expression of P2X2 and P2X3 receptor subunits in rat carotid body afferent neurones: role in chemosensory signalling. J Physiol. 537(Pt 3):667-77.

Qin Z, Lewis JE, Perry SF (2010) Zebrafish (*Danio rerio*) gill neuroepithelial cells are sensitive chemoreceptors for environmental CO_2. J Physiol 588:861–872.

Rahbar S, Pan W, Jonz MG (2016) Purinergic and Cholinergic Drugs Mediate Hyperventilation in Zebrafish: Evidence from a Novel Chemical Screen. PLoS One 11:e0154261.

Randall D (1982) the Control of Respiration and Circulation in Fish During Exercise and Hypoxia. J exp Biol ioo:275–288.

Randall DJ. SG (1963) The effects of changes in environmental gas concentrations on the breathing and heart rate of a teleost fish. Carbon N Y 9:229–239.

Rao MS, Van Vleet TR, Ciurlionis R, Buck WR, Mittelstadt SW, Blomme EAG, Liguori MJ. (2019) Comparison of RNA-Seq and Microarray Gene Expression Platforms for the Toxicogenomic Evaluation of Liver From Short-Term Rat Toxicity Studies. Front Genet. 9:636.

Regan KS, Jonz MG, Wright PA (2011) Neuroepithelial cells and the hypoxia emersion response in the amphibious fish *Kryptolebias marmoratus*. 214:2560–2568.

Reid SG, Perry SF (2003) Peripheral O2 chemoreceptors mediate humoral catecholamine secretion from fish chromaffin cells. Am J Physiol - Regul Integr Comp Physiol. 284(4):R990-9.

Rigual R, Gonzalez E, Gonzalez C, Fidone S (1986) Synthesis and release of catecholamines by the cat carotid body in vitro: Effects of hypoxic stimulation. Brain Res. 374(1):101-9.

Robertson CE, Wright PA, Köblitz L, Bernier NJ (2014) Hypoxia-inducible factor-1 mediates adaptive developmental plasticity of hypoxia tolerance in zebrafish, *Danio rerio*. Proc R Soc B Biol Sci. 281(1786):20140637.

Rombough P (2007) The functional ontogeny of the teleost gill: Which comes first, gas or ion exchange? Comp. Biochem. Physiol. - A Mol. Integr. Physiol. 148(4):732-42.

Rong W, Gourine A V., Cockayne DA, et al (2003) Pivotal Role of Nucleotide P2X2 Receptor Subunit of the ATP-Gated Ion Channel Mediating Ventilatory Responses to Hypoxia. J Neurosci. 23(36):11315-21.

Rudy B, Fishell G, Lee SH, Hjerling-Leffler J (2011) Three groups of interneurons account for nearly 100% of neocortical GABAergic neurons. Dev Neurobiol. 71(1):45-61.

Saltys HA, Jonz MG, Nurse CA (2006) Comparative study of gill neuroepithelial cells and their innervation in teleosts and Xenopus tadpoles. 323(1):1-10.

Schindelin J, Arganda-Carreras I, Frise E, et al (2012) Fiji: An open-source platform for biological-image analysis. Nat. Methods 9(7):676-82.

Shakarchi K, Zachar PC, Jonz MG (2013) Serotonergic and cholinergic elements of the hypoxic ventilatory response in developing zebrafish. J Exp Biol 216:869–880.

Shirahata M, Balbir A, Otsubo T, Fitzgerald RS (2007) Role of acetylcholine in neurotransmission of the carotid body. Respir Physiol Neurobiol 157:93–105.

Shirahata M, Sham JSK (1999) Roles of ion channels in carotid body chemotransmission of acute hypoxia. Jpn. J. Physiol. 49(3):213-28.

Smatresk NJ, Burleson ML, Azizi SQ (1986) Chemoreflexive responses to hypoxia and NaCN in longnose gar: Evidence for two chemoreceptor loci. Am J Physiol - Regul Integr Comp Physiol. 251(1 Pt 2):R116-25.

Sobrino V, González-Rodríguez P, Annese V, et al (2018) Fast neurogenesis from carotid body quiescent neuroblasts accelerates adaptation to hypoxia. EMBO Rep. 19(3):e44598

Sobrino V, Platero-Luengo A, Annese V, et al (2020) Neurotransmitter modulation of carotid body germinal niche. Int. J. Mol. Sci. 21(21):8231.

Stuart T, Butler A, Hoffman P, et al (2019) Comprehensive Integration of Single-Cell Data. Cell 177:1888-1902.e21.

Sugita S, Shen KZ, North RA (1992) 5-hydroxytryptamine is a fast excitatory transmitter at 5-HT3 receptors in rat amygdala. Neuron. 8(1):199-203.

Summers BA, Overholt JL, Prabhakar NR (1999) Nitric oxide inhibits L-type Ca^{2+} current in glomus cells of the rabbit carotid body via a cGMP-independent mechanism. J Neurophysiol. 81(4):1449-57.

Sundin L, Nilsson S (2002) Branchial innervation. J Exp Zool 293:232–248.

Sundin L, Reid SG, Rantin FT, Milsom WK (2000) Branchial receptors and cardiorespiratory reflexes in a neotropical fish, the tambaqui (*Colossoma macropomum*). J Exp Biol 203(Pt 7):1225-39.

Takeda N, Maemura K, Imai Y, et al (2004) Endothelial PAS domain protein 1 gene promotes angiogenesis through the transactivation of both vascular endothelial growth factor and its receptor, Flt-1. Circ Res. 95(2):146-53.

Tanaka H, Tajimi K, Matsumoto A, Kobayashi K (1990) Vasodilatory effects of milrinone on pulmonary vasculature in dogs with pulmonary hypertension due to pulmonary embolism: a comparison with those of dopamine and dobutamine. Clin Exp Pharmacol Physiol. 17(10):681-90.

Taupenot L, Harper KL, O'Connor DT (2003) The Chromogranin–Secretogranin Family. N Engl J Med. 348(12):1134-49.

Tello D, Balsa E, Acosta-Iborra B, et al (2011) Induction of the mitochondrial NDUFA4L2 protein by HIF-1α decreases oxygen consumption by inhibiting complex I activity. Cell Metab. 14(6):768-79.

Thompson EL, Ray CJ, Holmes AP, et al (2016) Adrenaline release evokes hyperpnoea and an increase in ventilatory CO_2 sensitivity during hypoglycaemia: a role for the carotid body. J Physiol. 594(15):4439-52.

Thompson RJ, Jackson A, Nurse CA (1997) Developmental loss of hypoxic chemosensitivity in rat adrenomedullary chromaffin cells. J Physiol. 498 (Pt 2)(Pt 2):503-10.

Varas R, Alcayaga J, Iturriaga R (2003) ACh and ATP mediate excitatory transmission in cat carotid identified chemoreceptor units in vitro. Brain Res. 988(1-2):154-63.

Varas R, Wyatt CN, Buckler KJ (2007) Modulation of TASK-like background potassium channels in rat arterial chemoreceptor cells by intracellular ATP and other nucleotides. J Physiol. 583(Pt 2):521-36.

Verna A, Roumy M, Leitner LM (1975) Loss of chemoreceptive properties of the rabbit carotid body after destruction of the glomus cells. Brain Res. 100(1):13-23.

Vicario I, Rigual R, Obeso A, Gonzalez C (2000) Characterization of the synthesis and release of catecholamine in the rat carotid body in vitro. Am J Physiol - Cell Physiol. 278(3):C490-9.

Vizek M, Pickett CK, Weil J V. (1987) Increased carotid body hypoxic sensitivity during acclimatization to hypobaric hypoxia. J Appl Physiol 63:2403–2410.

Voelkel NF, Tuder RM (2000) Hypoxia-induced pulmonary vascular remodeling: A model for

what human disease? J. Clin. Invest. 106(6):733-8.

Vulesevic B, McNeill B, Perry SF (2006) Chemoreceptor plasticity and respiratory acclimation in the zebrafish Danio rerio. J Exp Biol 209:1261–1273.

Wang F, Daugherty B, Keise LL, et al (2003) Heterogeneity of claudin expression by alveolar epithelial cells. Am J Respir Cell Mol Biol. 29(1):62-70.

Wang ZY, Bisgard GE (2002) Chronic hypoxia-induced morphological and neurochemical changes in the carotid body. Microsc Res Tech. 59(3):168-77.

Wang ZY, Olson EB, Bjorling DE, et al (2008) Sustained hypoxia-induced proliferation of carotid body type I cells in rats. J Appl Physiol. 104(3):803-8.

Wang ZZ, Stensaas LJ, Dinger B, Fidone SJ (1989) Immunocytochemical localization of choline acetyltransferase in the carotid body of the cat and rabbit. Brain Res. 498(1):131-4.

Wen L, Wei W, Gu W, et al (2008) Visualization of monoaminergic neurons and neurotoxicity of MPTP in live transgenic zebrafish. Dev Biol 314:84–92.

Westerfield M (2007) The Zebrafish Book. A Guide for the Laboratory Use of Zebrafish (*Danio rerio*), 5th Edition. Univ Oregon Press Eugene.

Williams SEJ, Wootton P, Mason HS, et al (2004) Hemoxygenase-2 is an oxygen sensor for a calcium-sensitive potassium channel. Science 306(5704):2093-7.

Worth AA, Shoop R, Tye K, et al (2020) The cytokine GDF15 signals through a population of brainstem cholecystokinin neurons to mediate anorectic signalling. Elife. 9:e55164.

Wyatt CN, Pearson SA, Kumar P, et al (2008) Key roles for AMP-activated protein kinase in the function of the carotid body? Adv Exp Med Biol. 605:63-8.

Wyatt CN, Peers C (1995) $Ca(^{2+})$-activated K^+ channels in isolated type I cells of the neonatal rat carotid body. J Physiol. 360:159-61.

Xu J, Yu H, Sun X (2020) Less Is More: Rare Pulmonary Neuroendocrine Cells Function as Critical Sensors in Lung. Dev Cell 55:123–132.

Yanagisawa M, Kurihara H, Kimura S, et al (1988) A novel potent vasoconstrictor peptide produced by vascular endothelial cells. Nature. 332(6163):411-5.

Yates AD, Achuthan P, Akanni W, et al (2020) Ensembl 2020. Nucleic Acids Res. 48(D1):D682-D688.

Youngson C, Nurse C, Yeger H, Cutz E (1993) Oxygen sensing in airway chemoreceptors. Nature 365:153–155.

Zaccone G, Cupello C, Capillo G, et al (2020) Expression of Acetylcholine- and G protein coupled Muscarinic receptor in the Neuroepithelial cells (NECs) of the obligated air-breathing fish, *Arapaima gigas* (Arapaimatidae: Teleostei). Zoology. 139:125755.

Zaccone G, Fasulo S, Ainis L, Licata A (1997) Paraneurons in the gills and airways of fishes. Microsc Res Tech. 37(1):4-12.

Zaccone G, Lauweryns JM, Fasulo S, et al (1992) Immunocytochemical Localization of Serotonin and Neuropeptides in the Neuroendocrine Paraneurons of Teleost and Lungfish Gills. Acta Zool. 73(3):177-183.

Zaccone G, Maina J, Germanà A, et al (2019) First demonstration of the neuroepithelial cells and their chemical code in the accessory respiratory organ and the gill of the sharptooth catfish, *Clarias gariepinus*: A preliminary study. Acta Zool.100(2):160-166.

Zachar PC, Jonz MG (2012a) Oxygen Sensitivity of Gill Neuroepithelial Cells in the Anoxia-Tolerant Goldfish. In: Advances in experimental medicine and biology. pp 167–172

Zachar PC, Jonz MG (2012b) Neuroepithelial cells of the gill and their role in oxygen sensing. Respir Physiol Neurobiol 184:301–308.

Zachar PC, Pan W, Jonz MG (2017a) Characterization of ion channels and O_2 sensitivity in gill neuroepithelial cells of the anoxia-tolerant goldfish (*Carassius auratus*). J Neurophysiol 118:3014–3023.

Zachar PC, Pan W, Jonz MG (2017b) Distribution and morphology of cholinergic cells in the branchial epithelium of zebrafish (Danio rerio). Cell Tissue Res 367:169–179.

Zhang L, Nurse C a, Jonz MG, Wood CM (2011) Ammonia sensing by neuroepithelial cells and ventilatory responses to ammonia in rainbow trout. J Exp Biol 214:2678–2689.

Zhang M, Buttigieg J, Nurse CA (2007) Neurotransmitter mechanisms mediating low-glucose signalling in cocultures and fresh tissue slices of rat carotid body. J Physiol. 578(Pt 3):735-50.

Zhang M, Fearon IM, Zhong H, Nurse CA (2003) Presynaptic modulation of rat arterial chemoreceptor function by 5-HT: Role of K^+ channel inhibition via protein kinase C. J. Physiol. 551(Pt 3):825-42.

Zhang M, Nurse CA (2000) Does endogenous 5-HT mediate spontaneous rhythmic activity in chemoreceptor clusters of rat carotid body? Brain Res 872:199–203.

Zhang M, Nurse CA (2004) CO 2 /pH Chemosensory Signaling in Co-Cultures of Rat Carotid Body Receptors and Petrosal Neurons: Role of ATP and ACh. J Physiol 92:3433–3445.

Zhang M, Zhong H, Vollmer C, Nurse C a (2000a) Co-release of ATP and ACh mediates hypoxic signalling at rat carotid body chemoreceptors. J Physiol 525:143–158.

Zhong H, Zhang M, Nurse CA (1997) Synapse formation and hypoxic signalling in co-cultures of rat petrosal neurones and carotid body type 1 cells. J Physiol. 503 (Pt 3)(Pt 3):599-612.

Zhou T, Chien MS, Kaleem S, Matsunami H (2016) Single cell transcriptome analysis of mouse carotid body glomus cells. J Physiol 594:4225–4251.